STRUCTURE-PROPERTY RELATIONSHIPS OF POLY(VINYLIDENE FLUORIDE) INDUCED BY STRESS RELAXATION

Maria Marjorie Contreras Ramos

Tese de Doutorado apresentada ao Programa de Pós-graduação em Engenharia Metalúrgica e de Materiais, COPPE, da Universidade Federal do Rio de Janeiro, como parte dos requisitos necessários à obtenção do título de Doutor em Engenharia Metalúrgica e de Materiais.

Orientadores: Celio Albano da Costa Neto
Marysilvia Ferreira da Costa

Rio de Janeiro
Agosto de 2018

STRUCTURE-PROPERTY RELATIONSHIPS OF POLY(VINYLIDENE FLUORIDE) INDUCED BY STRESS RELAXATION

Maria Marjorie Contreras Ramos

TESE SUBMETIDA AO CORPO DOCENTE DO INSTITUTO ALBERTO LUIZ COIMBRA DE PÓS-GRADUAÇÃO E PESQUISA DE ENGENHARIA (COPPE) DA UNIVERSIDADE FEDERAL DO RIO DE JANEIRO COMO PARTE DOS REQUISITOS NECESSÁRIOS PARA A OBTENÇÃO DO GRAU DE DOUTOR EM CIÊNCIAS EM ENGENHARIA METALÚRGICA E DE MATERIAIS.

Examinada por:

_____
Prof. Celio Albano da Costa Neto, Ph.D.

_____
Prof.ª Marysilvia Ferreira da Costa, D.Sc.

_____
Prof.ª Gabriela Ribeiro Pereira, D.Sc.

_____
Prof. Daniel Alves Castello, D.Sc.

_____
Prof. Karim Dahmouche, D.Sc.

_____
Prof. Otávio Bianchi, D.Sc.

_____
Dra. Christine Rabello Nascimento, D.Sc.

RIO DE JANEIRO, RJ - BRASIL
AGOSTO DE 2018

Ramos, Maria Marjorie Contreras

Structure-property relationships of poly(vinylidene fluoride) induced by stress relaxation/ Maria Marjorie Contreras Ramos. – Rio de Janeiro: UFRJ/COPPE, 2018.

XVI, 123 p.: il.; 29,7 cm.

Orientadores: Celio Albano da Costa Neto

Marysilvia Ferreira da Costa

Tese (doutorado) – UFRJ/ COPPE/ Programa de Engenharia Metalúrgica e de Materiais, 2018.

Referências Bibliográficas: p. 92 – 100.

1. Structural evolution. 2. Stress relaxation. 3. Poly(vinylidene fluoride). I. Costa, Celio Albano da *et al.* II. Universidade Federal do Rio de Janeiro, COPPE, Programa de Engenharia Metalúrgica e de Materiais. III. Título.

Dedicated with love to
my parents and
my brother

Acknowledgments

At first I want to thank my parents and my brother for their support and constant encouragement during my studies in the UFRJ. To them this work is dedicated.

I want to express my deep appreciation to my thesis advisors Prof. Marysilvia Ferreira da Costa and Prof. Celio A. Costa, for their advice and guidance during the realization of this thesis. Working with them has been a rewarding experience.

I am grateful to Dr. Christine Rabello for their help, enthusiasm, dedication and interest for this study. Likewise, I would like to thank Prof. Karim Dahmouche and Prof. Otavio Bianchi for their valuable help in this work. Their advices have been greatly appreciated. I would also like to thank Prof. Daniel A. Castello and Prof. Gabriela Ribeiro for serving as my committee member.

I want to thank the whole group of the LPCM (Laboratory of Materials Processing and Characterization) at the UFRJ for creating a friendly atmosphere of work.

I would like to thank Roberto Pinto Cucinelli of the Laboratory of Low Resolution Nuclear Magnetic Resonance, from the Institute of Macromolecules Professor Eloisa Mano (IMA) – UFRJ, for his help in the NMR measurements and his contribution in this work.

I would like to thank Prof. Cristiano L. P. Oliveira of the Complex Fluids Group, Institute of Physics – USP, for his help in SAXS experiments.

I want to thank Prof. Rossana Thire, Prof. Luis Marcelo Tavares, Agmar de Jesus, Inoussa Tougri, Rita Casia, Fabio Bruno, Javier Sanchez, Laercio Rosignoli, Nelson Souza, Roberto Medeiros and Aline Fernandes for their helping hand in all kinds of experiments and discussions on many subjects.

I also want to thank John Hernandez, Aynor Ariza, Eldred Grandez and Jorge Martinez from the Ocean Engineering program for their valuable help.

To my dear friends Andreina Figuera, Mariana Ladeira, Eveline Vasquez, Carolina Efio and Fiorella Aquino thank you for being my family away from home.

Finally, I want to thank the National Agency of Petroleum, Natural Gas and Biofuels (PRH35-ANP) and the Brazilian Agency CAPES for providing the scholarship and resources needed to develop this thesis.

Resumo da Tese apresentada à COPPE/UFRJ como parte dos requisitos necessários para a obtenção do grau de Doutor em Ciências (D.Sc.)

RELAÇÕES ESTRUTURA-PROPRIEDADES DE POLI(FLUORETO DE VINILIDENO) INDUZIDO POR RELAXAÇÃO DE TENSÃO

Maria Marjorie Contreras Ramos

Agosto/2018

Orientadores: Celio Albano da Costa Neto
Marysilvia Ferreira da Costa

Programa: Engenharia Metalúrgica e de Materiais

Poli(fluoreto de vinilideno) tem sido utilizado para realizar investigações sobre as relações entre estrutura e propriedades. Este polímero foi relaxado a diferentes temperaturas (23, 80 e 120 ºC) e deformações (3,5, 7 e 10%) durante 24 h. O material, como processado e relaxado a todas as condições, foi caracterizado por testes de tração e análise dinâmico mecânica (DMA) para determinar as propriedades mecânicas. Foram utilizadas as técnicas de ressonância magnética nuclear (RMN) e espalhamento de raios-X a baixo ângulo (SAXS) para detectar alterações morfológicas como resultado da relaxação de tensão. Os testes de tração após relaxação de tensão mostraram uma grande queda do módulo elástico, variando de 30 a 45% em relação ao polímero como processado. A técnica de RMN permitiu correlacionar a variação do módulo elástico com a evolução estrutural do material, isto é, diminuição da fração cristalina e aumento da região amorfa restrita devido à relaxação de tensão. No entanto, a fração amorfa livre não sofreu alteração significativa. As medidas de SAXS permitiram determinar as modificações dos parâmetros estruturais. Assim, a diminuição de período longo foi observada e atribuída à diminuição da espessura da camada amorfa, como resultado do recuo das cadeias. Por outro lado, a espessura lamelar cristalina não mudou após relaxação de tensão a 23 ºC. Em temperaturas mais elevadas (80 e 120 ºC), os resultados mostraram o crescimento da espessura da camada cristalina devido à cristalização por ativação de temperatura. A evolução estrutural descrita acima ocorreu em nanoescala.

Abstract of Thesis presented to COPPE/UFRJ as a partial fulfillment of the requirements for the degree of Doctor of Science (D.Sc.)

STRUCTURE-PROPERTY RELATIONSHIPS OF POLY(VINYLIDENE FLUORIDE) INDUCED BY STRESS RELAXATION

Maria Marjorie Contreras Ramos

August/2018

Advisors: Celio Albano da Costa Neto
Marysilvia Ferreira da Costa

Department: Metallurgical and Materials Engineering

Poly(vinylidene fluoride) have been utilized to carry out investigations on structure-property relationships. This polymer was relaxed at different temperatures (23, 80 and 120 ºC) and strains (3.5, 7 and 10%) during 24 h. The material, as processed and all relaxed conditions, was characterized by tensile tests, dynamic mechanical analysis (DMA) to determine mechanical properties; and solid-state nuclear magnetic resonance (NMR) and small angle X-ray scattering (SAXS) to detected morphological changes as a result of the stress relaxation. Tensile tests after stress relaxation showed a huge drop in the elastic modulus, varying from 30 to 45% compared to the as processed polymer. The NMR technique allowed to correlate the variation of the elastic modulus with the evolution of the structure inside the material, namely, decrease of crystalline fraction and increase of constrained amorphous region due to the stress relaxation. Nonetheless, the free amorphous fraction did not undergo a significant change. In addition, the SAXS measurements allowed to determine modifications of the structural parameters. It can be noted that the decrease of long period which was attributed to the decrease of amorphous layer thickness, as a result of the chains recoil. On the other hand, crystalline lamellar thickness did not change after stress relaxation at 23 ºC. However, at higher temperatures (80 and 120 ºC), the results showed the growth of the thickness of the crystalline layer due to crystallization by temperature activation. The structure evolution verified and described above occurred in nanoscale.

Content

Figures Index

Tables Index

Chapter 1

Introduction

The successfulness of a material's performance depends on its properties, which often depend on the microstructure it possesses. And, knowing the exact molecular mechanisms by which the structure and the properties are interrelated is a great challenge and has been the goal of many studies. Therefore, the understanding of the relationships between morphology and properties is of high importance with respect to the application of polymeric materials.

The present study was done to gain new insights on the structure-property behavior for poly(vinylidene fluoride) (PVDF) induced by stress relaxation. This material is a semicrystalline engineering polymer consisting of long molecular chains formed by a repetition of the molecular unit CH_2-CF_2, and alternating crystalline and amorphous regions [1-2]. The crystalline structures of PVDF involve spherulitic morphology which may reach a size of more than 100 μm under certain crystallization conditions [3]. The multiple covalent carbon-fluorine bonds give to PVDF excellent thermal stability and chemical resistance, and high mechanical properties [3-7]. These features promote its use in structural applications and in chemically aggressive environments, such as in demanding flexible lines in the oil and gas offshore industry, where it has to stand different chemicals up to 130 ºC. PVDF can present four different crystal structures, identified as α, β, γ and δ phase [8-9], being the non-polar α-phase the thermodynamically most stable one and, hence, the natural choice for structural applications [10-12]. Viscoelastic polymers suffer from stress relaxation, and their mechanical behavior is quite dependent on the thermal history, which can vary upon the crystalline morphology or introduce damage due to imposed strain or stress [13-14]. A typical application where stress relaxation is imposed is in internal pressure sheath in flexible lines (oil production) during winding on the spool or even during operation, which are crucial for guaranteeing the structural integrity of the lines. Nevertheless, only few investigations of stress relaxation behavior of PVDF were found in the

literature [2, 15], and they did not look upon structural modification and post relaxation properties. Different studies have been carried out to investigate the morphological changes during the deformation process of PVDF; however, structural evolution of PVDF after stress relaxation has not been found in the literature.

In order to more directly address the effect of morphology on the mechanical behavior of PVDF after stress relaxation, different techniques of characterization can be used including tensile tests, solid-state nuclear magnetic resonance (NMR) and small angles X-ray scattering (SAXS).

NMR technique provides valuable insights in structure and dynamics of semicrystalline polymers. ^{1}H NMR measurements investigates proton dipolar coupling strength which is an indicator for segmental dynamics in polymers. This technique is a suitable method for the study of chain dynamics in rigid-crystalline and mobile-amorphous domains of semicrystalline polymer. The differences in chain mobility between the individual phases of the polymer allow the detection of fraction of each domain. Moreover, a transition zone between crystalline and amorphous regions is detected as a portion of well-ordered chains which are characterized by partial order and restricted mobility of the chains segments as compared to the mobile-amorphous phase [16]. Therefore, two types of amorphous chains deserve to be distinguished, those which are interspherulitic amorphous domains (free amorphous regions), and those which are embedded within the spherulites or intraspherulitic amorphous domains (constrained amorphous regions) [17]. It is worth highlighting that the crystalline domains arrange themselves in stacks which form fibrils of the spherulites. The thickness in chain direction of these lamellar stacks is typically low, in the range of 10 nm, while the lateral lamellar extensions are in the micrometer range [3, 16]. Besides the phase structure of the polymer, also the molecular motions influence the mechanical properties [16]. Regarding structural evaluation, the solid-state NMR technique allowed obtaining local information on molecular dynamics (relaxation time) of the structure and phase composition quite suited for semicrystalline polymers evaluation [18]. The results showed a drop in the elastic modulus due to increase in the fraction of the constrained amorphous phase at the expense of the crystallinity.

Additionally, SAXS measurements allow establishing structural evolution of the polymer induced by stress relaxation. Structural studies employing SAXS usually assume a simple layer-like morphology [19], mainly due to their sensitivity to periodic structures. The semicrystalline polymers are usually characterized by the presence of a

structural periodicity of crystalline and amorphous phases with dimensions in the nanometer range, which form lamellar stacks embedded in the fibrils within a spherulitic structure [17, 19]. These different phases can only be distinguished on the basis of their electron density and not their mobility. The SAXS patterns are mostly analyzed using the linear correlation function $\gamma(r)$ method which allows to describe the variation of the electron density along the height of a lamellar stack and to determine the structural parameters of the stacks, namely, long period, crystalline lamellae and amorphous layers thickness. In this work, it was observed the decrease of long period which was attributed to the decrease of amorphous layer thickness inside fibrils, as a result of the chains recoil. As for the crystalline layer thickness, it was observed the increase of crystalline lamellae thickness at higher temperatures of stress relaxation due to crystallization induced by temperature. Meanwhile, at lower temperature the crystalline layer thickness practically did not change.

The aim of the present study is to determine phase composition using NMR technique, structural parameters by SAXS methods, and to discuss the effect of stress relaxation on structural evolution in relation to mechanical properties. Thus, this approach is very promising for gaining a better understanding the effect of stress relaxation on morphology and mechanical properties of PVDF.

Chapter 2

Literature review

The study of structure-property relationships in semicrystalline polymers is one of the principal topics in polymer science [16, 20]. The first part of this review focus on the morphology in semicrystalline polymers, emphasizing spherulitic morphology. In the second part of this chapter, some important properties concerned with the mechanical behavior of semicrystalline polymers are discussed. Moreover, a detailed review on NMR and SAXS techniques is included in this chapter. Some basics on these subjects need to be discussed and can serve as background for the investigations presented in this work.

2.1. Semicrystalline polymers

Polymers like PVDF are a very important class of engineering materials, and among them, semicrystalline polymers are of particular interest. Semicrystalline polymers that crystallize often have a spherulitic morphology. For semicrystalline polymers, there are three basic levels of microstructures that are important [16, 20]: the 0.2 to 2 nm level (interactions between neighboring chain segments in both the crystalline phase and the amorphous phase), the 10 to 30 nm (thickness of the crystalline lamellae and of the amorphous layers between the crystalline lamellae), and the 0.5 to 100 μm level (dimension of larger scale structures such as spherulites). Thus, semicrystalline polymers with a spherulitic morphology are considered as microstructural and mechanical complex systems, in which all the three levels of structure influence the mechanical behavior (for example deformation process) [16, 20]. However, all the three levels are not always present, as for example semicrystalline polymers that have already experimented extensive drawing [16, 20].

The morphology of semicrystalline polymers has been extensively studied [20-24]. The variety of morphologies of crystalline polymers includes those crystallized from

either solution or the melt state, either with or without external flow, and those undergone a large extent of plastic deformation in the solid state. Some common morphology (Figure 1) of semicrystalline polymers are, for example, spherulites, which are the crystalline aggregates for semicrystalline polymers crystallized from the melt; row structure, which represents the morphology for semicrystalline polymers crystallized from the melt in conditions of extensional strain or flow; and microfibril morphology, which is typical for ultra-drawn semicrystalline polymers in the solid state [20, 25]. The crystalline structures of PVDF, studied in this work, involve spherulitic morphology; therefore it will be discussed in the next section of this chapter.

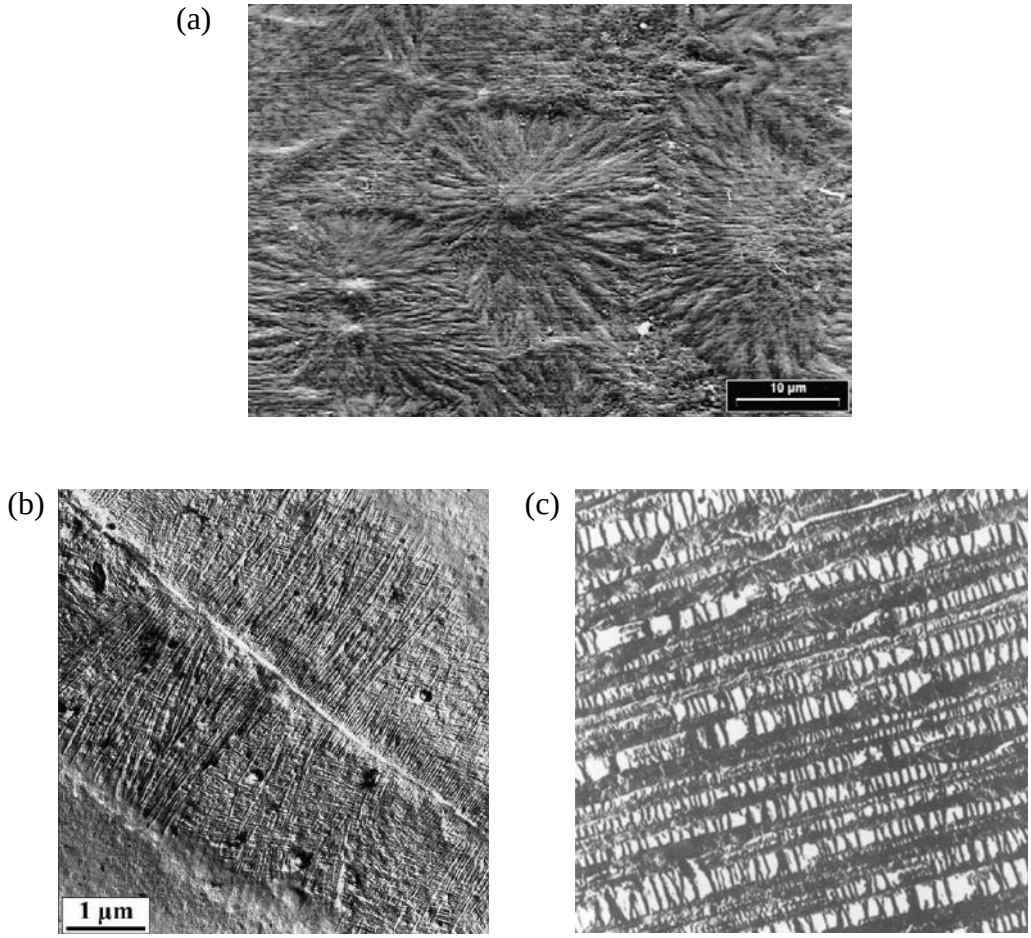

Figure 1. Electronic microscopy micrographs of morphology of semicrystalline polymers. (a) Spherulitic microstructure of compression-molded PVDF [25], (b) Row structure in isotactic polypropylene [26], (c) Microfibril structure of polyethylene sample drawn at 60 ºC to draw ratio of 13.5 [27].

Row morphology is a combination of two structures, fibril type crystals from the extended chains and chain-folding lamellae from the random chains [20]. For semicrystalline polymers, orientation can exist in both the crystalline phase and amorphous phase. Hence, there are two different ways towards this goal; stretching polymer chains in the melt or solution state first and then the subsequent crystallization, and drawing an initially unoriented crystalline polymer in the solid state to a large degree. Although a polymer chain cannot be extended fully due to chain overlaps or entanglements [20].

The original morphology of a spherulitic semicrystalline polymer in the solid state can be transformed into highly oriented microfibril morphology under sufficient uniaxial drawing [20]. The deformation processes of transformation from spherulitic into microfibril morphology are the following [20]. The stressed spherulitic lamellae shear into crystal blocks via chain tilt/slip within lamellae; then the blocks rotate such that the molecular chains align along the local principal stress direction; the crystal blocks decrease in width by chain slip and unfolding until microfibrils of alternating crystalline and amorphous regions are formed [20]. The lamellar stacks form many micronecks once the yield stress is reached, and each microneck is associated with the formation of a microfibril. The high alignment of chains in the microfibrils provide a high anisotropy of mechanical properties, a higher elastic modulus and tensile strength in the direction of drawing and a lower value perpendicular to it [27].

Crystal polymorphism is a frequent event for semicrystalline polymers. A good example for crystal polymorphism is PVDF which exhibits four crystalline forms: α, orthorhombic unit cell with a = 0.496 nm, b = 0.964 nm and c = 0.462 nm; β a orthorhombic unit cell with a = 0.858 nm, b = 0.491 nm, c = 0.256 nm; γ a monoclinic unit cell with a = 0.496 nm, b = 0.967 nm, c = 0.920 nm; δ which corresponds to the polar α-form [24, 28-30]. For the four crystalline phases, the α-form is the most encountered crystalline structure and it is obtained by crystallization from the polymer melt; the β-form structure can be obtained by cold drawing of the α-form film; the γ-form structure has been observed to occur in two coexisting crystalline phases (α and γ), by crystallization from the melt at temperatures above 155 °C and long crystallization times (~ 36 h); the δ-form can be obtained by applying an electric field (170 $MV.m^{-1}$) to the α phase [31]. The α- to β-phase transformation mechanism have been extensively investigated [8, 12, 24, 32-34], and it is associated to the microstructural change in which samples stretched lose the spherulitic structure to form a microfibrilar one [12]. It

have been reported for PVDF films that the α- to β-phase transition occurred at stretching at draw ratio (ratio of the initial and final lengths) of about 3 - 6 and at temperatures of 70 - 100 ºC. At temperatures between 70 - 80 ºC, mechanical deformation caused by drawing produces stresses sufficiently high to destroy the crystalline order. The percentage of β-phase increases with increasing the draw ratio. On the other hand, at temperature above 90 ºC the viscosity decreases and the consequent increase in chain mobility allows orientation of the crystals in the draw direction [34]. Hence, drawing above 90 ºC results in predominantly oriented α phase [34]. At least 300% strain is needed to convert all the α- to β-phase at a temperature below 100 °C [35]. At temperatures exceeding 120 ºC, the α-β transition took place only with draw ratio ≥ 6 [8, 32, 33]. The α-β transformation and chain orientation can be quantified by infrared spectroscopy. Sencadas *et al.* [12] stretched PVDF samples at 80 ºC with draw ratio of 1 (as used in this work) and microfibrilar structure was not observed and the β-phase fraction was 0%. To samples stretched at 80 ºC with draw ratio of 2 and 5 (Figure 2), the β-phase fraction found was 30 and 78% respectively. The β-phase of PVDF is characterized by an oriented microfibrilar structure. Additionally, Guo *et al.* [36] found that either α-β transformation or yielding in PVDF initiated at almost the same strain level, based on *in-situ* SAXS and WAXS (wide angle X-ray scattering) measurements.

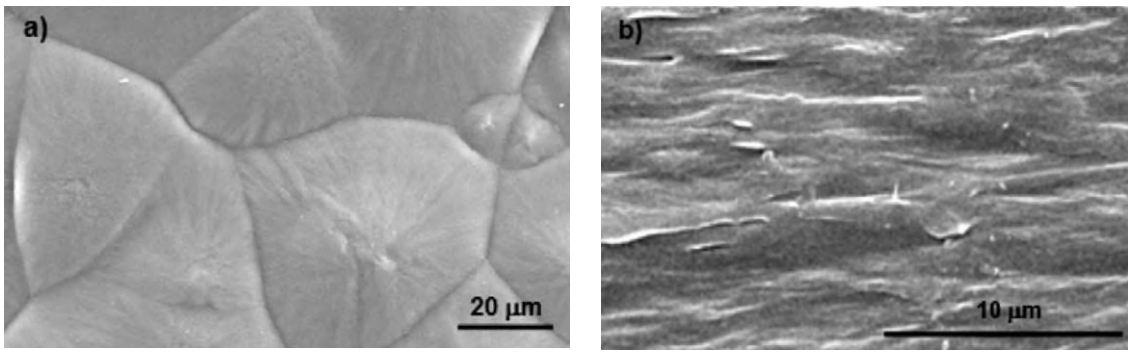

Figure 2. Scanning electric microscopy (SEM) images of PVDF. (a) Spherulitic structure of the α-phase, (b) Microfibrilar structure of β-phase (sample stretched at 80 ºC with draw ratio = 5) [12].

2.1.1. Spherulites

Spherulites are recognized as the most important morphology for melt-crystallized polymers. The diameter of the spherulites increases with increasing crystallization temperature, and it shows sizes between 0.5 to 100 μm [5, 20]. A spherulite often exhibits the characteristic Maltese cross pattern under inspection in the polarized optical microscope (as shown in Figure 3 a - b), and this characteristic can be explained by the birefringent nature of polymer chains [16, 20]. The Maltese cross pattern develops from the coincidence of the principle optical axis of the crystal with the direction of the polarizer and analyzer used in optical microscope [16, 20]. Figure 3 b - c presents polarized-light optical and electronic microscopy micrographs of spherulitic structure of PVDF extruded as pipes from 5 mm thickness, it reveals imperfect spherulites with a diameter between 2 and 5 μm [26].

A feature of spherulitic structure is the presence of fibrils sub-units, which grows radially outwards from the common central nucleus; see Figure 4 [37]. The fibrils consist of crystalline lamellae embedded in a matrix of amorphous material, and present dimensions just over 100 nm for the length and around 10 nm for the width [37]. The fibrils are a fundamental part of spherulitic structure; however the behavior of the spherulites do not depend solely of the properties of these fibrils, but also of the amorphous regions presents in the crystallized polymer [37].

The development of a spherulite can be described according the following steps: first, a chain-folding single lamella distributes by branching at its ends and grows into sheaflike multilayered lamellae. Then radial growth of the intermediate lamellar aggregate carries to a spherical and symmetric arrangement of fibrils (ribbon-like lamellae). The lamellae may branch by developing adjacent branches to meet the requirement of spacing filling, during the growth of the spherulite. Beside, the remaining chains may solidify by subsequent secondary crystallization, or remain amorphous material [16, 20].

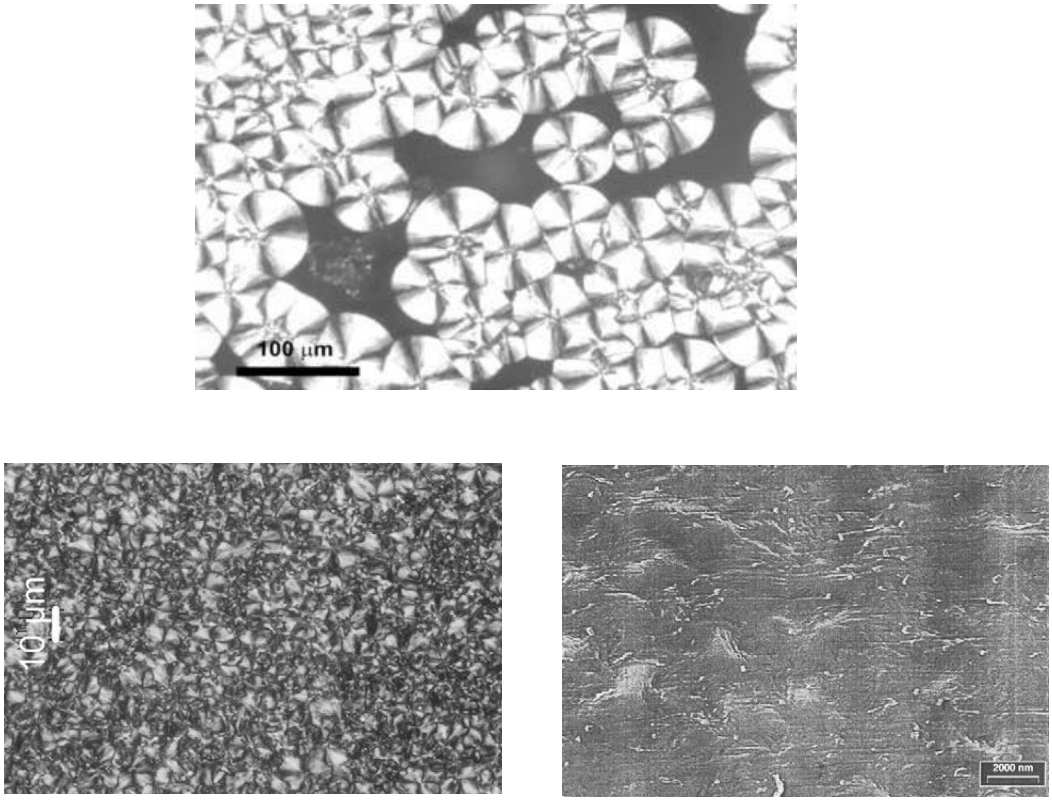

Figure 3. Spherulitic microstructure. (a) Polarized-light optical micrographs of PVDF samples crystallized at 150 ºC; (b) Polarized-light optical micrographs of extruded PVDF; (c) Scanning electronic microscopy micrographs of the spherulitic structure of extruded PVDF [5, 26].

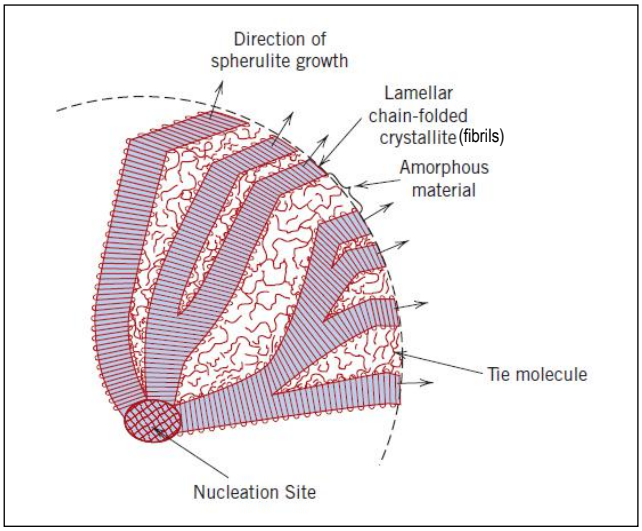

Figure 4. Schematic representation of the spherulitic structure. Adapted from [38].

2.2. Stress relaxation

From a mechanical point of view, stress relaxation is defined as the decrease of stress, which depends on time and temperature, in a solid due to the conversion of elastic into inelastic strain [39]. On the other hand, from a material point of view, stress relaxation occurs by slow slipping of the polymeric chains to each other, and by mechanical unwinding of the chains [40]. Furthermore, stress relaxation process can possibly take place due to break-up and restatement of secondary bonds between the chains. This process allows the material to spontaneously attain a low energy level if there is enough energy for the process to happen. Therefore, stress relaxation of polymers depends on temperature and time and is associated with the energy [40].

Investigations on stress relaxation behavior have been extensively carried on polymethyl methacrylate (PMMA) [41-43] and polypropylene (PP) [13, 44, 45]. In these studies, the stress relaxation was mechanically evaluated and modeled, however few information concerning the structural arrangement modification and its role on the tensile properties after stress relaxation has been established. Stachurski *et al.* [41] developed a micromechanism of stress relaxation for PMMA and showed that the movements of the polymeric main chains were responsible for stress relaxation. The polymeric chain segments will be twisted when the polymer is stretched. And the corresponding molecular rearrangement will result in stress relaxation of the chains. In addition, they proposed a theoretical model based on a rotation-translation process of the lateral groups, of the polymeric chains, partially responsible for the mechanical relaxations of PMMA. The physical manifestation of the rotation-translation process occurs as a result of the mechanical equilibrium disturbance. In stress relaxation, the phenomenon would be activated by the applied deformation. Andreassen [13] investigated the stress relaxation of PP fibers with different morphologies and determined that the stress relaxation behavior would be related to the effect of the molecular orientation or molecular weight parameters. Therefore, the relaxation rate was reduced by increasing molecular constraining and broadening the molecular weight distribution.

A variety of experimental techniques have been utilized to investigate the morphological changes during the deformation process of PVDF: optical microscopy (OM) [26, 32, 46], scanning electron microscopy (SEM) [23, 26], wide angle X-ray scattering (WAXS) [8, 21-24, 46-49], small angle X-ray scattering (SAXS) [21-24, 36,

47-49], Fourier transform infrared spectroscopy (FTIR) [21, 32], differential scanning calorimetry (DSC) [21-23, 32, 46, 49-50], dynamic mechanical analysis (DMA) [22-50], and stress-strain deformation [23, 26, 49, 51-52]. Nevertheless, structural evolution of PVDF after stress relaxation has not been found in the literature.

2.3. Mechanical properties

The complex structural of semicrystalline polymers hinders to form even general correlations for property predications; however, investigations about the molecular origins of a specific mechanical property are available [16, 20]. The stress-strain behavior is a function of temperature and strain rate because of the viscoelastic nature of the polymers [16, 20]. The elastic modulus, stress and strain at yield point, and stress and strain at break point are some important properties obtained from a tensile test. The elastic modulus and yield stress will be discussed in this section due to be the most studied properties for such investigations and the most important properties in the performance of engineering materials.

The elastic modulus depends on the low deformation elastic behavior of the materials [16, 20]. As a first approximation, the polymer can be considered as a composite of hard crystalline phase and soft amorphous phase stacked. Thus, it can be considered that the crystalline and amorphous phases are deformed in parallel, and therefore the elastic modulus is governed by the crystalline phase [16, 20]. The relationship between elastic modulus and crystallinity for semicrystalline polymer has been treated in the literature [53-55]. It has been shown that the higher crystallinity the higher should be the modulus. On the other hand, mechanical properties (elastic modulus) after stress relaxation were not found in the literature.

The other properties such as stress and strain at yield point, and stress and strain at break point are related to the plastic deformation behavior of the polymer. Other factors, namely molecular weight distribution, thermal annealing and orientation state of the crystalline phase, will also affect these properties; nevertheless, they will not be discussed in this work. The plastic deformation process for semicrystalline polymers can be described as the drawing process that transforms an isotropic spherulitic structure into a microfibril structure [16, 20]. The plastic deformation processes have been explained; the stressed spherulitic lamellae shear into crystal blocks by chain slip,

then the polymer chains align towards the local principal stress directions. During this step, the crystal blocks decrease in width by chain slip and/or lamellar break-up, until a microfibril structure is formed [16, 20]. Several investigations [21-24, 26, 36, 47-49] based on X-ray scattering and electron microscopy studies have been proposed to describe this process. This mechanism is supported by the observation that the long period detected from SAXS is a function of deformation and temperature and is independent of the initial lamellar thickness before drawing. Guo *et al.* [36] found for deformation of uniaxial stretched PVDF that the long period along tensile direction increases to a maximum and then drops into a lower value during the stage of plastic deformation. According to previous studies, the yield stress is correlated with the crystallinity; nevertheless, interpretation of such dependence has been concluded that the fundamental parameter is the crystalline lamellar thickness, and not the amount of crystalline phase [16, 20].

2.4. Nuclear magnetic resonance (NMR)

The macroscopic properties of semicrystalline polymers, such as tensile strength, rigidity, elasticity, etc., depend on molecular structure and dynamics of the chains as well [18, 56]. Nuclear magnetic resonance (NMR) spectroscopy measurements allow to detect spin interactions within and between molecules which provide local information on dynamics and structure of polymers [18, 56]. The structure of semicrystalline polymers usually consists of lamellae of highly ordered crystalline and disordered amorphous regions with high chain mobility. NMR spectroscopy is an appropriate method for the study of chain dynamics in crystalline and mobile-amorphous regions of semicrystalline polymers. Thus, the detection of crystallinity and domain sizes is possible due to differences in chain mobility between the individual regions [18, 56]. Overall, the dynamical processes in polymers include very fast segmental motions, slower cooperative motions of longer chain segments and motions of the whole chain [18, 56].

As already mentioned, the spherulitic structure is composed by fibrils which have crystalline lamellae arrange themselves in stacks. The transition zone between crystalline and mobile-amorphous, namely constrained amorphous phase, is

characterized by partial order and restricted chain mobility compared to mobile-amorphous region [18, 56].

The phase structure and dynamics in the material influence the mechanical properties. The morphology of the polymers is defined by parameters namely crystallinity or, in more general terms, the phase composition; the domain thicknesses and thickness distributions; and the extent and structure of the crystalline surface. The crystallinity represents the portion of crystalline material within a sample, and can be measured as mass fraction by DSC or NMR [18, 56]. The obtained values deviate according the experimental technique and the physical quantity used for the measurement. The crystalline lamellar and amorphous thickness inside fibrils can be determined from SAXS experiments. On the other hand, NMR spectroscopy is the most suitable method for the study of chain dynamics within crystalline and free and constrained amorphous phases [18, 56].

NMR theory is summarized in the next section to introduce to the application of ^{1}H time-domain NMR. In this work, NMR measurements permitted a distinction between crystalline, mobile-amorphous and intermediate region depending on the mobility of the polymer chains. And the mobility and composition of each phase were related to mechanical properties of PVDF after stress relaxation tests.

2.4.1. Nuclear spins and magnetization

NMR spectroscopy is based on the existence of the nuclear spin which is an intrinsic property of various atomic nuclei. The nucleus of the main isotope of hydrogen (^{1}H), contains a single proton and has a nuclear spin quantum number $I = 1/2$. A magnetic field can be generated by the circulation of electric currents, the magnetic moments of the electrons, and the magnetic moments of the atomic nuclei. The magnetic moments of electrons and nuclei are complex concepts. These fundamental particles both possess intrinsic magnetism i.e. they have a permanent magnetism (Figure 5), which is not due to a circulating current; as well they have spin angular momentum [18, 56-58].

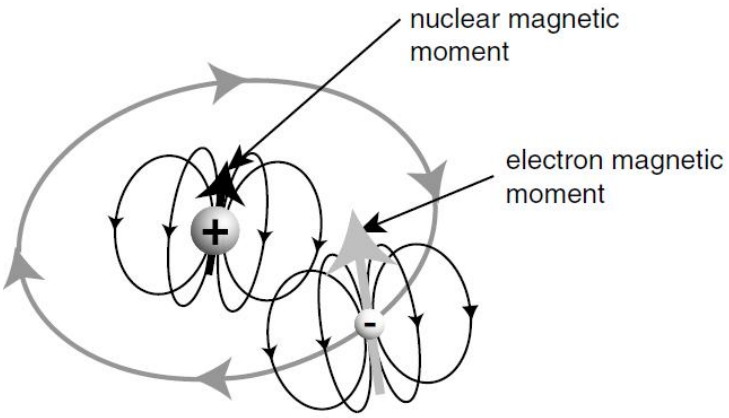

Figure 5. Electron and proton spin magnetism in a hydrogen atom [57].

As an additional contribution to ^{1}H behavior, if an electric current through the coil is turned on and off, it generates a magnetic field (B_1). In the majority of materials, the circulating electric currents exist on a molecular distance scale and are confined to the atoms or molecules [57]. For a hydrogen atom, the electron (in a *p*-orbital) circulates around the proton, building a small current loop that creates a magnetic field (Figure 6) [57].

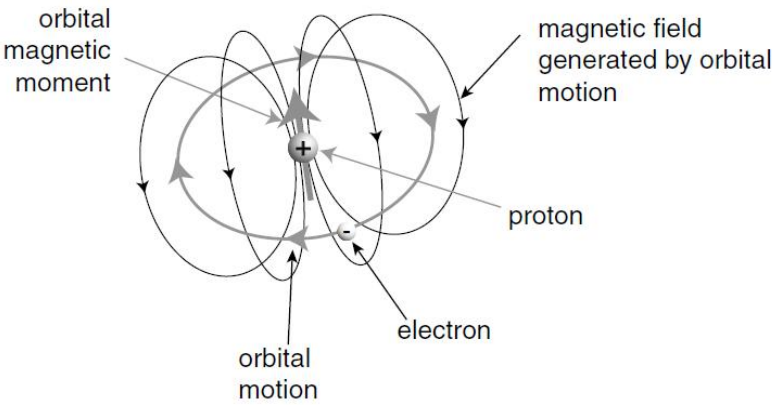

Figure 6. Orbital magnetism of the electron in a hydrogen atom [57].

Spin and magnetism are closely associated; thus, the nuclear spin (I) and the magnetic moment (μ) are proportional to each other and related as follows [18, 56, 57]:

$$\mu = \gamma \, . \, I \qquad (1)$$

where γ is the gyromagnetic ratio. The spin responds to the magnetic field causing a net magnetization vector which rotates around the direction of the applied magnetic field B_1. The rotation angle is described as $\theta = 2\pi.\gamma.\tau.B_1$; where τ is the time of duration of the magnetic field. The vectorial sum of the magnetization vectors, of all the spin groups which undergo the same magnetic field, is called net magnetization vector M [58, 59]. At equilibrium state, the net magnetization vector is leaded in the direction of the applied magnetic field (at equilibrium) B_o and is labelled the equilibrium magnetization (M_o) (Figure 7). The magnetic field and net magnetization vector at equilibrium are along the z axis according convention of NMR coordinate system, hence the component of magnetization is $M_z = M_o$. However, there are no components of magnetization transverse (M_x or M_y) [59]. A $\pi/2$ pulse of B_1 applied along x axis means that the magnetization vector rotates by 90° to the y axis (Figure 8) [59].

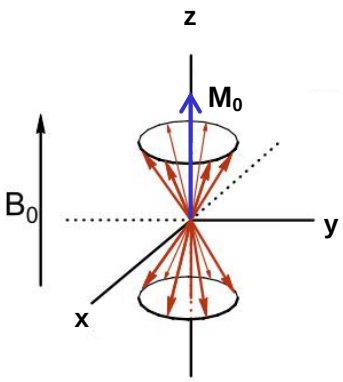

Figure 7. Net magnetization vector [59].

In NMR spectroscopy, a spin-echo is an effect of quantum mechanics in which the magnetization of a sample (or magnetic moment) is partially recovered after being lost. The spin-echo requires the application of a magnetic field during specific times (pulses)

and involves the refocusing of magnetization which is extremely sensitive to the translational motion of spins [60]. The spin-echo sequences are pulse sequences applied to a sample to produce a specific form of NMR signal or free induction decay (FID) [57, 59]. The detected FID signal is obtained as a voltage in the time domain. Then, Fourier transformation of the time-domain signal results in the frequency-domain spectrum (Figure 9) [61].

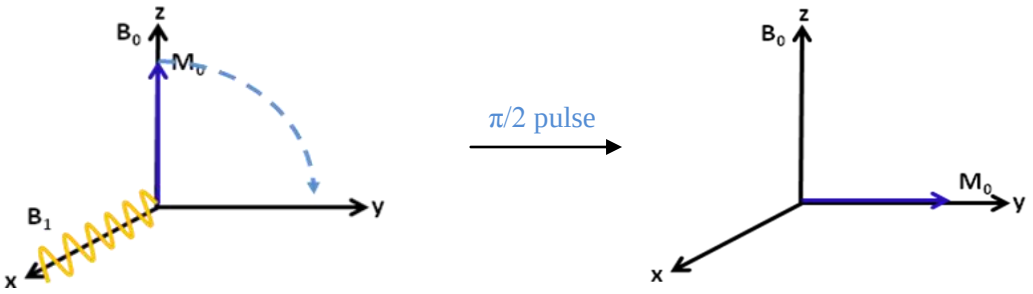

Figure 8. Pulsed magnetic field B_1 in x axis [59].

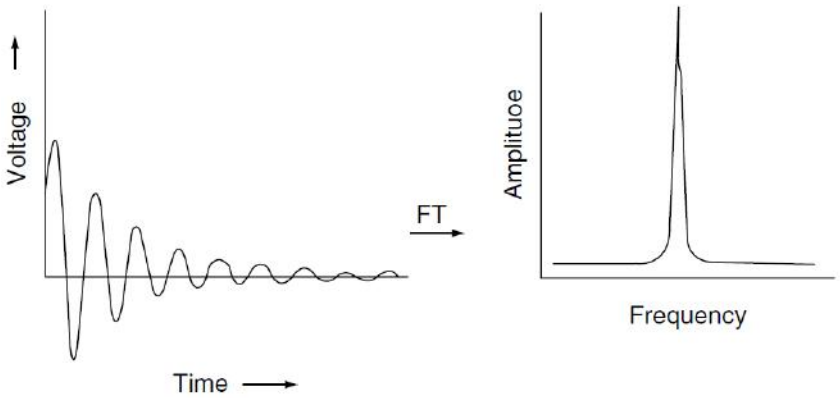

Figure 9. Fourier transformation (FT) of the time-domain FID [61].

2.4.2. Spin-lattice and transverse relaxation

The thermal equilibrium is first established in the absence of a magnetic field. Then when a magnetic field is applied, the system relaxes to the new equilibrium state [57]. The thermal equilibrium of the spins is disturbed during applying of field which excites the spins. After that, the relaxation processes will occur to return the system to equilibrium. The term relaxation is extensively used in the physical sciences to indicate the re-establishment of thermal equilibrium after some perturbation is applied [57]. There are two process of relaxation, namely, longitudinal and transversal relaxation [62]. The longitudinal relaxation is the process whereby the component of magnetization M_z returns to its equilibrium value (M_o) in the direction of B_o. The exponential time constant which characterizes this process is known as the spin-lattice relaxation time or the longitudinal relaxation time (T_1). The time-dependence of the longitudinal relaxation is described as follows [62]:

$$M_z = M_o \left[1 - \exp\left(-t / T_1\right)\right] \qquad (2)$$

The relaxation time T_1 depends on the nuclear isotope and the sample, including parameters such as temperature and viscosity; and the value of T_1 is in the range of milliseconds to seconds [57].

Additional, NMR spectroscopy can be measure the magnetization perpendicular to the field as well, which is called transverse magnetization [57]. The state immediately after the pulse corresponds to a net polarization along the y axis, perpendicular to the main field [57]. Then the nuclear magnetization rotates in the xy plane at Larmor frequency ($\omega = -\gamma.B_0 / 2\pi$), perpendicular to the main magnetic field. After rotation, the net magnetization begins to dephase due to that each spins experiences a slightly different magnetic field and rotates at its Larmor frequency. The constant time which describes the return to equilibrium of the transverse magnetization M_{xy} is labelled spin-spin relaxation time or transversal relaxation time (T_2) [57, 62].

$$M_{xy} = M_{xy_o} . \exp\left(-t / T_2\right) \qquad (3)$$

The transversal relaxation is usually faster than the longitudinal, therefore $T_2 \leq T_1$. The transversal relaxation times depend on rotational reorientation and translational displacement of nuclear spins, which are related to the structure of the sample [62]. Two factors contribute to the decay of transverse magnetization: molecular interactions due to fluctuating microscopic magnetic fields (lead to pure T_2 molecular effect), and inhomogeneities due to the variation of the macroscopic magnetic field B_o over the volume of the sample, due to instrumental imperfections (lead to inhomogeneous T_2 effect). The relation between the T_2 from molecular processes and from inhomogeneities in the magnetic field is given by the time constant T_2*.

$$\frac{1}{T_2^*} = \frac{1}{T_2} + \frac{1}{T_{2\,\text{inhomog}}} \qquad (4)$$

The combined time constant T_2* is linked to the width of the resonance lines ($\Delta\upsilon$) of the high resolution spectra. The molecular motions result in a narrowing of the resonance lines of the high resolution spectra ($\Delta\upsilon \; \alpha \; 1 / T_2^*$) [63].

The more relevant spin interactions for ^{1}H solid state NMR are the chemical shielding interaction (indirect magnetic interaction between the external magnetic filed and the nuclear spins) and the dipolo-dipolo coupling of nuclear spins. The dipolar coupling depends on the distance (r) between the nuclei and the angle (ϑ) of spin-spin interaction vector (with respect to the magnetic field B_0), as shown in Figure 10 [18, 56]. NMR experiments can measured phase composition based on diferences in dipolar coupling strength between the phases in the polymer. Furthermore, NMR is suited to study chain mobility in polymers. In semicrystalline polymers, the polymer chains of the crystalline phase are packed regularly and densely; in consequence proton distances are slightly smaller than in amorphous phases [18, 56]. The protons within the crystalline region are subject to strong dipolar coupling leading faster decaying FID signal, broad ^{1}H NMR spectrum, and short T_2 relaxation time. In contrast, the amorphous regions show fast mobility resulting in partial dipolar coupling (reduced coupling strength), narrow spectrum, and slow signal decay with long T_2 [18, 56]. The signal of crystalline and amorphous domains can be differentiated by the widhts of their spectral line [18, 56]. Besides the time-domain NMR signals are decomposed and fitted with different methods to determine, for example, phase fractions. The dipolar couplings on the NMR signal is sensitive to segmental mobility in polymer; thus, it is

very suitable to study the phase composition and chain mobility of each domain in the polymer [18, 56]. In this study, inversion-recovery and the Magic Sandwich Echo methods were applied to these investigations and will be discussed in the next sections.

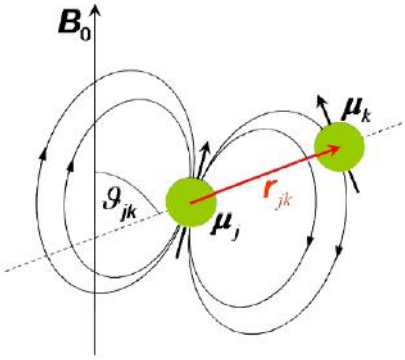

Figure 10. Dipolar coupling between magnetic dipole moments [56].

2.4.3. Inversion-recovery (IR) method

The usual technique to measure the longitudinal relaxation time T_1 of the spins is called inversion-recovery [57]. This pulse sequence method consists of two pulses separated by an interval τ (as shown in Figure 11). The pulse sequence is repeated with different values of τ, and the results compiled in a two-dimensional data matrix. The first pulse in the sequence is a 180º pulse which generates an inverted spin population distribution. The spins relax back towards thermal equilibrium state during the interval τ, and their progress is monitored by the second pulse (90º) which induces an NMR signal [57]. The NMR signal is a function of the interval τ and the time t after the last pulse and reflects the history of the longitudinal relaxation [57].

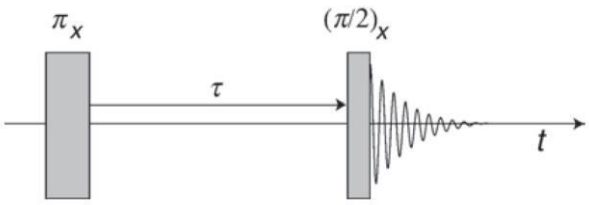

Figure 11. Inversion-recovery pulse sequence [57].

2.4.4. The magic sandwich echo (MSE) method

The magic sandich echo pulse sequence consists of a 90° pulse followed by a delay τ and a sequence of duration 4τ so-called sandwich part comprising two 90° pulses of the same pulse phase with two pulse blocks (consisting of four 90° pulses each), as shown in Figure 12 [18, 56]. The pulses within each block display the same phase, and the phases of the second block are inverted. The echo signal is generated after another delay τ [18, 56]. MSE sequence is explained as a time reversal of the effects of dipolar couplings on the spin system, that is, the system at t = 6τ is in a state where the dipolar couplings were leaving to zero [18, 56].

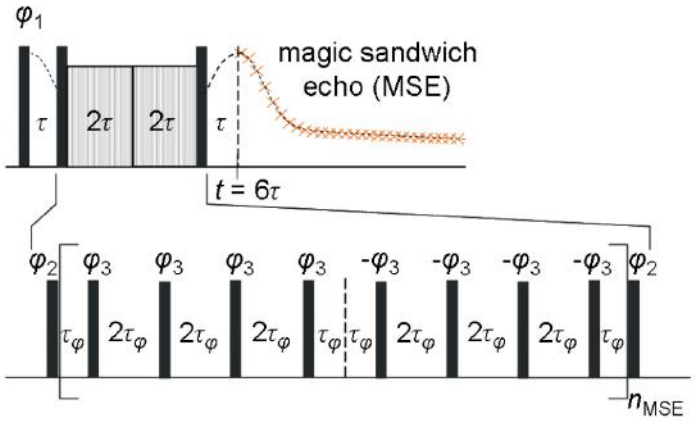

Figure 12. Magic sandwich echo pulse sequence [57].

The MSE signal exhibits the typical features of the time-domain curves for semicrystalline polymers; hence it can be decomposed into three signal contributions and fitted using a weighted sum of three functions [18, 56]:

$$f(t) = g_c.e^{-0.5(at)^2}\frac{\sin bt}{bt} + g_i.e^{-(t/T_{2i}^*)^{\nu_i}} + g_a.e^{(t/T_{2a}^*)^{\nu_a}} \quad (5)$$

where g_c, g_i and g_a are weighting factors; and a ($a = 1 / T_{2c}^*$), b, T_{2i}^*, T_{2a}^*, ν_i and ν_a are the shape parameters of the polymer phases [18, 56]. The first component corresponds to the crystalline (rigid) phase with low chain mobility and fast signal decay due to the strong dipolar coupling [18, 56, 64]. The second component of the MSE signal is assigned to a rigid-amorphous intermediate region which could be considered as part of signal of the amorphous phase. The signal contribution of intermediate region shows a decay time constant between rigid-crystalline and mobile-amorphous state in terms of dynamics, hence it is subject to intermediate dipolar coupling strengths [18, 56]. An exponential function is used to fit the intermediate and amorphous components [64]. The shape of the ^{1}H MSE signal is governed by the interaction of numerous proton spins [18, 56]. The MSE signal fitted according to Equation 5 permits to determine sample mass fractions and molecular dynamics (relaxation times T_2^*) of each phase in the polymer [18, 56]. It is worthy to note that the intensities of the NMR signals provide information about phase composition only if these polymer phases exhibit differences in NMR interactions, namely, dipolar coupling strength, relaxation times and chemical shift [18, 56].

Different MSE NMR investigations of polymers, such as polyethylene, poly(ε-caprolactone), polystyrene-polybutadiene block copolymers, blends of polycaprolactone and poly(3-hydroxybutyrate), are found in the literature [18, 56, 65-68]. Litvinov *et al.* [68] studied the molecular mobility and phase composition of ultrahigh molecular weight polyethylene fibers (fibrillar morphology), at the final stages of drawing, by MSE NMR method. The results indicated increase of rigid fraction at the expense of intermediate fraction, with increasing drawing. Nonetheless, the mobile fraction did not change with draw ratio. In adition, they found that the T_2^* of the amorphous region increased (from 500 to 1500 μs) upon drawing at high draw ratios. This increase in

chain mobility was attribuited to some local disorder and voiding (presence of nanovoids) [68].

On the other hand, Roos *et al.* [19] studied the dynamic of the intermediate region of poly(ε-caprolactone), semicrystalline polymer, using proton MSE NMR and NMR spin diffusion method. They found that a part of the mobile phase must be in direct contact with the rigid phase. Thus, they proposed an island-like distribution of the intermediate region or its placement within the rigid (crystalline) phase; concluing that a significant direct contact of the intermediate phase with the crystalline. And it excluded an arrangement of uniform gradation from rigid to semirigid to mobile material. Thus, the phases in the polymer are distinguished on the basis of their different mobility without relying on periodic structures [19].

2.5. Small angle X-ray scattering (SAXS)

Small-angle X-ray scattering (SAXS) is a well-established technique for the structural investigation in semicrystalline polymers, as it allows to characterize the morphological information (1 - 100 nm) of the material [16, 20, 69]. SAXS investigates relatively large-scale structures compared to wide-angle X-ray diffraction (WAXD) that deals principally with the atomic structure of crystals [70]. SAXS includes the diffraction of large lattice spacing, of the order of tens, hundreds, or even thousands of interatomic distances [70]. Moreover, whereas WAXD is described by the fundamental relation named the Bragg equation, $n\lambda = 2d \sin\theta$ (where 2θ is the scattering angle, λ is the X-ray wavelength; and d is the lattice spacing), the scattering of semicrystalline or amorphous materials is often explained in terms of electron density (in reciprocal or Fourier space) [70].

The information of SAXS measurements can often be extracted after some complex data analysis which implies the use of the correlation function $\gamma(r)$ and the interface distribution function g(r) [69]. The calculation of these functions involves knowledge of Porod's law parameters at high scattering angles. And besides the interpretation of these functions it requires the assumption of a morphological model (finite lamellar stacks model) used to calculate morphological variables such as long period (L_p), lamellar thickness (L_c) and amorphous layer thickness (L_a) [69]. The assumed model implies that the crystalline lamellae are isotropic stacks of plates with an infinitely extended lateral

dimension [16, 20]. Lamellar thickness for a specific polymer arises from its chemistry and crystallization kinetics and is related to the thermal and mechanical properties [16, 20]. Accordingly, it is of interest to be able to determine the lamellar thickness [16, 20].

In this study, the morphological variables were determined by the calculation of the correlation function $\gamma(r)$ from SAXS data. This calculation was made possible by using a lamellar model, since this analysis is suitable for crystalline polymers. The correlation function $\gamma(r)$ revealed the morphological parameters such as long period, lamellar thicknesses of both constituting phases and interface thickness. Therefore, the evaluation of morphological parameters allowed to study structural modification after stress relaxation, which is extensively related to the properties of the material.

The next sections consist of an introduction of the basics of SAXS and data analysis which primarily have been used for the investigations presented here.

2.5.1. Basics of SAXS

SAXS is based on the scattering of X-rays on optical inhomogeneities of the sample with the size of the order of several tens of nanometers [71]. X-ray small angle scattering is observed only if there are electron density inhomogeneities in the sample [72]. This implies that in order to establish contrast in SAXS, the particles must have an electron density different than that of the surrounding matrix material [73]. SAXS is a technique to study structural features of nanometers size [72]. It is worth pointing that with scattering techniques the whole illuminated sample volume is investigated; therefore, average values of the structure parameters are obtained by SAXS. The average is taken over all objects and over all orientations of the objects [73].

Scattering process is defined by a reciprocity law which gives an inverse relation between particle sizes and scattering angle [72]. The scattered waves are coherent which means that the scattering amplitudes can be added, and the intensity is the given by the square of the resulting amplitude [72]. The amplitudes differ by their phase φ which depends on the position of the electron in the space and is $2\pi/\lambda$ times the difference between the optical path and a reference point [72]. The path difference of a point P and the origin, defined as vector r, is $-\vec{r}\,(\vec{S} - \overrightarrow{S_0})$; being unit vector $\overrightarrow{S_0}$ the direction of the incident beam, and $\vec{S}$ of the scattered beam, as illustrated in Figure 13 [72]. The phase

is $\varphi = -(2\pi/\lambda)\vec{r}\,(\vec{S} - \vec{S_0})$. At small angles, the scattering is assumed to be purely elastic (i.e. incoherent scattering can be neglected), thus the phase can be written as [74]:

$$\varphi = -\vec{q} \cdot \vec{r} \qquad (6)$$

being $\vec{q}$ the scattering vector, $\vec{q} = (4\pi / \lambda)\sin\theta$, where 2θ is the scattering angle [72].

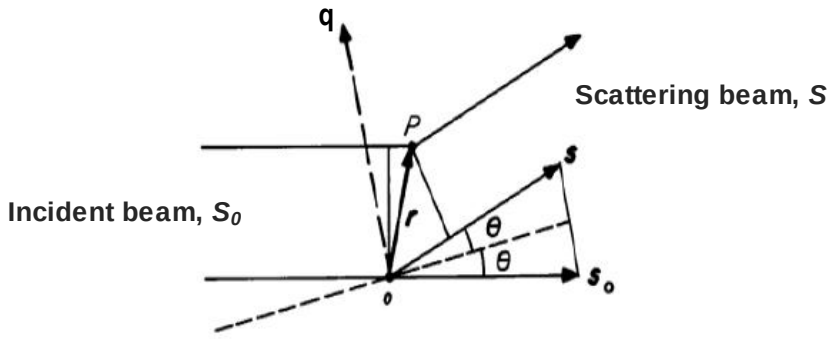

Figure 13. Scattering by two points centers [72].

The resulting amplitude, A(q), is given by summing up of all the waves scattered by every portion of the material [72, 74]. However, considering the huge amount of electrons and that a single electron cannot be identified, thus the summation can be substituted by integration over the whole volume irradiated by the incident beam [72]:

$$A(\vec{q}) = \int_V dV\, \rho(\vec{r})\, e^{-i\vec{q}\vec{r}} \qquad (7)$$

where $\rho(r)$ is the electron density at r, V is the entire volume irradiated by the X-ray beam [74]. The intensity I(q) observed is proportional to the absolute square of the amplitude, derivate from the conjugated complex ($I(q) = A(q).A^*(q) = |A(q)|^2$), and defined as [74]:

$$I(\vec{q}) = \int\int \rho(\vec{r}_1)\rho(\vec{r}_2)\, e^{-i\vec{q}(\vec{r}_1 - \vec{r}_2)}\, dV_1 dV_2 \qquad (8)$$

The scattering intensity depends on the relative movement of scattering centers and on variations in the density of these centers [74]. Considering that only two electron densities provide the structural contrast; then the mean density is subtracted, and a correlation function is define by [74]:

$$\gamma(\vec{r}) = \overline{(\Delta\rho)^2} V \int dV \left(\rho(\vec{r}_2)\rho(\vec{r}_2 - \vec{r}) - \bar{\rho}^2 \right) e^{-i\vec{q}\vec{r}} \qquad (9)$$

where $\vec{r} = \left(\vec{r}_2 - \vec{r}_1\right)$, $\bar{\rho}^2$ is the square of the average electron density, V is the total volume irradiated by the X-ray beam, and $\overline{(\Delta\rho)^2}$ is the mean square electron density contrast. Thus, the fundamental scattering equation is written as [74]:

$$I(\vec{q}) = \overline{(\Delta\rho)^2} V \int dV \, \gamma(\vec{r}) \, e^{-i\vec{q}\vec{r}} \qquad (10)$$

The scattering intensity is registered as a function of scattering angle in the region of small angles, for scattering vector of $0 < q < 0.2$ [71]. The analysis of scattering intensity allows obtaining information on the mean particle size (or inhomogeneity regions) in the sample as well as estimating the shape and distribution of particles [71]. Semicrystalline polymers show electron density contrast within the correlation length covered by this technique (1 - 100 nm), and their structure can be described by assuming the electron density variations occur in one coordinate direction [72]. The interpretation of scattering intensity from polymers requires an elaborate treatment to be presented in the next section.

2.5.2. SAXS analysis

In the SAXS analysis, semicrystalline polymers can be considered as condensed systems of structural periodicity composed of two types of regions of different electron density, namely, crystalline lamellae and amorphous layers, with a diffuse transition layer between them [75]. The alternating crystalline and amorphous layers form stacks which can be distinguished inside spherulites of the polymer. The structure of stacks consists of layers (not ideally parallel) which may be curved or undulated and with

orientation in space changing continuously [75]. For SAXS analysis, the scattering from layered structures can be described using a model in which the layers are perfectly parallel to one another and have infinite size, this is due to the lateral dimensions of stacks are higher than the X-rays wavelength. Therefore, the scattered intensity is established by the electron density variations taking place in only one direction (perpendicularly to the layers) [75]. The distribution of electron density along the height of a lamellar stack can be described by the one dimensional electron density correlation function [17]. Thus, the linear correlation function γ(r) represents the probability of finding fluctuation of electron density at the point r in relation with the fluctuation at the origin [17]. The procedures for determining the structural parameters of semicrystalline polymers based on the analysis of the linear correlation function has been reported in the literature [17, 69, 76, 77], and will be explained in detail below.

The scattering SAXS intensity, I(q), measured from an isotropic three-dimensional object can be transformed to the one-dimensional intensity, $I_1(q)$, by Lorentz correction as follows [17, 69]:

$$I_1(q) = cI(q)q^2 \qquad (11)$$

where c is a proportionality constant. Figure 14 shows SAXS intensities and Lorentz-corrected SAXS profiles for PVDF samples.

The linear correlation γ(r) function is defined by [17, 69]:

$$\gamma(r) = \frac{1}{Q}\left[\int_0^{+\infty} q^2 I_1(q)\cos(qr)dq\right] \qquad (12)$$

where Q is the invariant defined as follows [69]:

$$Q = \int_0^{+\infty} I_1(q)dq = \int_0^{+\infty} I(q)q^2 dq \qquad (13)$$

In the case of highly oriented system (high module fiber or film), Equation 12 can be applied directly with I(q) without Lorentz correction, since intensity I(q) along the

meridional direction is similar to the one-dimensional integrated intensity profile, $I_l(q)$ [69].

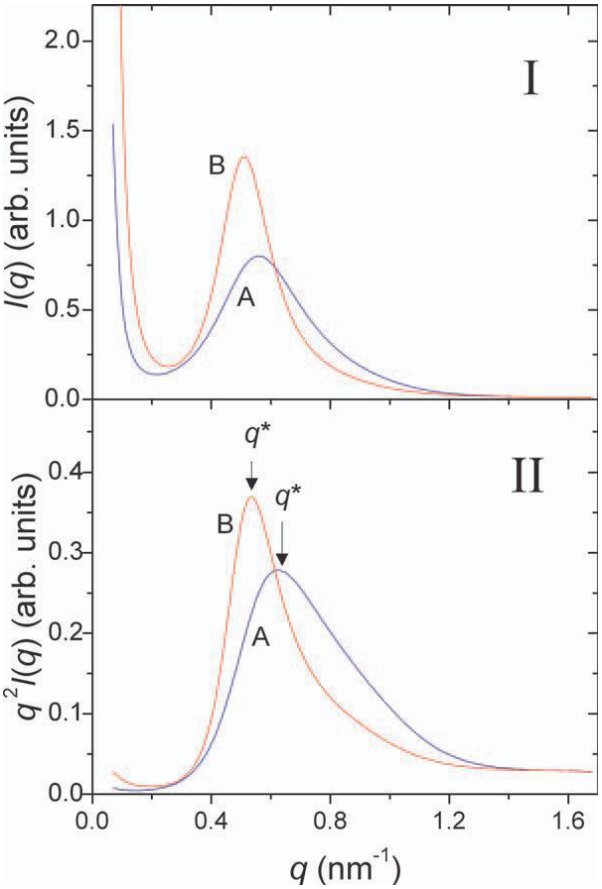

Figure 14. (I) SAXS intensities for (A) PVDF and (B) PVDF stretched at 130 ºC with draw ratio = 4. **(II)** The Lorentz correction for obtaining the one-dimensional intensity $I_1(q) = I(q)\, q^2$ [21].

For the above equations, all integrations must be carried out in the range: $0 \leq q \leq \infty$. However, this is not viable experimentally due to the both limits are beyond the resolution of any detector [69]. Thus, the total integration can be divided into three parts, considering that the limits for the detector are q_l and q_2. Then, the invariant Q can be obtained by [69]:

$$Q = \int_0^{q_1} I(q)q^2dq + \int_{q_1}^{q_P} I(q)q^2dq + \int_{q_P}^{\infty} I(q)q^2dq \qquad (14)$$

The first component of the integral is the area of a triangle with base q_l and height $I(q_1)q_1^2$; the second component is the integral of the experimental data; and the third component can be determined by Porod's law, where q_p is the starting value of the Porod region ($q_p < q_2$) [69]. The Porod's law is applied at high q and for sharp phase boundaries ($q > 1/T$, T: minimum thickness of the phases) [21]. When the phases show variations in the electron densities in a molecular level, then the Porod's law would present positive deviations [21]. The scattering intensity in the Porod region is defined by:

$$\lim_{q\to\infty} I(q) = K_P / q^4 \qquad (15)$$

where K_p is the Porod constant. Then, Equation 13 can be written as [69]:

$$Q = \frac{1}{2} I(q_1) q_1^3 + \int_{q_1}^{q_P} I(q) q^2 dq + \frac{K_p}{q} \qquad (16)$$

The typical measured scattering intensity I(q) includes the contributions from 'background' scattering, $I_b(q)$ and the finite interface between the two phases. Thus, the Porod's law can be written as [17, 69]:

$$\lim_{q\to\infty} I(q) = I_b + \frac{K_P}{q^4} \exp(-\sigma_{ln}^2 q^2) \qquad (17)$$

where I_b is a constant background scattering due to electron density fluctuations within the phases and σ_{ln} is related to the width of the interface [69, 76]. These parameters are estimated using a first plotted in a $I(q)q^4$ versus q^4 diagram; thus, as a first approximation, I_b can be considered as a constant and extracted from the slope of the straight line [17, 69]. Then the data is plotted in a $Ln[(I(q) - I_b)q^4]$ versus q^2 diagram. The values of K_p and σ_{ln} are obtained from intercept and slope, respectively [17]. An example of these plots for PVDF samples are shown in Figure 15.

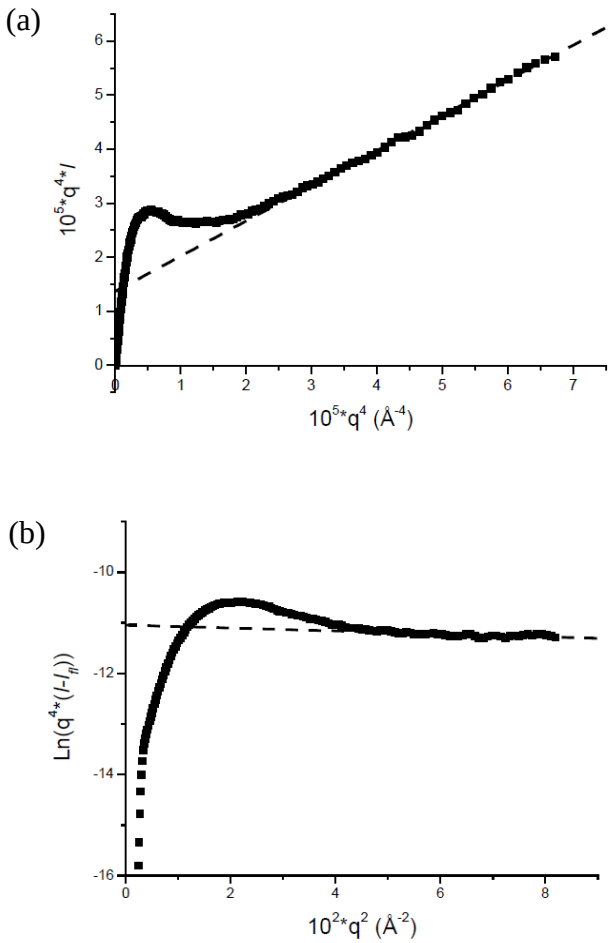

Figure 15. (a) Porod plots of $I(q)q^4$ versus q^4 for PVDF samples. (b) Plots, after the background subtraction, of $Ln[q^4(I(q) - I_b)]$ versus q^2 [21].

The limits for the Porod region are estimated, and it is considered that the Porod region is identical for all scattering profiles [69]. After that, the corresponding linear correlation function γ(r) is determined using Equation 7 (by an inverse Fourier transform of the intensity distribution). The γ(r) function allows the determination of several important parameters of stacks, such as long period, the thicknesses of crystalline lamellae and amorphous layers, thickness of the transition layer (interface), local (or linear) crystallinity and volume crystallinity. The analysis of the linear correlation function γ(r) by the two-phase model (or finite lamellar stacks model) is suitable for most semicrystalline polymers and has been demonstrated in detail previously [17, 69, 76, 77]. This model is represented by an isotropic arrangement of randomly oriented stacks which are composed of crystalline lamellar and amorphous

layers (Figure 16) [75]. Stacks are characterized by the long period which is composed of the average values of crystalline lamellar thickness and amorphous layer thickness; and these thicknesses statistically fluctuate independently of one another [75].

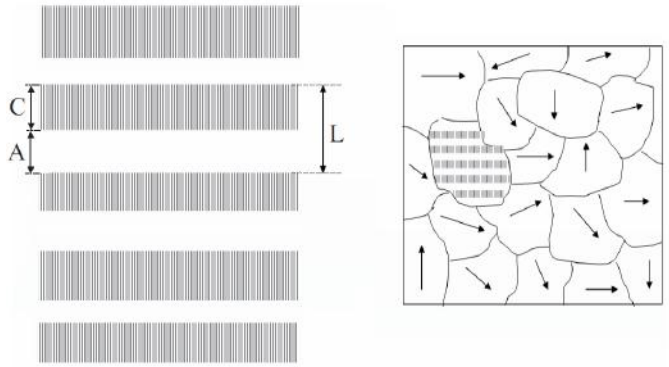

Figure 16. (a) Scheme of a stack and (b) a model of polymer structure assumed in the SAXS method (C: crystalline lamellar thickness, A: amorphous layer thickness, and L: long period; the arrows indicate random orientation of stacks in the polymer volume) [75].

The morphological parameters of the lamellar stacks are determined from the γ(r) function, according procedures reported in the literature [17, 69, 76-80]. The long period (L_p) can be determined from the position of the first maximum in the γ(r) function (Figure 17) [77]. And this parameter represents the most probable distance between the centers of gravity between two adjacent crystalline lamellar [77]. The long period minimum or L_{pmin} is calculated as twice the first minimum value of the γ(r) function, and is the most probable distance between the centers of gravity of a crystalline lamellar and its adjacent amorphous region [77]. In the case of a one-dimensional ideal lattice, both (L_p and L_{pmin}) values coincide [77]. In an ideal case, the thicknesses of crystalline lamellae and amorphous layers are constant and the borders between the phases are sharp [75]. Nevertheless, in the case of real stacks, the thicknesses of crystalline lamellae and amorphous layers, and consequently the long period, show a certain distribution; and the boundaries between the phases are not sharp [75]. Therefore, for a not ideal lattice, the position of the L_p and L_{pmin} in the γ(r) function may be slightly displaced [77].

The average crystalline thickness L_c is given by the intersection of the straight line ($d\gamma(r)/dr$) with the tangent at the first $\gamma(r)$ minimum which belongs to a self correlation triangle [17]. The average amorphous layer thickness L_a is deduced by $L_a = L_{pmin} - L_c$ [17]. In addition, the average interface thickness (IT) can be calculated by: $IT = L_c^2/L_{pmin}$ [17]. Another important parameter is the degree of crystallinity within the lamellar stacks called linear (or local) crystallinity, $\chi\,\% = L_c/L_{pmin}$ [17]. On the other hand, the volume crystallinity is determined as $X\,\% = A/(A + \gamma_{max})$, where $A = -\gamma_{min}$ (defined in Figure 17) [17]. Finally, the non-ideality parameter, $NI = \left[(L_p - L_{pmin})/L_p\right]^2$, defined as the deviation from a ideal two-phase model [17].

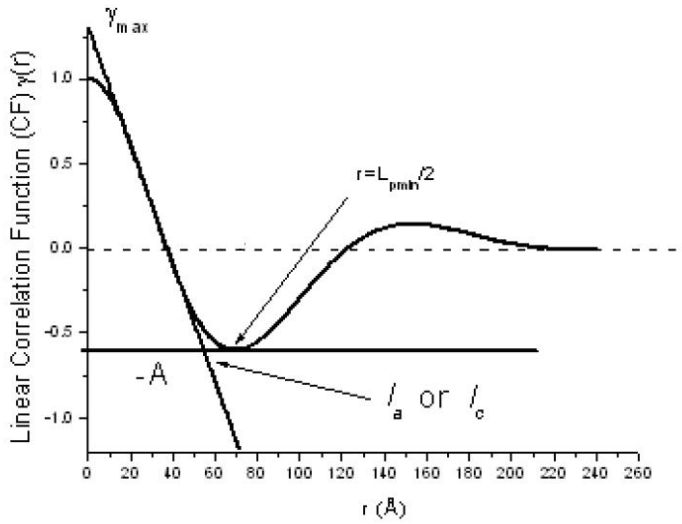

Figure 17. Linear correlation function γ (r) for PVDF sample and its general properties for a lamellar two-phase system [17].

It is worth pointing that the structural parameters can be calculated from different methods, such as conventional analysis by Bragg's law, linear correlation function and interface distribution function. The long period values obtained by these different methods are different; however, their trends are usually similar [69]. The different long periods denotes the heterogeneity of the lamellar distributions in the morphology [69]. Long period can also be obtained by Bragg's law (Bragg long period $L_B = 2\pi/q_{max}$),

where q_{max} is the position of the maximum of the scattering. However, the method based on the analysis of the linear correlation function and interface distribution function permits a more elaborate evaluation [76, 77].

Structural study of semicrystalline polymer from SAXS method has been presented previously [17, 21-23, 46-48, 76, 81, 82]. Chinaglia *et al.* [21] studied the nanostructural modifications of PVDF samples after the stretching process (at 130 ºC with draw ratio of 4) using SAXS technique. Those stretching conditions were used because they practically do not cause α-β transformation, and only oriented α-phase predominates. The linear correlation function γ(r) method was used to determine the morphological parameters, and the results showed that the growth of the crystalline layer thickness induced by the stretching process occurs at expense of the interface and amorphous layer thickness [21]. Guo *et al.* [36] investigated the structural evolution of PVDF during tensile deformation at 60, 140 and 160 ºC, by *in-situ* SAXS technique. The analysis of the obtained scattering results indicated that the initial lamellar structure along tensile direction of PVDF can be destroyed and oriented with elongation, resulting in yielding. And the deformation induced lamellar modifications under stretching after yielding lead to α-β transformation. Moreover, the long period, along tensile direction, showed an increase-decrease variation which was related to the extension of lamellae by stretching and orientation of lamellar fragments [36]. Liu *et al.* [46] presented an *in-situ* SAXS investigation of the deformation process of PVDF/poly(butylene succinate) blends. The results showed crystalline transition from α to β-PVDF during deformation (at around 100% strain). And the final microstructure of the blends contained PVDF microfibrils with poly(butylene succinate) chains distributed in the inter-fibrillar region [46].

Chapter 3

Experimental part

The PVDF used is of a typical commercial grade, with properties quite similar to those grades applied to pressure sheaths of flexible pipes. The experimental proposal herein is to submit the PVDF to a stress relaxation, a condition imposed to flexible pipes during fabrication, storage and operation for the oil and gas offshore industry. The test conditions imposed will be bounded by API 17B.

Stress relaxation involves inelastic deformation of a complex structure, acting on chain segments, crystalline lamellae and amorphous layers between adjacent lamellae, within spherulites in the polymer.

In order to investigate the structure-property relationships due to stress relaxation of the polymer, specific characterization techniques were employed. Mechanical properties were determined by tensile tests and dynamic mechanical analysis (DMA); crystallinity was characterized by differential scanning calorimetry (DSC); information on chain dynamics and structure by solid-state nuclear magnetic resonance (NMR); and crystalline lamellae thickness, amorphous layers thickness, and long period by small angle X-ray scattering (SAXS).

3.1. Material

The PVDF studied was commercial homopolymer within 3 to 5% plasticizer. This grade of PVDF has a density of 1.62 $g.cm^{-3}$ and melt flow index of 3 $g.10^{-1}$ min^{-1} (at 230 °C and 10 kg), approximately.

This material was supplied as extruded pipes with 6 m length, 110 mm external diameter and wall thickness of 5 mm. The samples were machined from the PVDF pipe, longitudinally, per ASTM D 638 [83] Type I specimens, having 13 mm width and 3.2

mm thickness in the gage length, and overall length of 165 mm, as shown in Appendix I.

3.2. Stress relaxation

The stress relaxation (in tension) tests were performed in a Zwick/Roell machine (Kappa Multistation model) with a 5 kN load cell. These tests were conducted at three different temperatures (23, 80 and 120 ºC) and, for each temperature, three different strains (3.5, 7 and 10%). Each test was performed with a crosshead speed of 5 $mm.min^{-1}$ until the sample reached the target strain, at the given temperature, and then kept for 24 h. The strain was measured by a video extensometer. The maximum temperature was limited a little bit below the maximum temperature specified for PVDF application (130 ºC). The strains imposed were selected in accordance with API 17B standard (Recommended Practice for Flexible Pipes) [84], being the strain of 10% an extreme condition. For tests at higher temperatures (80 and 120 ºC), the samples were stabilized during 2 h (ASTM D 618 [85] – Conditioning Plastics for Testing). Three samples were tested for each condition, and the results were very homogeneous.

3.3. Characterization

Characterization study was carried out for samples after the stress relaxation tests and also for as processed PVDF. To evaluate the mechanical properties, tensile tests and DMA experiments were performed. Crystallization behavior was verified by DSC technique. The structural changes induced by stress relaxation were investigated by NMR and SAXS.

3.3.1. Tensile tests

Uniaxial tensile tests (triplicate) were performed on a universal testing machine Instron (model 5567) at room temperature (23 ºC) with crosshead speed of 5 $mm.min^{-1}$.

The elastic modulus (E) was calculated from the slope of the initial part of the engineering stress-strain curve, in strain range between 0.05 - 0.5%.

3.3.2. Dynamic mechanical analysis (DMA)

Samples (duplicates) with dimensions of 60 x 10 x 3.2 mm were carefully cut directly from the useful area of PVDF specimens. DMA tests in three-point-bending were conducted using a Netzsch DMA 242C instrument, under nitrogen atmosphere. In these tests, dynamic load and amplitude were 4 N and 50 μm, respectively. Temperature was increased from -80 to 120 °C at a heating rate of 2 °C.min^{-1}, and at a frequency of 1 Hz. The dynamic mechanical parameters of storage modulus (E') and loss factor (Tan δ) were analyzed from DMA curves at 1 Hz frequency.

3.3.3. Differential scanning calorimetry (DSC)

Crystallinity was studied via DSC in Netzsch DSC 204 F1 Phoenix calorimeter. Two heating and cooling cycles were applied in a temperature range from 27 to 200 ºC. Samples (duplicates) of about 6 mg were heated from 27 to 200 ºC at a heating rate of 10 ºC.min^{-1} under nitrogen atmosphere and held at 200 ºC for 5 min. Afterward, the sample was cooled to 27 ºC at a cooling rate of 10 ºC.min^{-1}. The melting temperature (T_m), melting enthalpy (ΔH_m) and crystallization temperature (T_c) were obtained from the DSC analysis. The crystallinity degree (X_c) was calculated considering that the melting enthalpy for 100% crystalline PVDF was 104.7 J/g (ΔH_0) [23], in accordance with the following equation [7, 10]:

$$X_c = \frac{\Delta H_m}{\Delta H_0} \times 100\% \qquad (18)$$

where ΔH_m is the melting enthalpy of the samples obtained in this study.

3.3.4. Solid-state nuclear magnetic resonance (NMR)

The NMR measurements were carried out at IMA / UFRJ using a MARAN Ultra spectrometer with an electromagnetic field of 0.54 T (23.4 MHz for ^{1}H) and probe diameter of 18 mm. Samples with dimensions of 13 x 13 x 3.2 mm were tested at 28 ± 2 ºC. Two techniques were used to analyze the samples: the inversion-recovery (IR) and the free induction decay refocused through magic sandwich echo (MSE-FID) pulse sequence.

- Inversion recovery (IR) consisted of a conventional spin echo sequence preceded by a 180º inverting pulse. This technique is sensitive to mobility in domains of the order of 13 nm and allows to determine the longitudinal relaxation times ($T_{1,n}H$). IR pulse sequence was used to assess domains on a larger dimensional scale than MSE-FID technique. The data obtained were adjusted according to the following function:

$$M_z(t) = \sum_n M_n \left[1 - 2.\exp\left(\frac{-t}{T_{1,n}H} \right) \right] + k \qquad (19)$$

where M is the initial magnetization of the n-th group of protons, n is the number of domains (n = 2), and k is offset from the equipment or baseline of the relaxation signal [65]. Two different domains with relaxation times $T_{1,1}H$ and $T_{1,2}H$ were found. The domain with the lowest longitudinal relaxation time ($T_{1,1}H$) refers to the population of hydrogen with greater mobility, while $T_{1,2}H$ is the longitudinal relaxation time of the rigid domain. The fraction of each domain indicates the size of the domain, i.e. the percentage of hydrogen that formed each region. The mean square distance of the process of diffusion of the magnetization (L) between the mobile and rigid domains was determined according to the following equation:

$$L = \sqrt{2n'Dt} \qquad (20)$$

where n' is a factor related to the geometry of the rigid domain (n' = 1 for lamellar system, e.g. nanoparticles; n' = 2 for cylinders in a matrix, e.g. fibers, clays; and n' = 3 for spheres or cubes in a matrix, e.g. polymers); in this work n' = 3 was considered [65]. D is the diffusion coefficient of the magnetization, D ~ 0.5 $nm^2.ms^{-1}$ characteristic of

semicrystalline polymers [65]. t is the $T_{1,n}H$ ponderal relaxation time ($t = \sum_n f_n.T_{1,n}H$, where f_n is the fraction of each domain) [65].

- The MSE-FID technique is sensitive to segmental mobility, and allows to determine percentage fraction of the rigid, intermediate and mobile region, and the transversal relaxation time (T_2^*) of each region. The MSE-FID experiment consisted of a pulse 90º followed by a period of evolution τ_{MSE} [65, 67]. The excitation pulse 90º was calibrated to $\tau p\ 90 = 7.5$ μs of duration. The central part of this sequence was formed by a symmetrical standard of 8 pulses 90º spaced at $t\varphi = 6$ μs. After this step, other pulse 90º was applied and the same time of evolution from the beginning of the sequence before the acquisition of the signal (FID) was waited. The formation of a stimulated echo occurred after τ_{MSE} ($2\tau p90 + 3t\varphi = 33$ μs), which contains information regarding the crystalline and amorphous regions in each sample [65]. The signal obtained was normalized and fitted according to the equation [64, 65, 86]:

$$A(t) = f_{rigid}.\exp\left[-\frac{1}{2}\left(\frac{t}{T^*_{2,rigid}}\right)^2\right]\left(\frac{\sin(2\pi\nu t)}{2\pi\nu t}\right) + f_{inter}.\exp\left[-\left(\frac{t}{T^*_{2,inter}}\right)^{\beta_i}\right] + f_{mobile}.\exp\left[-\left(\frac{t}{T^*_{2,mobile}}\right)^{\beta_a}\right] + k \quad (21)$$

where f_{rigid}, f_{inter} and f_{mobile} (%) are amplitudes or fractions of rigid, intermediate (non-rigid segments confined between rigid domain) and mobile regions, respectively. T_2^* is the transversal relaxation time of each of these regions, ν is the sinusoidal oscillation constant of the rigid component based on the second and fourth moments of Van Vleck [64, 65]. β_i and β_a are shape parameters, in which β_i varies from 1 to 2 and β_a from a value close to zero to 1. k is the offset or baseline of the relaxation signal that compensates for the influence of noise during non-linear adjustment [64, 65]. The signal fitted is composed of three different regions; the first is related to the ^1H nuclei of high rigidity and obeys an Abragamian function, whereas the second is governed by ^1H of intermediate mobility and is fitted by a Gaussian function, and finally, the third is related to ^1H of higher mobility with higher T_2^* values exhibited a decay of exponential

behavior [64, 65, 86]. Thus, the percentage fraction of each domain can be calculated according to the following function:

$$\text{Fraction} = \frac{f}{f_{rigid} + f_{inter} + f_{mobile}} \times 100 \qquad (22)$$

$f = f_{rigid}$, f_{inter} or f_{mobile}.

3.3.5. Small angle X-ray scattering (SAXS)

SAXS measurements were carried out at the Institute of Physics – USP, São Paulo using a NanoSTAR SAXS system (Bruker AXS) coupled to Cu Kα radiation source Xenocs (Genix 3D Cu ULD) and to a Bruker Vantech 2000 detector. The measurements were carried out at room temperature, and samples of 10 x 10 x 1 mm were used. The wavelength of the X-ray radiation was 0.154 nm. The sample-to-detector distance was 66.7 cm, generating scattering vectors q ($q = 4\pi\sin\theta / \lambda$, where 2θ is the scattering angle and λ is the wavelength) in the effective range from 0.01 to 0.36 $Å^{-1}$ (2θ: 0 to 4.9º). Each SAXS pattern was collected within 30 min. SAXS intensities were corrected and normalized by subtracting parasitic scattering (empty holder) and background (vitreous carbon scattering). The data processing was performed by the SUPERSAXS software developed by Prof. Cristiano L. P. Oliveira from the Institute of Physics, USP.

In order to analyzed the SAXS data, two independent procedures were used to determine the structural parameters of the studied polymer. The first was based on Bragg's law; and the second, the analysis by the linear correlation γ(r) function.

- The data were treated using the OriginPro8.0 software. The scattering SAXS intensity I(q) and the Lorentz-corrected SAXS profiles $I(q)q^2$ were plotted as a function of the wave scattering vector q. The Bragg long period (L_B) was obtained from Bragg's law [17, 21] as:

$$L_B = \frac{2\pi}{q_{max}} \qquad (23)$$

where q_{max} is the position of the first maximum Bragg peak of the Lorentz-corrected SAXS profiles. The transformation $I_1(q) = I(q)q^2$ is known as Lorentz-correction. In addition, the average domain size can be calculated according the equation:

$$\text{Average domain size} = \frac{4\pi}{\Delta l} \qquad (24)$$

where Δl is the full width at half maximum of the peak of the Lorentz-corrected SAXS profiles.

- The linear correlation function $\gamma(r)$ procedures involved calculating the function $\gamma(r)$ by the cosine transformation of the Lorentz-corrected SAXS intensity distribution, according to the equation [17, 76, 78, 80]:

$$\gamma(r) = \frac{\int_0^{\infty} I(q)q^2\cos(qr)dq}{\int_0^{\infty} q^2 I(q)dq} = \frac{1}{Q}\int_0^{+\infty} q^2 I_1(q)\cos(qr)dq \qquad (25)$$

where r is the direction perpendicular to the lamellae surfaces, Q is the so-called second moment or invariant which represents the electron density difference between the two amorphous and crystalline phases.

Prior to the determination of the linear correlation $\gamma(r)$ function, the experimental curves were extrapolated to high q values by applying Porod's law (curves shown in Appendix II) [17, 21] given by:

$$\lim_{q\to\infty} I(q) = I_b(q) + \frac{A_p}{q^4}\exp(-\sigma_{In}{}^2 q^2) \qquad (26)$$

where A_p is the Porod constant, I_b is a constant background scattering due to electron-density fluctuations within the phases, and σ_{In} is a parameter characterizing the thickness of the transition layer. To calculate the linear correlation function $\gamma(r)$, the SAXS intensities were exported to Wolfram Mathematica 11.2 program, then the function $\gamma(r)$ was calculated by Equation (25).

The data were analyzed in terms of a one-dimensional stack model, the semicrystalline polymer is considered as a system of stacks of lamellar crystals separated by amorphous layers [17, 21, 76, 78, 80]. The lamellar structure parameters such as long period (L_p), crystalline lamellar thickness (L_c) and amorphous thickness (L_a) can be determined from the function $\gamma(r)$ and calculated according to the following procedure:

- The long period (L_p): L_p corresponds to the r value of the first maximum of the $\gamma(r)$ outside the self-correlation triangle.

- The minimum long period (L_{pmin}): L_{pmin} corresponds to the double of the r value that belongs to the first $\gamma(r)$ minimum in ideal lamellar structure.

- The average crystalline thickness (L_c): L_c is obtained by the intersection of straight line $d\gamma(r)/dr$ with the baseline at γ_{min}, the baseline is defined as the horizontal tangent at the first minimum of the $\gamma(r)$, which belongs to the self-correlation triangle.

- The average amorphous thickness (L_a): L_a is estimated by subtracting average crystalline thickness by minimum long period.

$$L_a = L_{pmin} - L_c \qquad (27)$$

- The average interface thickness (IT): IT (between crystalline and amorphous phases) is obtained by relation of the average crystalline thickness and minimum long period.

$$IT = \frac{L_c^2}{L_{pmin}} \qquad (28)$$

- The non-ideality (NI), or deviation from the ideal two phase model, was obtained by the equation:

$$NI = \left(\frac{L_p - L_{pmin}}{L_p} \right)^2 \quad (29)$$

- The linear crystallinity (χ) was obtained by the relation:

$$\chi\,(\%) = \frac{L_c}{L_{pmin}} \quad (30)$$

3.4. Statistical analysis

In order to an adequate understanding of the results of this work, statistical treatment was performed. The Statistica 10 software was used for this purpose and the results are showed in Appendix III.

Chapter 4

Results and discussion

This chapter presents the stress relaxation results and the studies of the relationships between properties and morphology of PVDF. It includes the studies on tensile properties, the dynamic mechanical analysis and differential scanning calorimetry and structural modifications detected by solid-state NMR and SAXS as a result of the effect of stress relaxation.

4.1. Stress relaxation behavior

Figure 18 shows the stress relaxation curves representative of each test condition, namely, 23, 80 and 120 ºC and, for each temperature, 3.5, 7 and 10% strain. If complementary information is needed, the strain versus time and stress versus strain are presented in Appendix II.

It can clearly be seen that the stress relaxation curves (Figure 18) at 23 and 80 ºC were mainly straight lines parallel to each other after 200 s, independent of the strain applied. For the tests conducted at 120 ºC, a short period of linearity was reached after 1000 s for 7 and 10% strain and no-linearity was observed for 3.5% strain; furthermore, after 20000 s there was a stress recovery process for all strain imposed, which is opposite to the stress relaxation expected. The results of testes at 120 ºC will be addressed later on.

The stress relaxation behavior at 23 and 80 ºC is typically reported in the literature, where the macroscopic behavior is explained by the viscosity reduction due to temperature increase and, therefore, lower motion resistance that facilitates chain slippage [40]. Looking at the molecular scale, the chains are mechanical unwinding, rotating [40] and aligning as they are stretched, higher strain leading to higher alignment [43]. Furthermore, these movements could lead to phase transformation or change in crystallinity fraction, an intrinsic structure modification [23, 55].

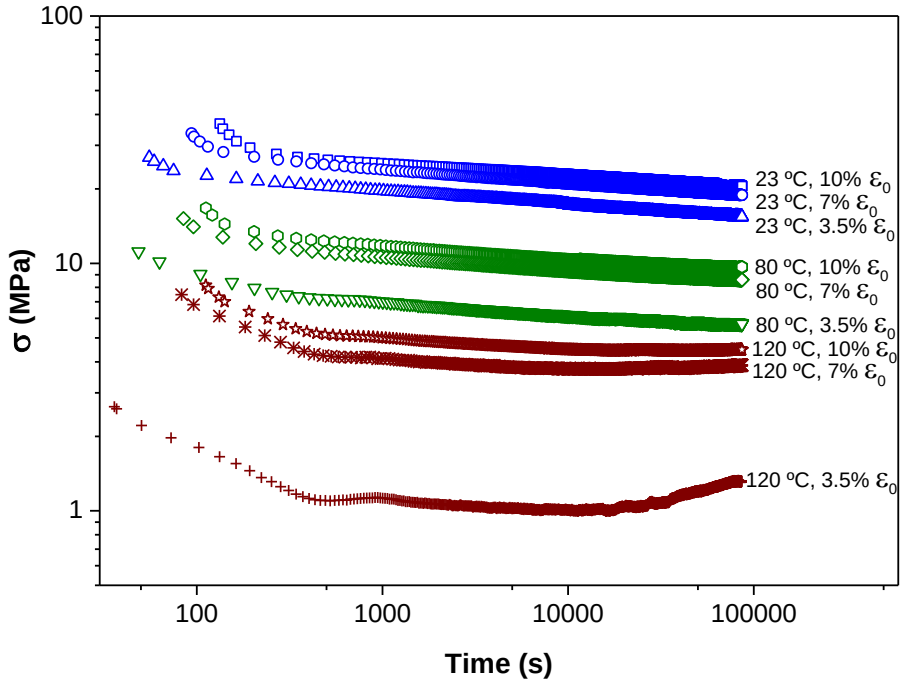

Figure 18. Stress relaxation curves at different temperatures and strains. ε0: strain of the stress relaxation test.

4.2. Tensile behavior after stress relaxation

The tensile mechanical properties were characterized before and after stress relaxation, all test conducted at 23 ºC. The representative stress-strain curves of as processed PVDF and relaxed samples are shown Figure 19 - 21. The properties of elastic modulus (E), yield stress (σ_y) and strain (ε_y), and breaking strain (ε_b) were determined from these curves and they are listed in Table 1 (Table 1 shows the average values).

It can be noted that the elastic modulus decreased significantly after stress relaxation at all conditions, as shown in Figure 22. PVDF as processed presents an elastic modulus of 1292 MPa. The elastic modulus of samples relaxed at 23 and 80 ºC (at all three strains) decreased to 951 - 797 MPa which representing a reduction between 30 - 40%. Besides, the samples relaxed at 120 °C presented lower values of elastic modulus (762 - 724 MPa), a reduction around 45%. Figure 23 and 24 shows values of yield stress and strain of as processed PVDF and relaxed samples. Yield stress (σ_y) of as processed

PVDF was around 38 MPa. That practically did not change for samples relaxed at 80 ºC. For samples stressed at 23 and 120 ºC, the σ_y values slightly decreased to 35 MPa, which was not a significant change. On the other hand, yield strain of as processed PVDF was 15%, which practically did not change for samples relaxed at 23 and 80 ºC. For stress relaxation at 120 ºC it was observed the increase in ε_y values for 19%. As for the elongation at break, there was a large dispersion of these values for all samples (as shown in stress-strain curves in Appendix II). However, the average values of elongation at break indicating decrease of this property for relaxed samples at all conditions.

- The elastic modulus will be the focus of the following discussion, since it is the most studied property for this investigation. This property is directly related to the crystallinity and crystalline lamellar thickness in the polymer. Moreover, the relative changes in the values of the modulus with changes in structure (crystallinity and crystalline lamellae thickness) and molecular constitution are significant. Previous investigations [53, 54] assessed the dependence of elastic modulus on the crystallinity level which indicated a continuous decrease in the modulus with lower crystallinity fraction. Furthermore, in reference to structural parameters, the crystalline lamellae thickness for a polymeric chain is related to the rigidity (elastic modulus). A variance of rigidity will give a variation of crystalline lamellae thickness. However, the crystalline lamellae thickness cannot be only a function of the rigidity; it is also dependent on the molecular weight and temperature [53]. The behavior of elastic modulus was explained and related to the structural evolution detected by NMR (crystalline, constrained amorphous and amorphous region fractions) and SAXS (crystalline lamellae and amorphous layer thickness, and long period) measurements, and it will be presented later.

- The elongation at break of a sample depends only on entanglement density in the interlamellar amorphous region; and it does not depend on crystallinity level, crystalline thickness, or other elements of structure that describe the semicrystalline state [54]. Since the entanglements are constrained between the crystalline lamellae and they can act as cross-links. A decrease of elongation at break will be attributed to decrease in entanglement density which depends on the molecular weight. The entanglement density (molecular weight) of this material was not determined nor identified by manufacturer, which prevented further discussion on this matter.

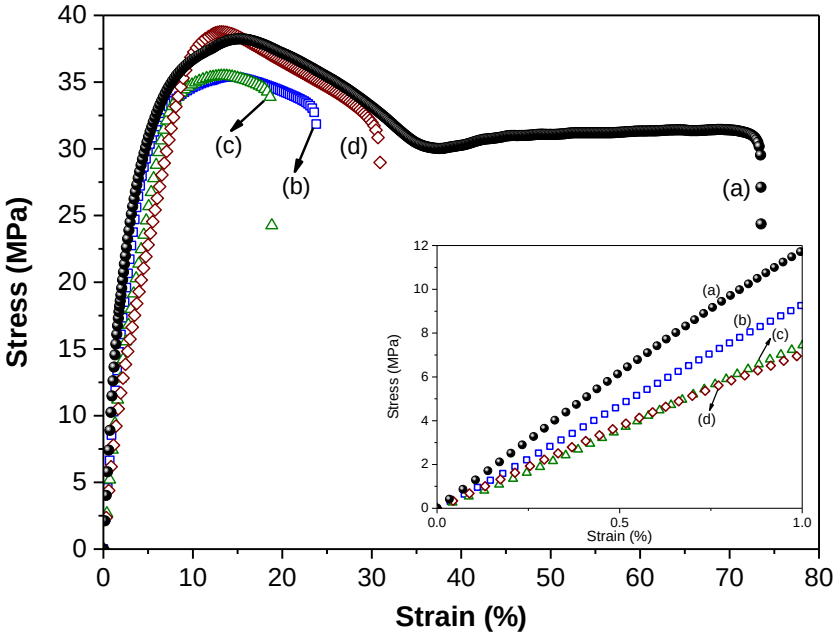

Figure 19. Representative strain-stress curves of PVDF as processed and samples relaxed at 23 ºC, tested at 23 ºC. (a) PVDF as processed; (b) PVDF relaxed at 23 ºC, 3.5% ε_0; (c) PVDF relaxed at 23 ºC, 7% ε_0 and (d) PVDF relaxed at 23 ºC, 10% ε_0.

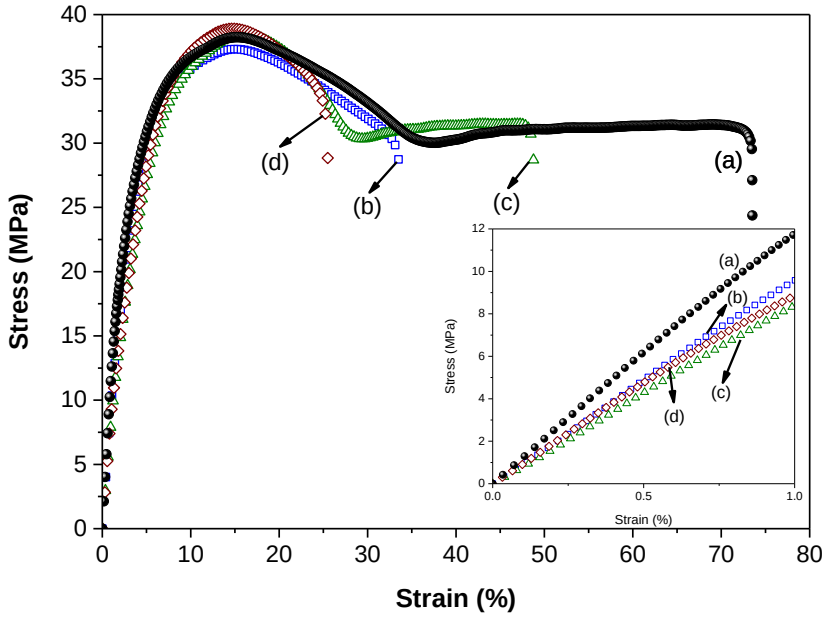

Figure 20. Representative strain-stress curves of PVDF as processed and samples relaxed at 80 ºC, tested at 23 ºC. (a) PVDF as processed; (b) PVDF relaxed at 80 ºC, 3.5% ε_0; (c) PVDF relaxed at 80 ºC, 7% ε_0 and (d) PVDF relaxed at 80 ºC, 10% ε_0.

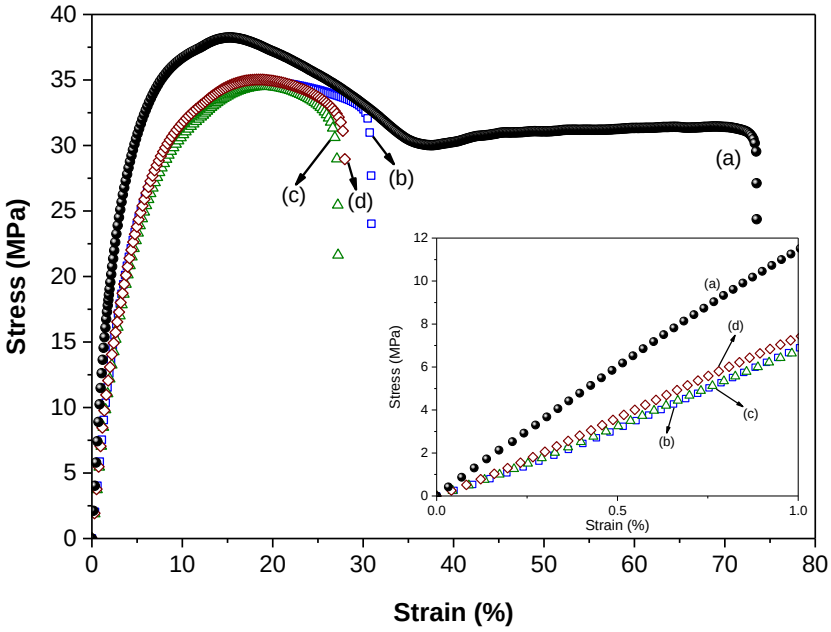

Figure 21. Representative strain-stress curves of PVDF as processed and samples relaxed at 120 ºC, tested at 23 ºC. (a) PVDF as processed; (b) PVDF relaxed at 120 ºC, 3.5% ε_0; (c) PVDF relaxed at 120 ºC, 7% ε_0 and (d) PVDF relaxed at 120 ºC, 10% ε_0.

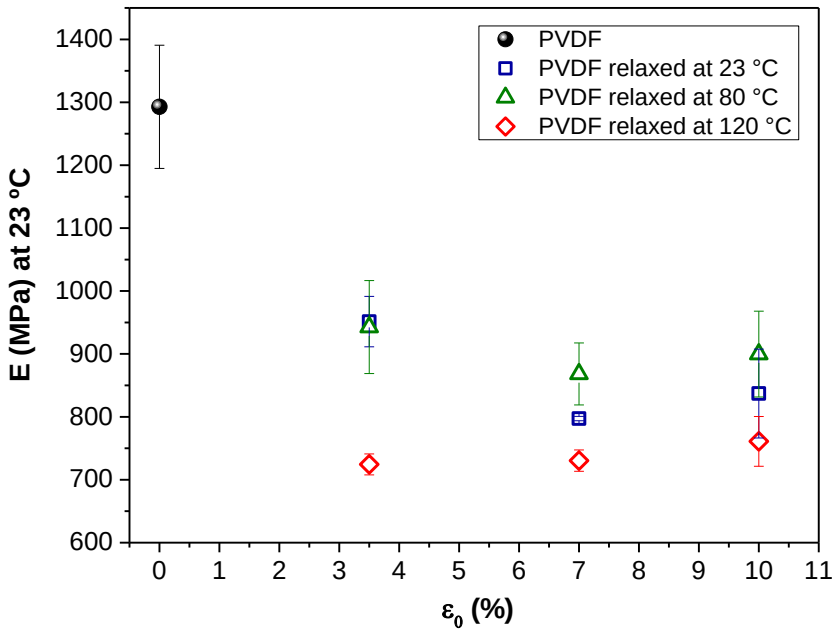

Figure 22. Elastic modulus (E) obtained from tensile tests at 23 ºC of as processed PVDF and relaxed samples. ε_0: strain of the stress relaxation test.

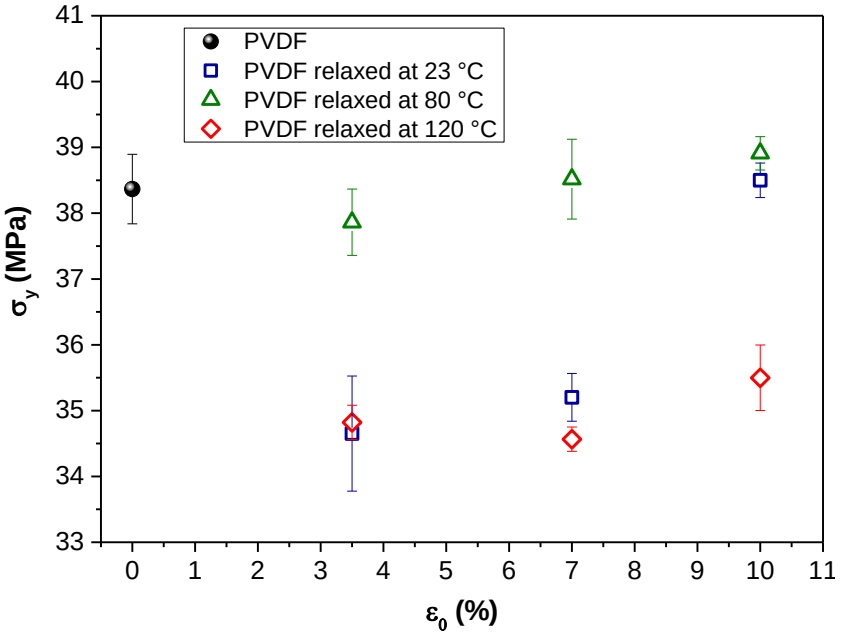

Figure 23. Stress at yield point (σ_y) obtained from tensile tests at 23 ºC of as processed PVDF and relaxed samples. ε_0: strain of the stress relaxation test.

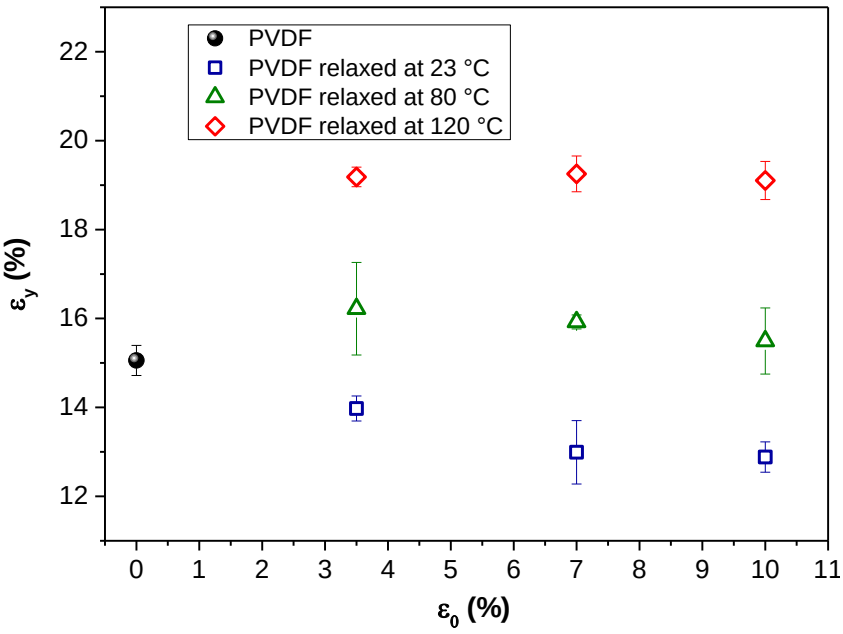

Figure 24. Strain at yield point (ε_y) obtained from tensile tests at 23 ºC of as processed PVDF and relaxed samples. ε_0: strain of the stress relaxation test.

Table 1. Mechanical properties from tensile testing for as processed PVDF and relaxed samples.

Sample	E [a] (MPa)	σ_y [b] (MPa)	ε_y [c] (%)	ε_b [d] (%)
PVDF	1292 ± 98	38 ± 0.5	15 ± 0.3	66 ± 28
PVDF relaxed at 23 °C, 3.5% ε_0	951 ± 40	35 ± 0.9	14 ± 0.3	23 ± 2
PVDF relaxed at 23 °C, 7% ε_0	797 ± 4	35 ± 0.4	13 ± 0.7	21 ± 3
PVDF relaxed at 23 °C, 10% ε_0	837 ± 71	39 ± 0.3	13 ± 0.3	56 ± 26
PVDF relaxed at 80 °C, 3.5% ε_0	942 ± 74	38 ± 0.5	16 ± 1.0	47 ± 24
PVDF relaxed at 80 °C, 7% ε_0	868 ± 49	39 ± 0.6	16 ± 0.2	52 ± 5
PVDF relaxed at 80 °C, 10% ε_0	899 ± 68	39 ± 0.3	16 ± 0.7	53 ± 24
PVDF relaxed at 120 °C, 3.5% ε_0	724 ± 17	35 ± 0.3	19 ± 0.4	37 ± 6
PVDF relaxed at 120 °C, 7% ε_0	730 ± 170	35 ± 0.2	19 ± 0.4	32 ± 6
PVDF relaxed at 120 °C, 10% ε_0	761 ± 40	36 ± 0.5	19 ± 0.2	31 ± 4

[a] E = elastic modulus

[b] σ_y = yield stress

[c] ε_y = yield strain

[d] ε_b = breaking strain

4.3. DMA tests

DMA was carried out to detect segment relaxation and transitions of PVDF. Figure 25 present the loss factor (tan δ) curves of the as processed and relaxed PVDF samples, in the temperature range from -80 to 120 ºC at 1 Hz of frequency.

a) It can be observed in Figure 25 three thermal transitions: β, β' and α. The lower temperature peak obtained from the tan δ plots may be assigned to the β-transition which corresponds to the glass transition temperature (T_g) and hence to Brownian motion in the amorphous phase [9, 87, 88]. This transition process is assigned to the cooperative segmental chain motions of the amorphous region of the material [11, 12]. Tan δ is related to the reduction of vibration of the materials which is associated to the free volume. For the onset of glass transition, a specific free volume fraction (0.025) is required according to the free volume theory [9]. The β-transition was detected at T_g = -39.8 ºC for as processed and all stress relaxed conditions of this PVDF grade, as showed

in Table 2. Therefore, the stress relaxation did not affect the T_g significantly, indicating no variation of the mobility of polymeric chains in the amorphous regions.

b) The β'-transition was observed to occur from 0 up to 30 ºC, as shown in Figure 5. For as processed PVDF, the β' was 14.2 ºC. This peak may be considered a transition quite similar to the glass transition and ascribed to relaxation of the chains at the constrained amorphous region (or intermediate region) [9, 89]. It was observed that the peak was displaced to higher temperatures and broadened for the stress relaxed conditions, compared to the as processed one, indicating the increase of constrained amorphous region in the polymer [9, 89].

c) The third transition, α-transition, was observed at 86.2 ºC peak for the as processed PVDF (Figure 25). It might be attributed to the relaxation of polymeric chains in the crystalline phase [11]. According to Mano *et al.* [11], this relaxation involves flip motions of 180º in the crystalline lamellae which includes both rotation and translation movements of the chains. Samples relaxed (at 23 ºC at all three strains, and 120 ºC at 3.5 and 7% strain) showed slightly decrease of α-transition temperature (T_α) than as processed PVDF. It was observed that the T_α of samples relaxed at 80 ºC at all three strains did not change significantly. However, the T_α values of PVDF relaxed at 120 ºC at 10% strain increased suggesting that these conditions of high temperature and strain influenced the transition process of the crystalline phase.

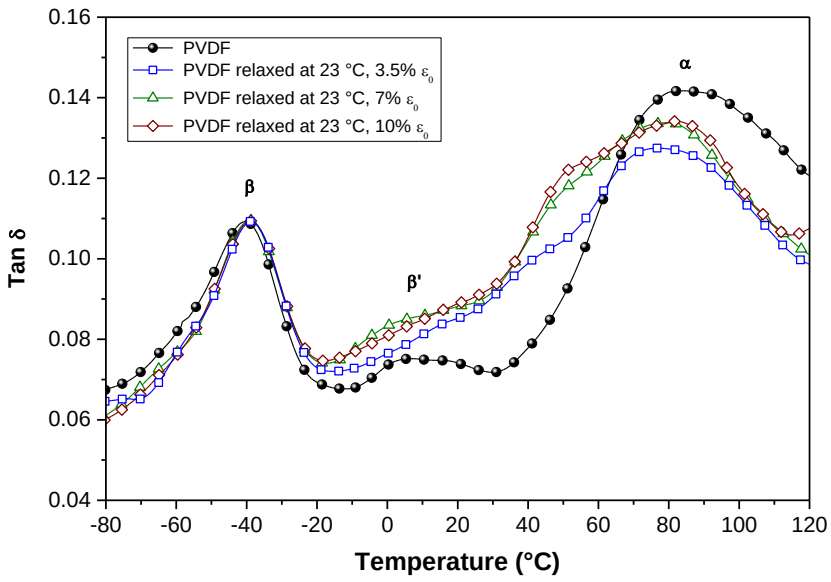

(a) PVDF relaxed at 23 ºC

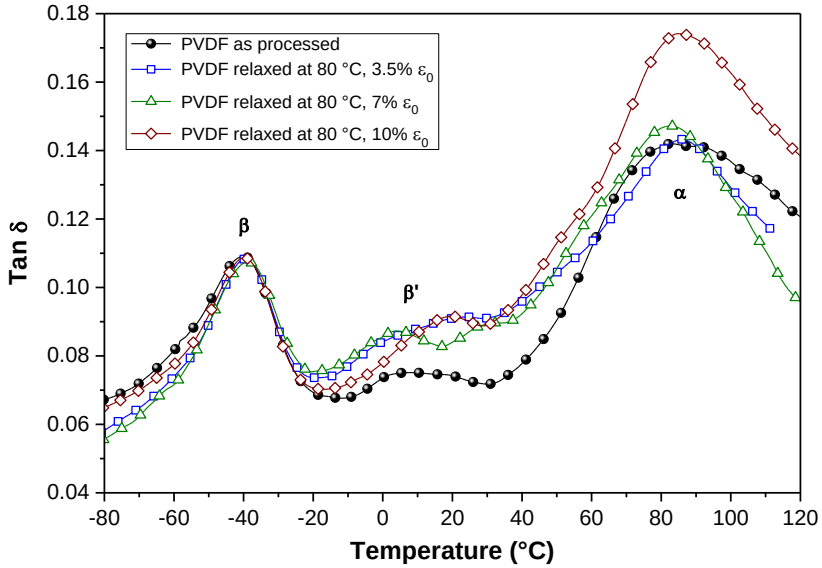

(b) PVDF relaxed at 80 ºC

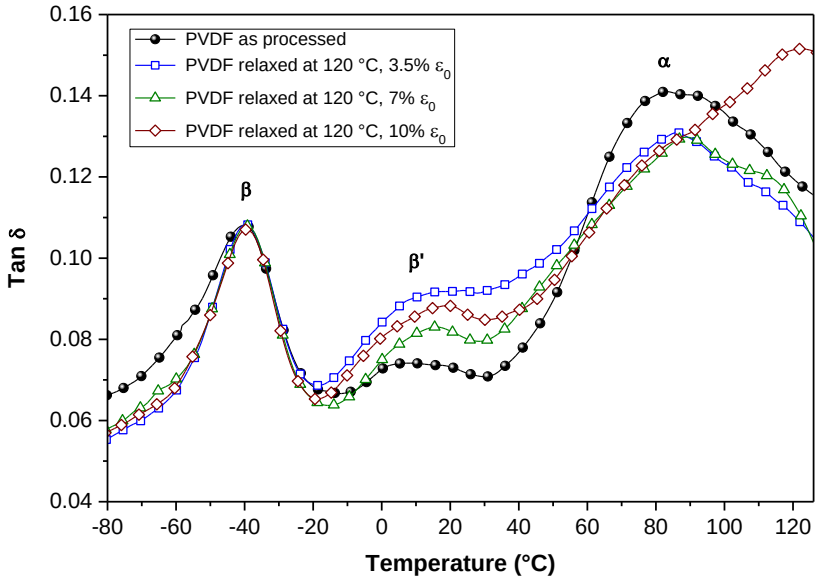

(c) PVDF relaxed at 120 ºC

Figure 25. DMA results obtained at a frequency of 1Hz of as processed PVDF and relaxed samples at: (a) 23 ºC, (b) 80 ºC and (c) 120 ºC.

Figure 26 shows the curves of dynamic storage modulus (E') versus temperature, at 1 Hz, for as processed PVDF and relaxed samples. It can be observed that the as processed PVDF presents a high E' value of 1650 MPa at 23 °C (Table 2), which is attributed to its rigid structure due to its ease of crystallization during the cooling from the melt. Moreover, it can also be observed that E' have high values in the region of low temperatures, between -80 and -60 °C, where the polymer is in the vitreous state (below the glass transition temperature). For all curves, it is observed that E' decreased with the increases in temperature, and then it showed a sharp drop in the glass transition region which occurs due to the increase of the mobility of the polymer chains above T_g. In addition, relaxed samples showed practically similar or slightly lower values of E' (at 23 ºC) compared with as processed PVDF, as shown in Table 2. However, the decrease of modulus was not significant. This variation of E' was observed at temperatures from 20 to 60 °C, including the T_g' range.

Table 2. DMA parameters of as processed PVDF and relaxed samples.

Sample	T_g [a] (ºC)	T_g' [b] (ºC)	T_α [c] (ºC)	E' [d] (MPa)
PVDF	-39.8	14.2	86.2	1650 ± 50
PVDF relaxed at 23 ºC, 3.5% ε_0	-38.6	19.1	75.9	1665 ± 137
PVDF relaxed at 23 ºC, 7% ε_0	-39.4	22.0	78.4	1694 ± 9
PVDF relaxed at 23 ºC, 10% ε_0	-39.1	21.9	79.5	1719 ± 95
PVDF relaxed at 80 ºC, 3.5% ε_0	-39.5	21.8	84.8	1545 ± 132
PVDF relaxed at 80 ºC, 7% ε_0	-38.8	27.2	82.2	1492 ± 100
PVDF relaxed at 80 ºC, 10% ε_0	-38.9	20.8	87.2	1543 ± 84
PVDF relaxed at 120 ºC, 3.5% ε_0	-39.1	17.5	87.3	1590± 124
PVDF relaxed at 120 ºC, 7% ε_0	-38.8	15.4	86.8	1624 ± 149
PVDF relaxed at 120 ºC, 10% ε_0	-39.5	21.4	120.9	1540 ± 121

[a] T_g = glass transition temperature (or β-transition temperature).

[b] T_g' = β'-transition temperature.

[c] T_α = α-transition temperature.

[d] E' = storage modulus (at 23 °C).

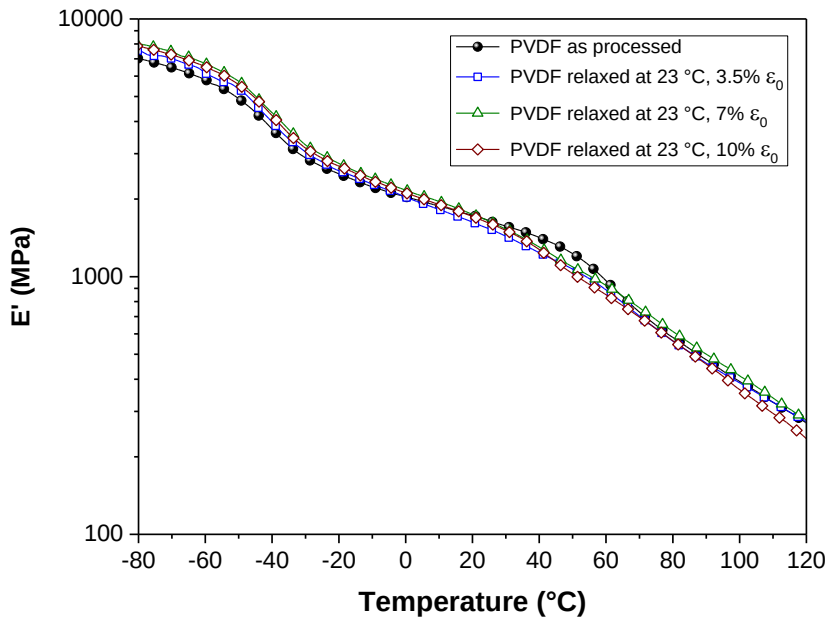

(a) PVDF relaxed at 23 ºC

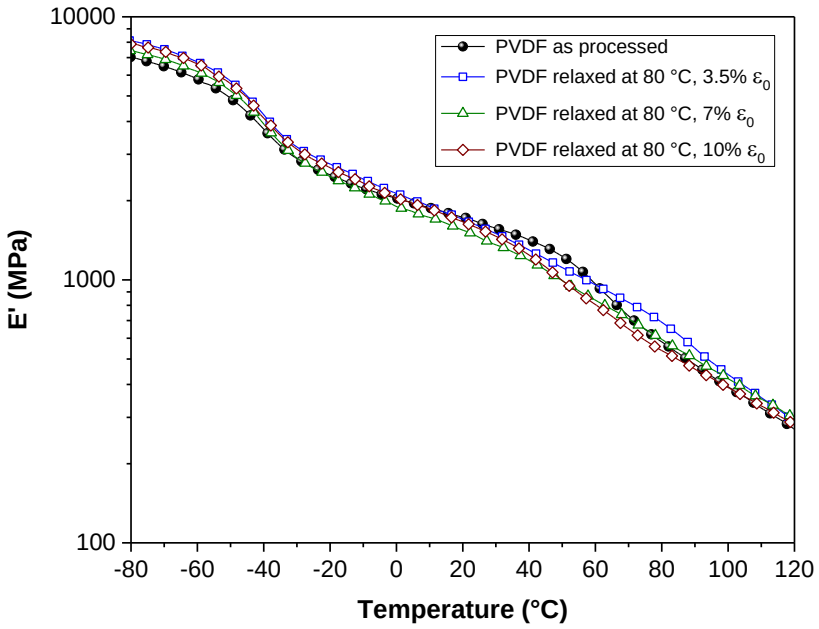

(b) PVDF relaxed at 80 ºC

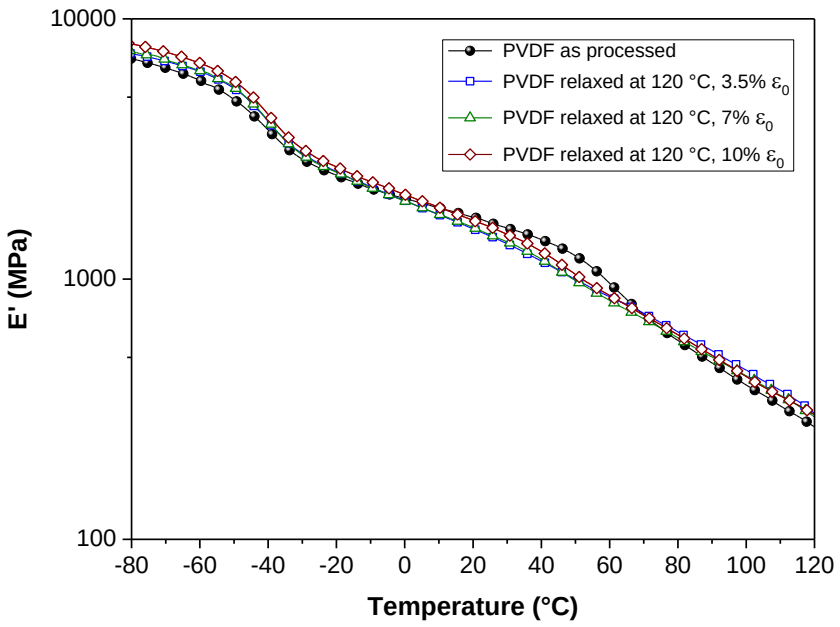

(c) PVDF relaxed at 120 ºC

Figure 26. Storage modulus versus temperature at a frequency of 1Hz of as processed PVDF and relaxed samples at: (a) 23 ºC, (b) 80 ºC and (c) 120 ºC.

4.3.1. Effect of stress relaxation on Tan δ

Recalling the tan δ data for relaxed samples, which were presented in Figure 25, they showed that the peaks temperature of β'-transition was displaced at higher temperatures. The results obtained showed a significant difference of the transition of the chains occurs at the constrained amorphous region (or also called intermediate region). This could indicate that the stress relaxation would improve more constrained or intermediate phase. Therefore, the possible effects of the morphological changes due to the stress relaxation tests should be related to the changes in the intermediate region, instead of only the amount of amorphous phase in the sample. In order to quantify the change of the constrained amorphous or intermediate region, NMR measurements were carried out and the results were shown later.

Thus, the recovery of the stress relaxation curves at 120 ºC (showed in Figure 18) could be related to constrain of chains in the intermediate region. For stress relaxation at

80 ºC, the process energy would not be enough for the transition molecular of the chains.

Besides that, stress relaxation at 120 ºC and 10% strain resulted in an increase of α-transition temperature. The α-transition is regarded as an intralamellar process which is found to be dependent on the crystalline lamellar thickness. Thus, the increase of this α-transition temperature could be related with increase of crystalline lamellar thickness which will be measured by SAXS method (shown later).

4.4. DSC tests

The representative DSC heating curves obtained on as processed PVDF and relaxed samples are showed in Figures 27 - 29. For as processed PVDF, the endothermic peak of the first (Figure 27a, 28a and 29a) and second (Figure 27b, 28b and 29b) heating run, assigned to the melting of its crystalline region, was visible on two runs around 168.3 °C for as processed PVDF and maintained constant after stress relaxation. The melting enthalpy (ΔH_m) of as processed PVDF was measured around 52.5 J/g which corresponds to about 50% crystallinity index (X_c) and kept roughly the same after stress relaxation, in the first and second heating cycle. The data of melting enthalpy and melting temperature, for as processed PVDF and relaxed samples, are summarized in Appendix II. The X_c values were determined considering the heat fusion of 104.7 J/g for 100% crystalline PVDF [23, 47, 90, 91], and are presented in Figure 30 and summarized in Table 3.

In Figure 29a, the first heating curve of PVDF relaxed at 120 °C revealed a minor endothermic peak (shoulder) around 120 and 140 °C for all three strains applied. The shoulder before the melting peak has been assigned to melting of small and/or imperfect crystallites [92, 93]. This shoulder is a low endotherm corresponding to melting of PVDF secondary crystals [92, 93]. The formation of secondary crystals occurs in the amorphous phase and induced conformational constraints in the chains, such as loops and tie-chains [92]. This peak disappeared in the second heating run performed after cooling from the melt. The enthalpy of this peak was estimated around 1 J/g and corresponds to 2% of the melting enthalpy; similarly to those reported in the literature [92, 93]. The presence of shoulders leads to a small increase in the crystallinity index, reaching around 51.5% here, which was not significant.

Additionally, the representative DSC cooling curves of as processed PVDF and relaxed samples are presented in Appendix II. Temperature of crystallization (T_c) of as processed PVDF on two runs was around 145.7 ºC and did not change significantly after stress relaxation.

No changes were observed by DSC measurements. It should be pointed out that stress relaxation does not affect the fraction of the crystalline phase, its melting and the crystallization temperature of this PVDF, meaning high material stability.

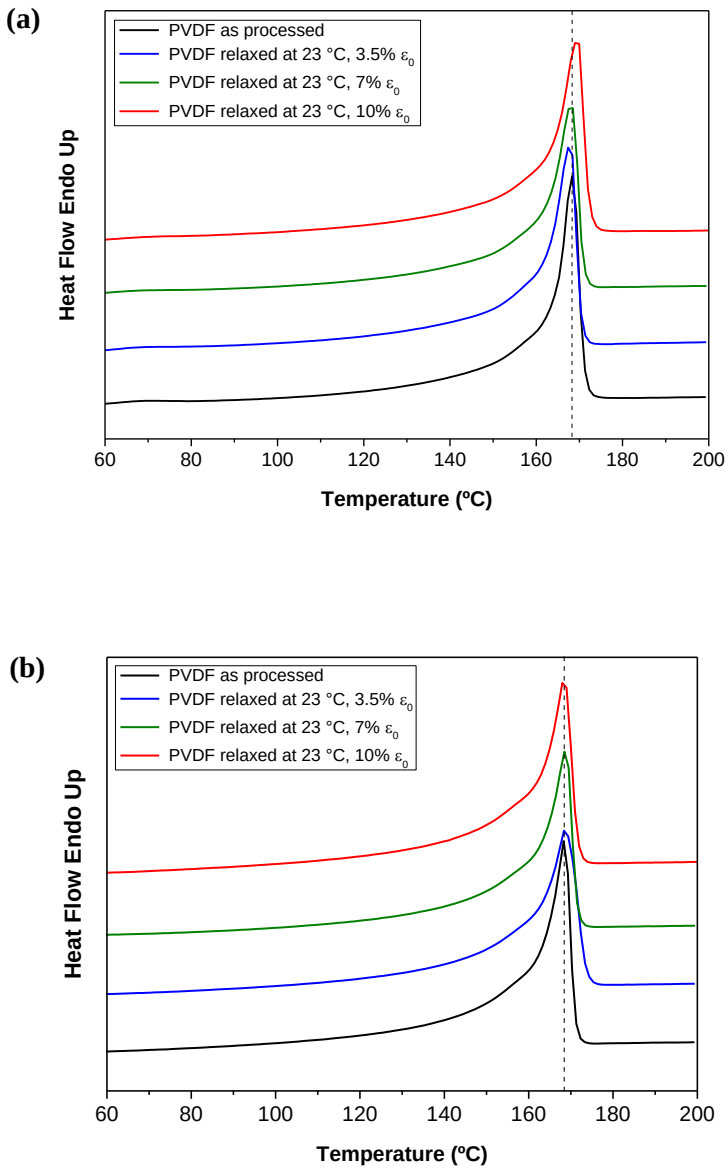

Figure 27. Representative DSC thermograms of PVDF as processed and samples relaxed at 23 ºC. (a) First heating, (b) Second heating.

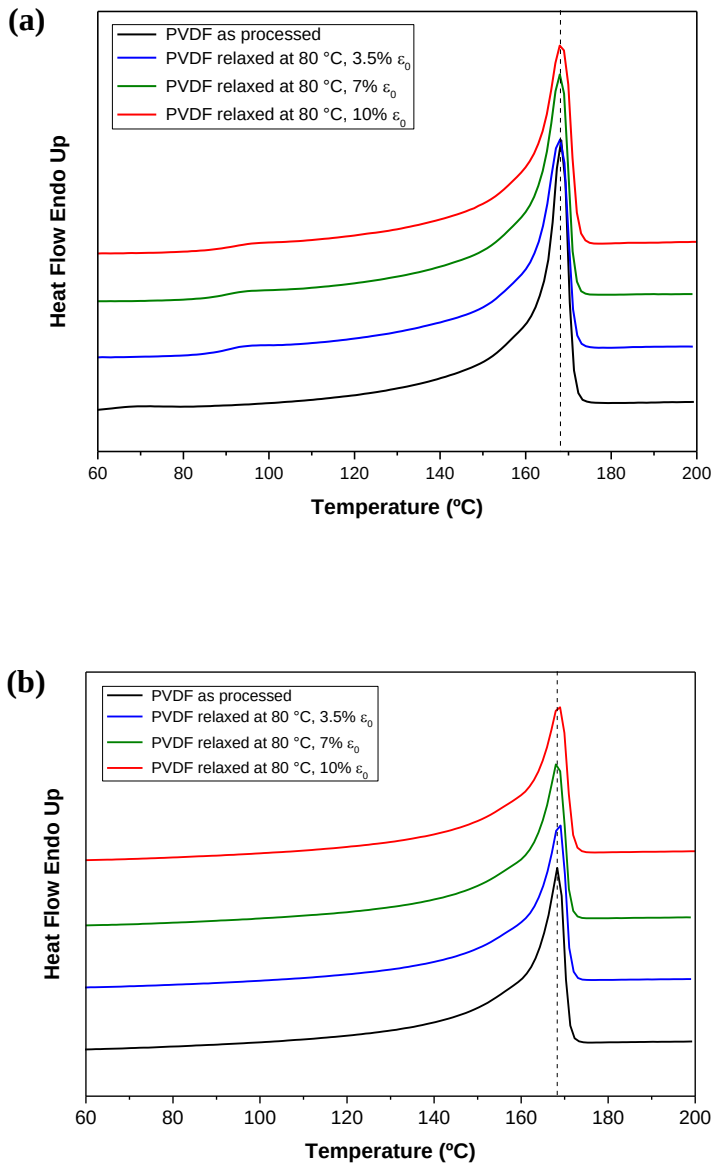

Figure 28. Representative DSC thermograms of PVDF as processed and samples relaxed at 80 ºC. (a) First heating, (b) Second heating.

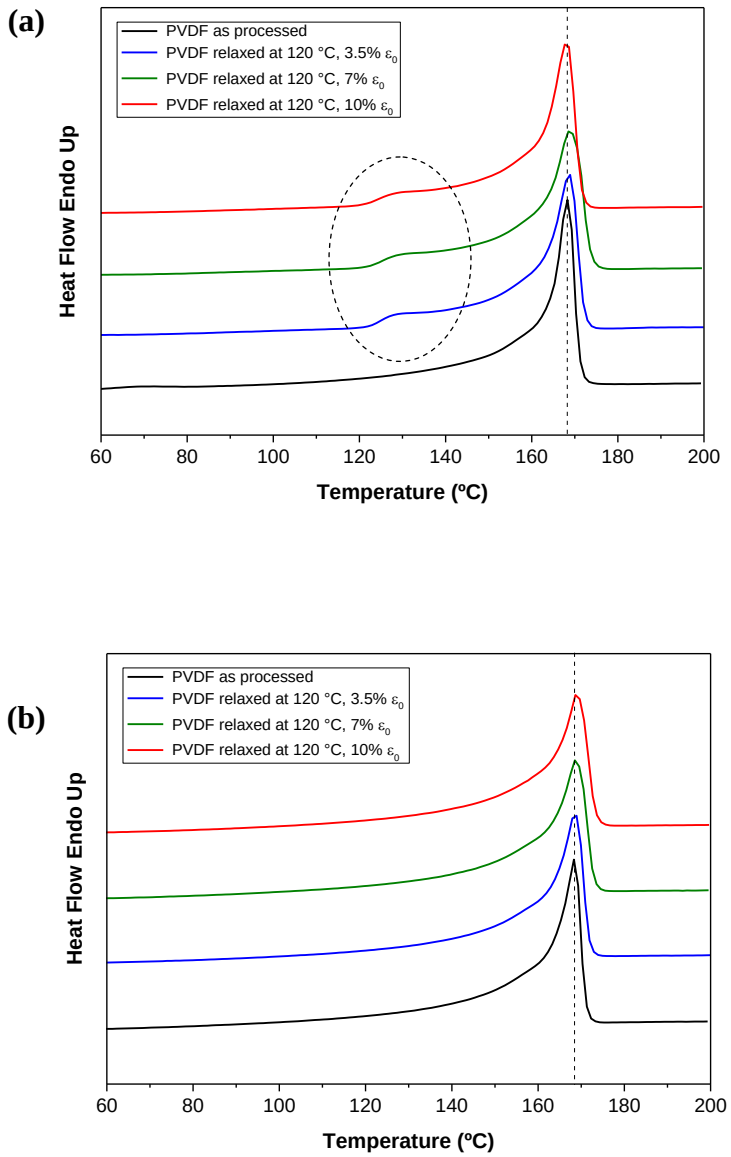

Figure 29. Representative DSC thermograms of PVDF as processed and samples relaxed at 120 ºC. (a) First heating, (b) Second heating.

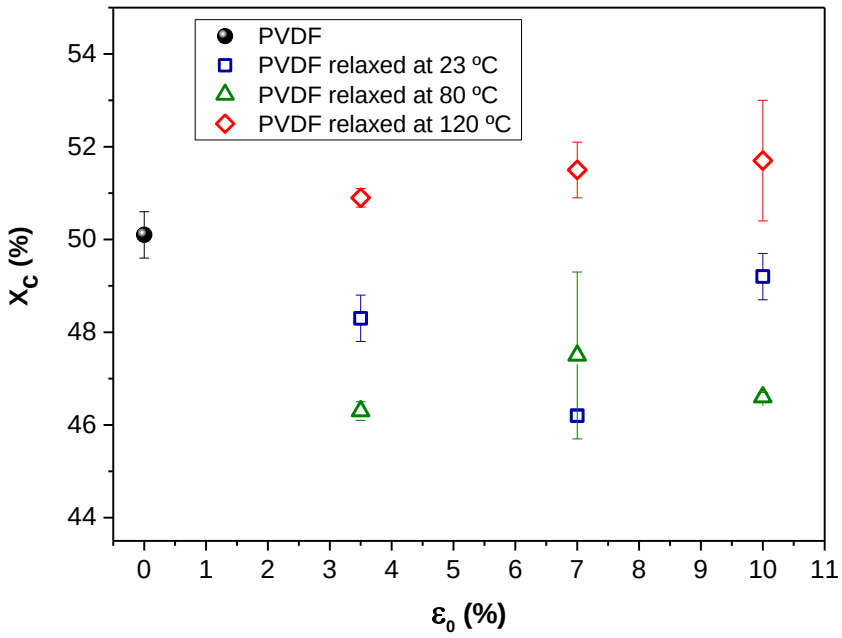

Figure 30. Crystallinity index (first heating) values obtained by DSC of as processed PVDF and relaxed samples. ε_0: strain of the stress relaxation test.

Table 3. Crystallinity index obtained by DSC technique.

Sample	X_c [a] (%)	
	First heating	Second heating
PVDF	50.1 ± 0.5	51.0 ± 0.2
PVDF relaxed at 23 ºC, 3.5% ε_0	48.3 ± 0.5	49.0 ± 0.6
PVDF relaxed at 23 ºC, 7% ε_0	46.2 ± 0.1	49.0 ± 0.3
PVDF relaxed at 23 ºC, 10% ε_0	49.2 ± 0.5	50.0 ± 0.5
PVDF relaxed at 80 ºC, 3.5% ε_0	46.3 ± 0.2	47.9 ± 0.7
PVDF relaxed at 80 ºC, 7% ε_0	47.5 ± 1.8	48.0 ± 0.2
PVDF relaxed at 80 ºC, 10% ε_0	46.6 ± 0.1	48.2 ± 0.7
PVDF relaxed at 120 ºC, 3.5% ε_0	50.9 ± 0.2	48.4 ± 0.2
PVDF relaxed at 120 ºC, 7% ε_0	51.5 ± 0.6	48.7 ± 0.2
PVDF relaxed at 120 ºC, 10% ε_0	51.7 ± 1.3	48.5 ± 0.4

[a] X_c = crystallinity index.

4.5. Molecular dynamics determined by NMR

The nuclear magnetic resonance was used to evaluate the structural modifications of the PVDF. This technique allows obtaining information on relaxometry of each part of the material structure, namely: crystalline, amorphous and constrained amorphous (intermediate) phases.

a) The inversion-recovery pulse sequence was used because it allows to obtain the longitudinal relaxation time from relaxation curves fitted with Equation (19) (showed in the experimental part). Typical relaxation curves of the samples are shown in Figure 31. The value of $T_{1,1}H$ and $T_{1,2}H$ for the as processed and for all stress relaxed PVDF were measured to be around 15 ms and 91 ms, respectively. Longitudinal relaxation time $T_{1,1}H$ refers to the population of hydrogen with greater mobility, associated to the amorphous phase. And the longitudinal relaxation time $T_{1,2}H$ is related to the population of hydrogen of the rigid region (crystalline phase). The value of $T_{1,1}H$ and $T_{1,2}H$ for the as processed and for all stress relaxed PVDF were measured to be around 15 ms and 91 ms, respectively. These results showed that the longitudinal relaxation time was not altered even by severe strain (10%) and temperature (120 ºC) up to 24 h. At the time being, the structure of the material has being quite stable under all tests condition and analytical methods used.

The longitudinal relaxation time of the inversion-recovery pulse technique is related to the mean square distance of the process of diffusion of the magnetization (L), which had the value of 13 nm (determined from Equation (20)) for as processed PVDF and relaxed samples. In this case, all morphological changes detected in the material had to be 13 nm or higher; in other words, any chain movements below 13 nm in dimension could not be measured. Therefore, a sequence sensitive to segmental dynamics was required.

b) The MSE-FID technique was then used to understand dimensions smaller than 13 nm, once it can detect morphological movements lower than 13 nm; in fact, its resolution starts at dimensions of 4 carbon atoms (about 0.6 nm) [40], 21 times better in resolution, comparatively. This technique allows to determine the transversal relaxation time and percentage fraction of the rigid, mobile and intermediate phases. The determination of the transversal relaxation times and fractions of these three regions is obtained through the curve shown in Figure 32. The signal obtained by MSE-FID pulse sequence was fitted with Equation (21) (showed in the experimental part). Then this

curve is deconvoluted in three functions: a Abragamian function, representing the rigid phase fraction with low chain mobility; a Gaussian function, governed by segments of intermediate mobility and less ordered, standing for the constrained amorphous fraction; and an exponential decay function, governed by hydrogens of higher mobility, representing the free amorphous phase.

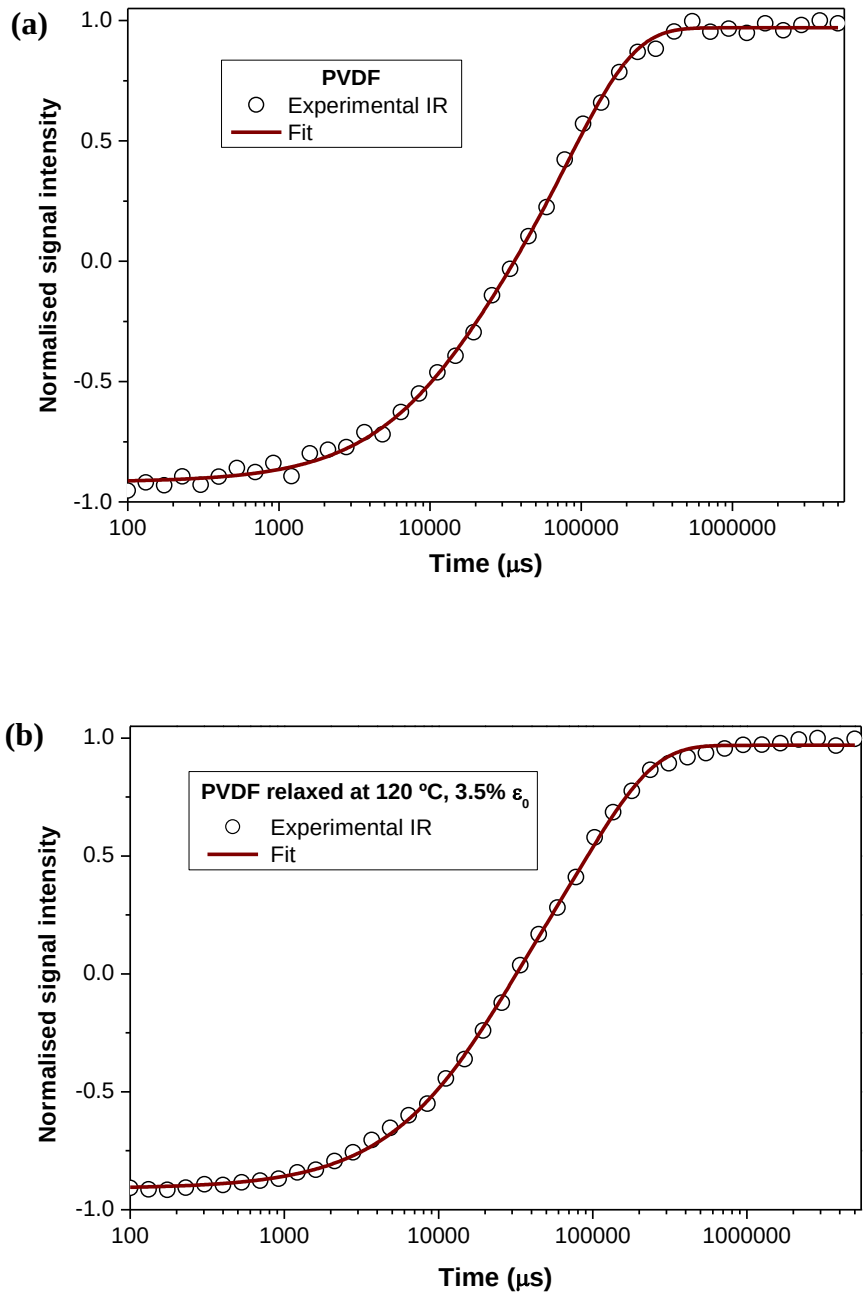

Figure 31. ^{1}H NMR FID of: (a) as processed PVDF and (b) PVDF relaxed at 120 ºC, 3.5% ε_0.

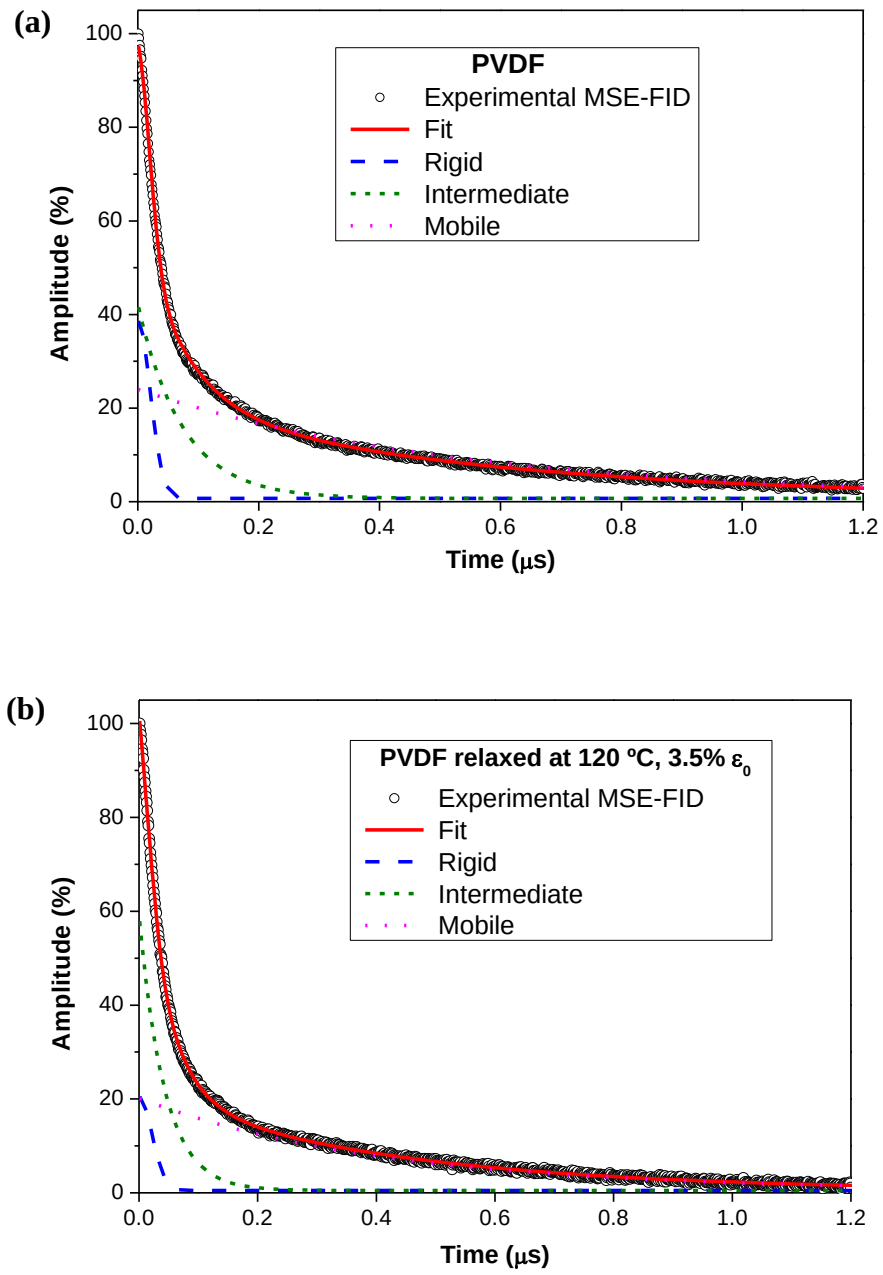

Figure 32. Decomposition of ^{1}H NMR MSE-FID into different signal fraction according to Equation (21) for: (a) as processed PVDF and (b) PVDF relaxed at 120 ºC, 3.5% ε_0.

The MSE-FID allowed to calculate the fraction of each region in the as processed and all relaxed PVDF samples, shown in Figures 33 - 35. Meanwhile, Table 4 and 5 show corresponding values of fraction and the transversal relaxation time, respectively, obtained for as processed PVDF and relaxed samples. The MSE-FID measurements

provided information about rigid, mobile and intermediate regions, which are difficult to obtain by other techniques. This technique served to gain information about interactions of neighboring proton spins via the investigation of spin dynamics [56]. These measurements provide information of the regions which are distinguished on the basis of their different molecular mobility [19]. Figure 36 presents the typical arrangement of the spherulitic structure of semicrystalline polymers, such as PVDF. It can be observed that the rigid phase corresponds to the fibrils (ribbon-like chain-folded crystallites) of the spherulites. Meanwhile, the intermediate region is located between fibrils within the spherulites. The mobile region is assigned to amorphous regions composed of randomly oriented molecules, in between the spherulites.

- It is interesting to observe in Figures 33 - 35 the combined behavior of the three regions present in the polymer. It can be observed that the fraction of the rigid phase (f_{rigid}) decreased with the increase of the stress relaxation temperature, reaching its lowest values at 120 ºC. The fraction of the mobile region (f_{mobile}) remained unchanged for all relaxed samples at all temperatures. The intermediate region (f_{inter}), increased at the expense of the rigid region (crystalline phase), for instance, it increased dramatically with the increase of the temperature test (120 ºC). The increase in test temperature leads to a reduction in viscosity due to a high molecular mobility, especially on the amorphous region. The increase of the percentage of the intermediate region (constrained amorphous phase) seems to influence the decrease of the elastic modulus, calculated by the tensile tests, as explained below.

On the other hand, comparing results of samples relaxed at the same temperature, it is important to note that this trend was less marked in cases of higher strain (10%) and lower temperatures (23 and 80 ºC) (results showed in Table 4). It was expected that with the advancement of the strain up to 10%, there would be a higher migration of chain segments from rigid phase to the intermediate phase. Nevertheless, the results of rigid and intermediate fraction (for stress relaxation at 23 and 80 ºC, at 10% strain) indicated that the increase of strain could lead to strain-induced crystallization. However, the percentage crystalline fraction for PVDF relaxed at 120 ºC and 10% strain was lower than results at 23 and 80 ºC, at 10% strain.

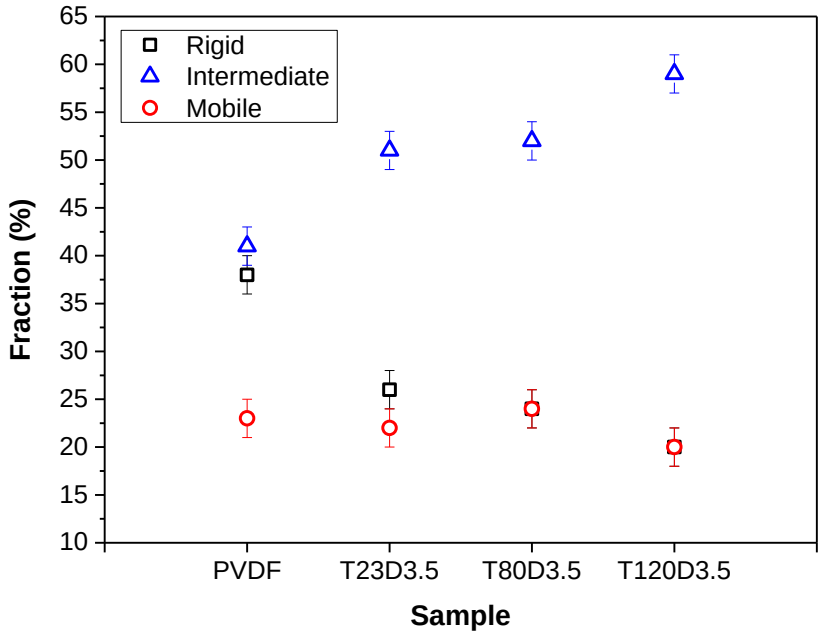

Figure 33. Fraction of the rigid, intermediate and mobile region obtained at 27 °C. Sample T23D3.5: PVDF relaxed at 23 °C and 3.5% ε_0; T80D3.5: PVDF relaxed at 80 °C and 3.5% ε_0 and T120D3.5: PVDF relaxed at 120 °C and 3.5% ε_0.

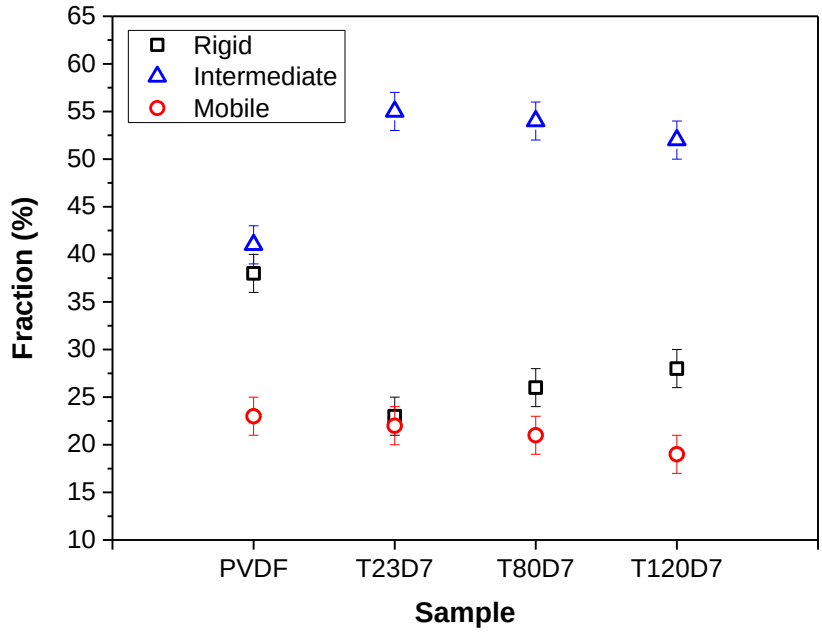

Figure 34. Fraction of the rigid, intermediate and mobile region obtained at 27 °C. Sample T23D7: PVDF relaxed at 23 °C and 7% ε_0; T80D7: PVDF relaxed at 80 °C and 7% ε_0 and T120D7: PVDF relaxed at 120 °C and 7% ε_0.

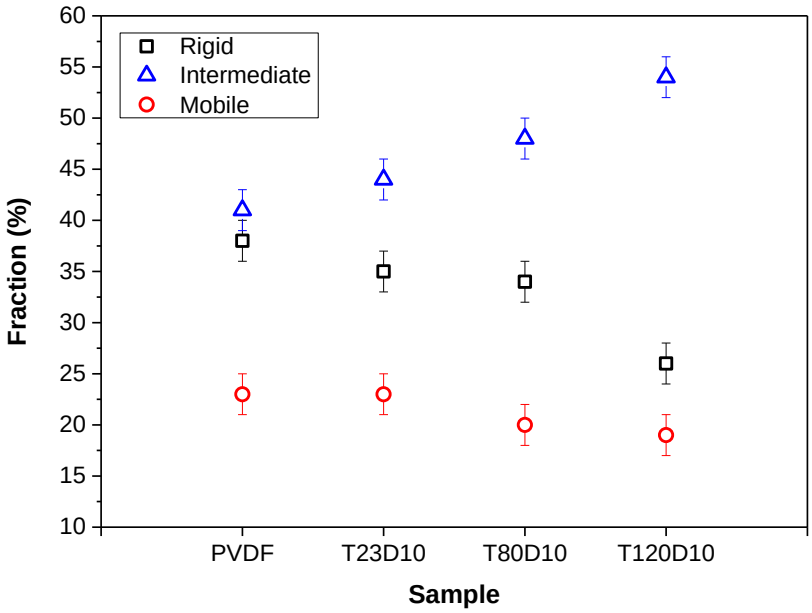

Figure 35. Fraction of the rigid, intermediate and mobile region obtained at 27 °C. Sample T23D10: PVDF relaxed at 23 °C and 10% ε_0; T80D10: PVDF relaxed at 80 °C and 10% ε_0 and T120D10: PVDF relaxed at 120 °C and 10% ε_0.

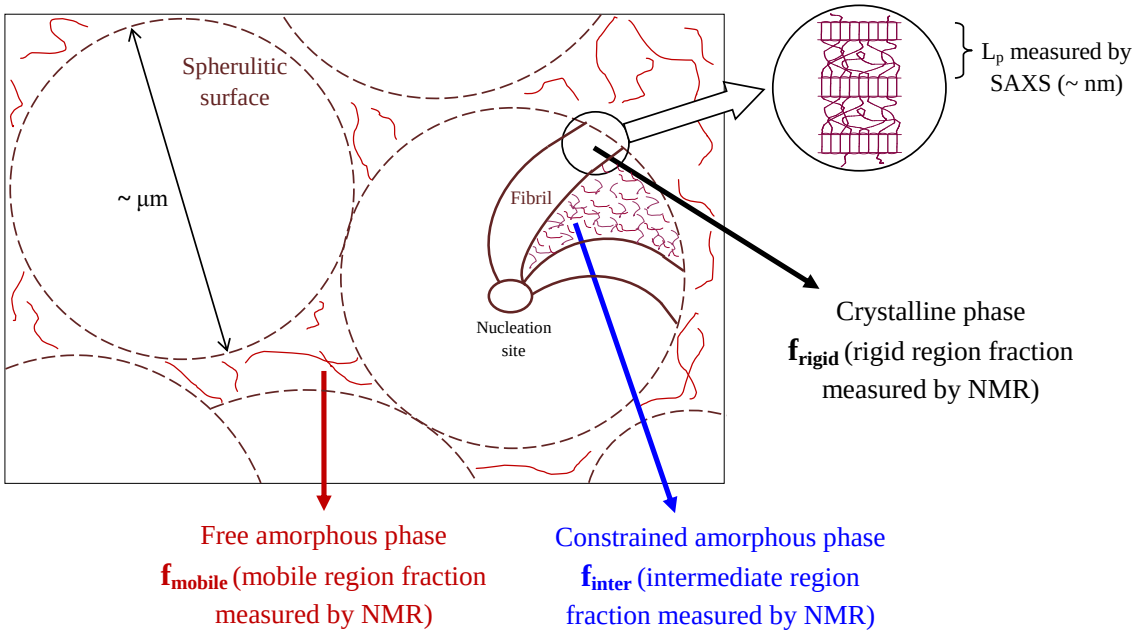

Figure 36. Schematic representation of the spherulitic structure of semicrystalline polymers.

Table 4. Fraction of the rigid, intermediate and mobile region obtained by MSE-FID technique.

Sample	f_{rigid} [A] (%)	f_{inter} [A] (%)	f_{mobile} [A] (%)
PVDF	38	41	23
PVDF relaxed at 23 ºC, 3.5% ε_0	26	51	22
PVDF relaxed at 23 ºC, 7% ε_0	23	55	22
PVDF relaxed at 23 ºC, 10% ε_0	35	44	23
PVDF relaxed at 80 ºC, 3.5% ε_0	24	52	24
PVDF relaxed at 80 ºC, 7% ε_0	26	54	21
PVDF relaxed at 80 ºC, 10% ε_0	34	48	20
PVDF relaxed at 120 ºC, 3.5% ε_0	20	59	20
PVDF relaxed at 120 ºC, 7% ε_0	28	52	19
PVDF relaxed at 120 ºC, 10% ε_0	26	54	19

[A] Standard deviation ± 2%.

The general behavior indicates, although not linear, a decreasing of the rigid region (crystallinity fraction) as the stress relaxation temperature increased, for each strain imposed; meanwhile, the intermediate region (constrained amorphous phase) increased in amount and the mobile region (free amorphous phase) did not undergo significant change. This behavior clearly shows that the chain segments that previously formed the crystalline phase migrate (or pulled-out) to the constrained amorphous phase, becoming segments confined between the remaining crystallites. Therefore, the stress relaxation process only induced the migration of chain segments from the crystalline phase to the constrained amorphous phase, keeping the free amorphous phase unchanged. It is worth pointing out that such modifications are to be linked to changes in the elastic modulus.

- The MSE-FID allowed to obtain the transversal relaxation time (T_2^*) of each region in the structure. The as processed PVDF presented T_2^* values of 21, 149 and 512 μs for the rigid, intermediate and mobile regions, respectively, as shown in Figures 37 - 39 (the MSE-FID tests were conducted at 28 °C). It can be noted that the transversal

relaxation time of the rigid phase ($T^*_{2,\,rigid}$) did not vary for all relaxed samples and had the lowest T^*_2 value, which is expected since it is the least sensitive to temperature and strain. $T^*_{2,\,rigid}$ values in the same order of magnitude (about 20 μs) are reported in the literature for other systems such as the blend (carboxyl terminated polybutadiene (CTPB)/clay), poly(3-hydroxybutyrate) (PHB) and polyethylene [65, 66, 68]; also, the molecular weight varied quite well for these materials tested, that range from 5000 g/mol to 400000 g/mol [8, 55]. The $T^*_{2,\,rigid}$ was also reported to be constant when tested up to 50 ºC for CTPB [66], showing the rigid region to be quite resilient to small changes in temperature due to its own stiffness.

Additionally, the intermediate and mobile regions have considerable higher transversal relaxation time compared to the rigid phase, about 6 and 20 fold higher, respectively. This behavior is related to the self-mobility of the chains, which vary from being highly constricted in between crystals to almost full possibilities of movement when in the mobile region. The stress relaxation process involves chains rearrangement and modifications in the fraction of their regions (rigid, intermediate and mobile), as shown above. It was observed that in the extreme condition of stress relaxation, 120 ºC and 10% strain, the $T^*_{2,\,inter}$ decreased slightly and the $T^*_{2,\,mobile}$ showed a higher drop. This reduction of $T^*_{2,\,inter}$ was due to chain stretching alignment, reducing the mobility of the segments and making them closer to each other (crystal-like situation), which is a typical behavior seen in deformed polymers [68]. However, samples relaxed at 23 and 80 ºC and at 10% strain showed $T^*_{2,\,inter}$ and $T^*_{2,\,mobile}$ closer to those determined for as processed PVDF (see Table 5). On the other hand, samples relaxed at 3.5 and 7% strain at all three temperatures followed a behavior standard on which $T^*_{2,\,inter}$ and $T^*_{2,\,mobile}$ were lower than as processed PVDF. Thus, intermediate and mobile segments tended to become less mobile with increasing temperature of the stress relaxation test. The reduction of T^*_2 was evidently greater in the amorphous fraction, where the segments had more mobility for a morphological rearrangement.

The effect of the stress relaxation process in the polymer can be described as: disorganization of the crystalline region and, as consequence, organization (alignment) of the constrained amorphous phase. Hence, free amorphous region fraction did not undergo a significant change. In addition, for stress relaxation at 23 and 80 ºC, at higher

strain (10%), it was determined alignment of the chains and strain-induced crystallization in the constrained amorphous phase. The crystallization was the preponderant effect in those conditions. Also, a similar development was found for stress relaxation at 120 ºC, an increase in the crystalline region fraction was obtained with increase of the strain. In this case, the effect of strain-induced crystallization was more predominant than alignment.

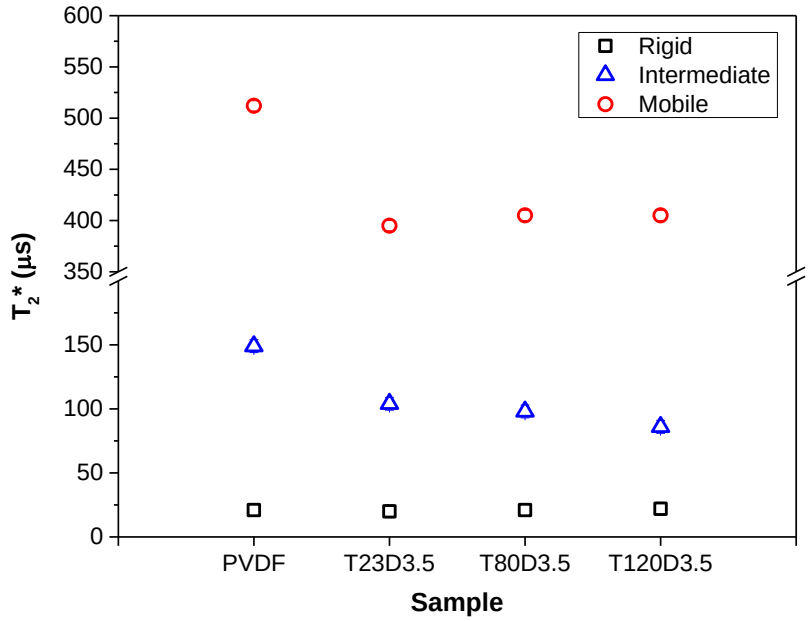

Figure 37. Transversal relaxation times of each region. Sample T23D3.5: PVDF relaxed at 23 °C and 3.5% ε_0; T80D3.5: PVDF relaxed at 80 °C and 3.5% ε_0 and T120D3.5: PVDF relaxed at 120 °C and 3.5% ε_0.

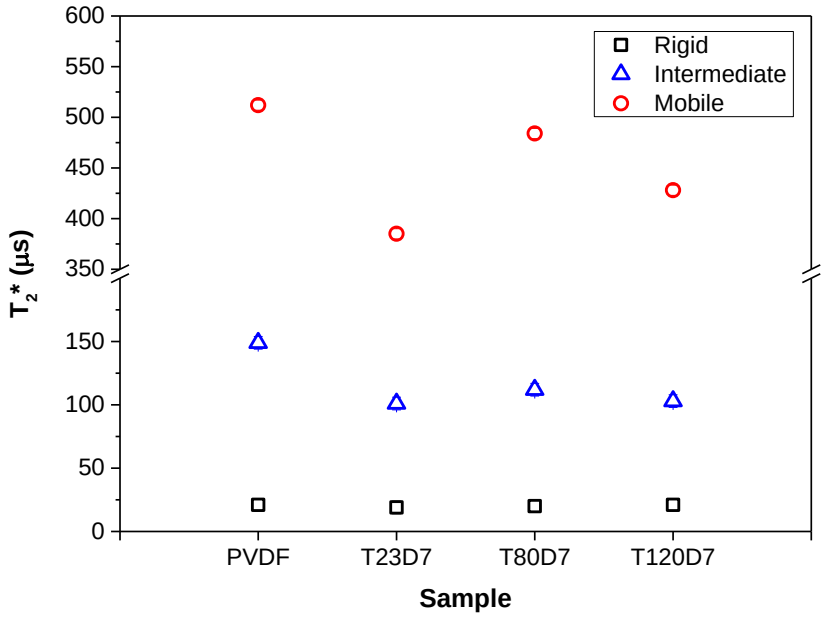

Figure 38. Transversal relaxation times of each region. Sample T23D7: PVDF relaxed at 23 °C and 7% ε_0; T80D7: PVDF relaxed at 80 °C and 7% ε_0 and T120D7: PVDF relaxed at 120 °C and 7% ε_0.

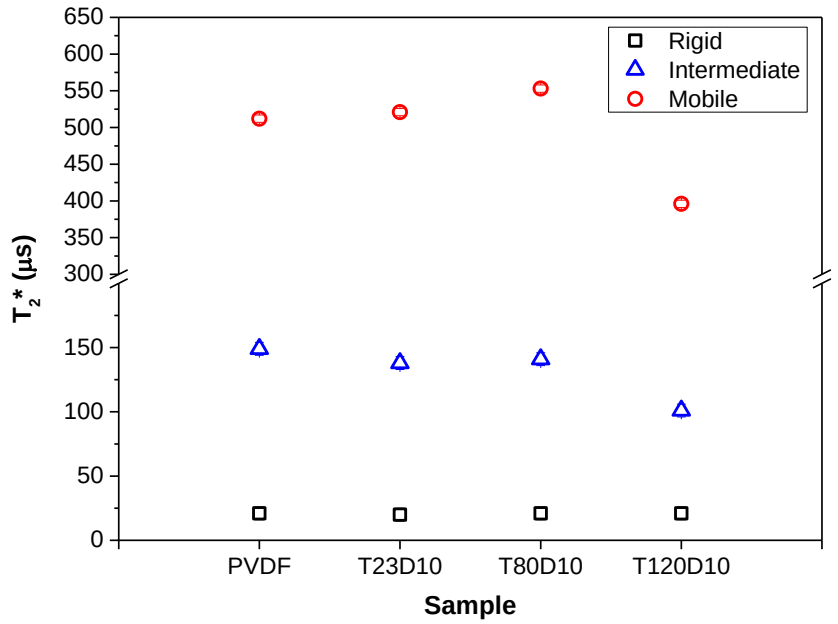

Figure 39. Transversal relaxation times of each region. Sample T23D10: PVDF relaxed at 23 °C and 10% ε_0; T80D10: PVDF relaxed at 80 °C and 10% ε_0 and T120D10: PVDF relaxed at 120 °C and 10% ε_0.

Table 5. Transversal relaxation times of each region obtained by MSE-FID technique.

Sample	$T_{2*, rigid}$ [A] (μs)	$T_{2*, inter}$ [A] (μs)	$T_{2*, mobile}$ [A] (μs)
PVDF	21	149	512
PVDF relaxed at 23 ºC, 3.5% ε_0	20	104	395
PVDF relaxed at 23 ºC, 7% ε_0	19	101	385
PVDF relaxed at 23 ºC, 10% ε_0	20	138	521
PVDF relaxed at 80 ºC, 3.5% ε_0	21	98	405
PVDF relaxed at 80 ºC, 7% ε_0	20	112	484
PVDF relaxed at 80 ºC, 10% ε_0	21	141	553
PVDF relaxed at 120 ºC, 3.5% ε_0	22	86	405
PVDF relaxed at 120 ºC, 7% ε_0	21	103	428
PVDF relaxed at 120 ºC, 10% ε_0	21	101	396

[A] Standard deviation ± 5 μs.

4.6. Structural study using SAXS measurements

SAXS measurements were employed for the structural investigation of PVDF before and after stress relaxation. It is worth noting that SAXS provides an estimation of the average lamellar thickness, as shown in Figure 40. Lamellar stacks are composed of crystalline lamellae and interlamellar amorphous region. The SAXS analysis was performed assuming that the crystalline lamellae are isotropic stacks of plates with an infinitely extended lateral dimension [16]. Thus, the lateral size and the curvature radius of the crystalline lamellae are assumed to be much greater than the long period [17].

In order to analyzed the SAXS data, two independent procedures were used to determine the structural parameters of the studied polymer. These methods were based on Bragg's law and the analysis of the linear correlation γ(r) function.

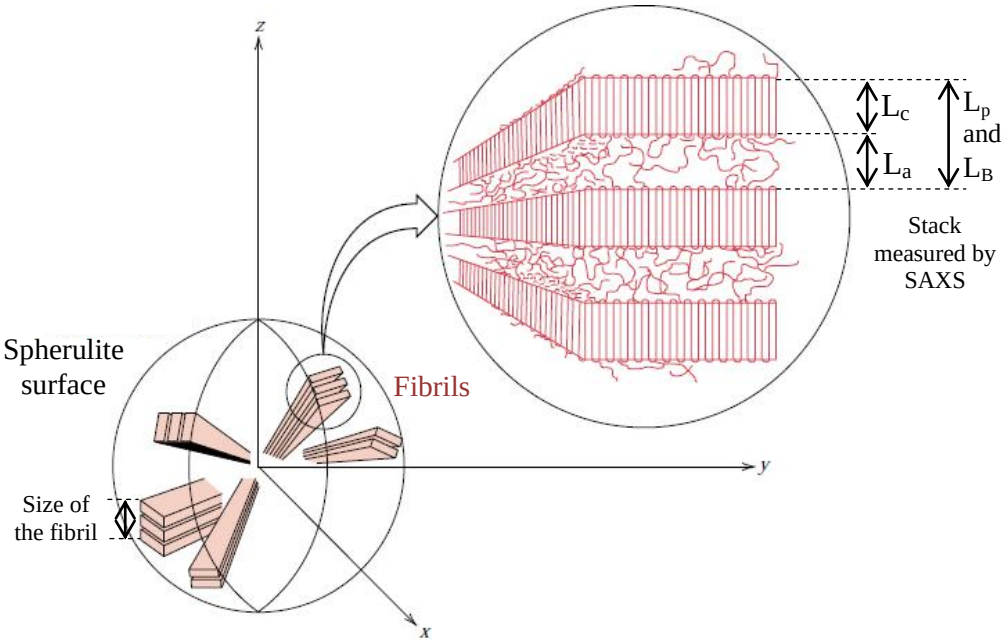

Figure 40. Structure in PVDF spherulite. Adapted from [38].

Figure 41 shows the scattered SAXS intensity profiles of as processed PVDF and relaxed samples. The SAXS profiles exhibit a scattering peak (first maximum) associated to the crystalline-amorphous structure of the semicrystalline PVDF. The SAXS profiles for samples relaxed at 120 ºC presented well defined and thinner peak. It also can be observed that the scattering peaks of the relaxed samples were progressively shifted to higher angles.

The SAXS profiles were properly corrected (e.g. Lorentz correction) using the transformation $I_1(q) = I(q)q^2$. The Lorentz-corrected SAXS profiles presented a well-defined Bragg peak for each sample as shown in Figure 42. The Bragg peak appears at $q_{max} = 0.0455$ Å^{-1} for as processed PVDF. The peak was shifted to higher q values for relaxed samples. The average Bragg long period (L_B) and average domain size were calculated according Equation (23) and (24) (showed in the experimental part), respectively, and the values are given in Table 6. The L_B is the sum of average thicknesses of crystalline layers and amorphous layers; however, this method does not directly provide any values of these two thicknesses. The L_B value of processed PVDF was 13.8 nm. Moreover, it can be observed the decrease of L_B values for all condition relaxed samples. The lowest values of Bragg long period (11.9 nm) were obtained for sample relaxed at 120 ºC at 3.5 % strain. On the other hand, the average domain size

represents the size of the fibrils (in the spherulites), see Figure 40. This dimension is inversely related to the half-width of the Bragg peak.

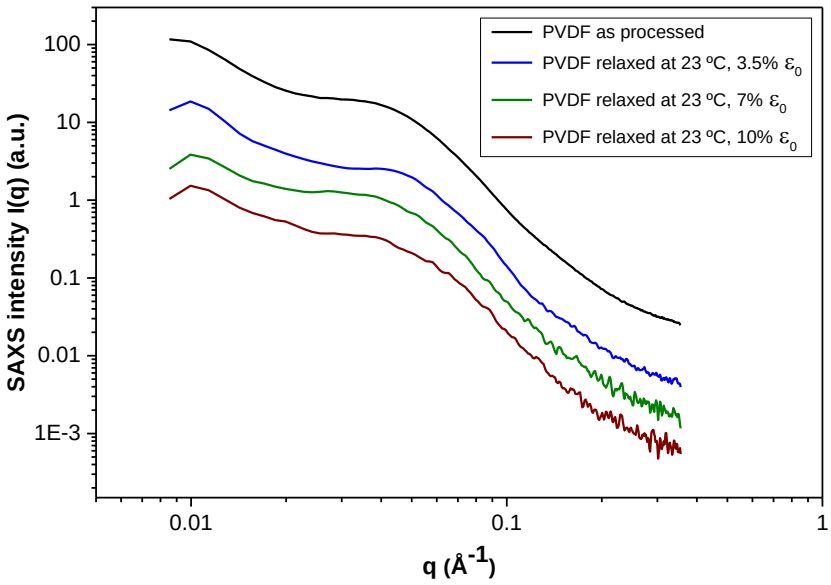

(a) PVDF relaxed at 23 ºC

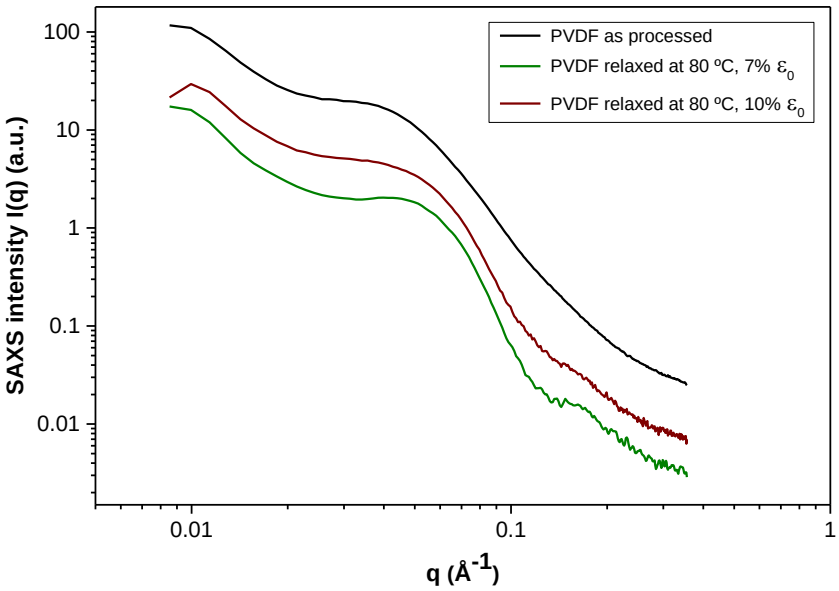

(b) PVDF relaxed at 80 ºC

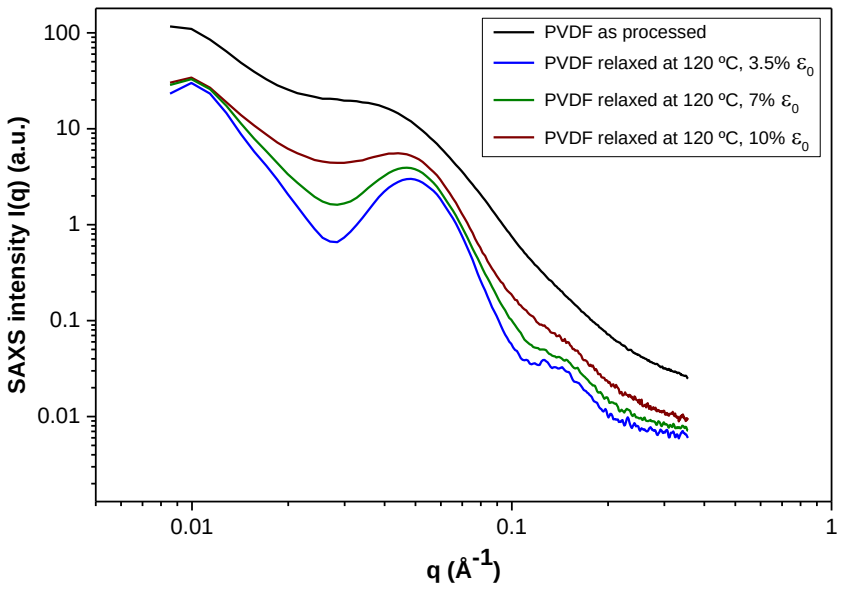

(c) PVDF relaxed at 120 ºC

Figure 41. I(q) SAXS intensity profiles for as processed PVDF and samples relaxed at (a) 23 ºC, (b) 80 ºC and (c) 120 ºC.

The average domain size of as processed PVDF was 36.9 nm, it indicates that a fibril would be conformed of three lamellar stacks. The relaxed samples at 80 and 120 ºC showed higher values of average domain size with the increase of stress relaxation temperature. This means that the structure of relaxed samples was more organized or presented lower values of the long period. These results were expected due to the narrowing of the peaks in the Lorentz-corrected SAXS intensity profiles. In the case of PVDF relaxed at 120 ºC at 3.5 % strain (L_B = 11.9 nm), the obtained average domain size was 46.8 nm indicating that a fibril contains four lamellar stacks. The higher values of average domain size (or size of the spherulite fibril) could be explained by the growth of the crystallites induced by the increase in temperature.

The linear correlation γ(r) function was used to determine structural parameters of the lamellar stacks in the investigated polymer. The data were analyzed in terms of a one-dimensional stack model, in which the stacks consist of crystalline lamellae separated by amorphous layers. This model holds in the case of stacks of parallel lamellae, densely packed and isotropically distributed. The γ(r) function of the electron density heterogeneities for a single stack of the ideal lamellar model varies in one

direction (x-direction) [21]. The γ(r) function in the x-direction can be obtained by the cosine transformation of the Lorentz-corrected SAXS intensity profiles according Equation (25) (shown in experimental part). Figure 43 presents the linear correlation γ(r) function of as processed PVDF and relaxed samples. The structural parameters (long period L_p, crystalline lamellar thickness L_c, amorphous thickness L_a, interface thickness, non-ideality parameter and linear crystallinity) were calculated from γ(r) function according to the procedure detailed in the experimental part.

The long period (L_p) was determined from the position of the first maximum in the γ(r) function (see Figure 44). The L_{pmin} values were determined as twice the value obtained from the first minimum of the γ(r) function. Other important parameters such as average crystalline lamellae thickness L_c, average amorphous thickness L_a, average interface thickness (IT), non-ideality parameter (NI) and linear crystallinity (χ) were obtained by γ(r) function and the values are summarized in Table 7. Moreover, the calculated parameters are compared in Figures 45 - 47.

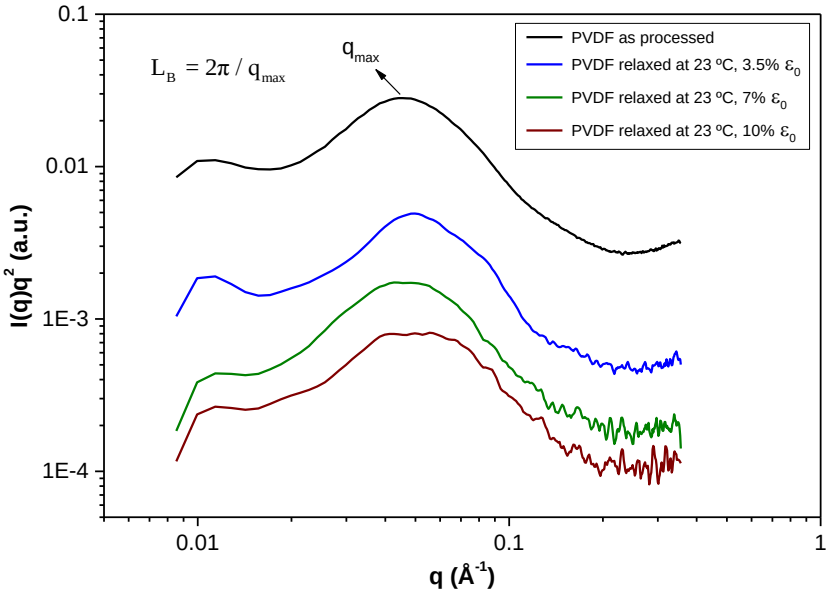

(a) PVDF relaxed at 23 ºC

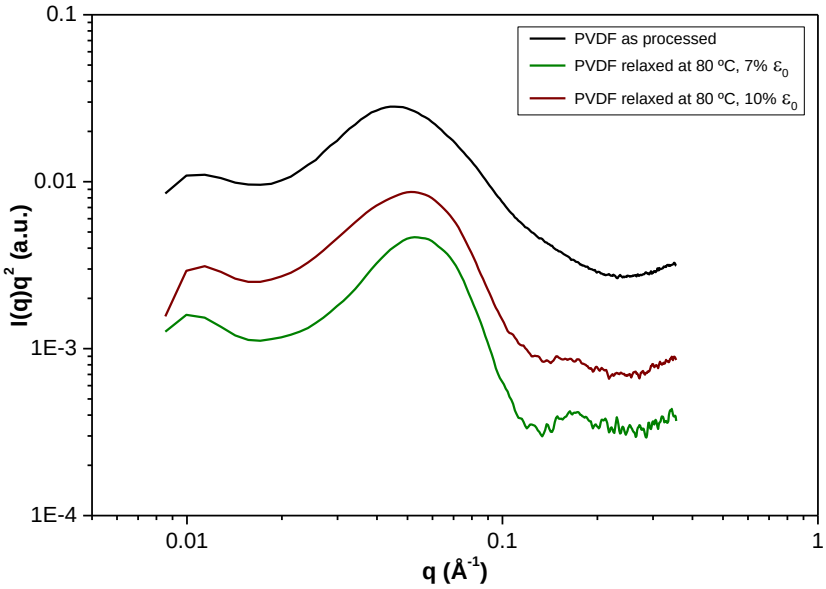

(b) PVDF relaxed at 80 ºC

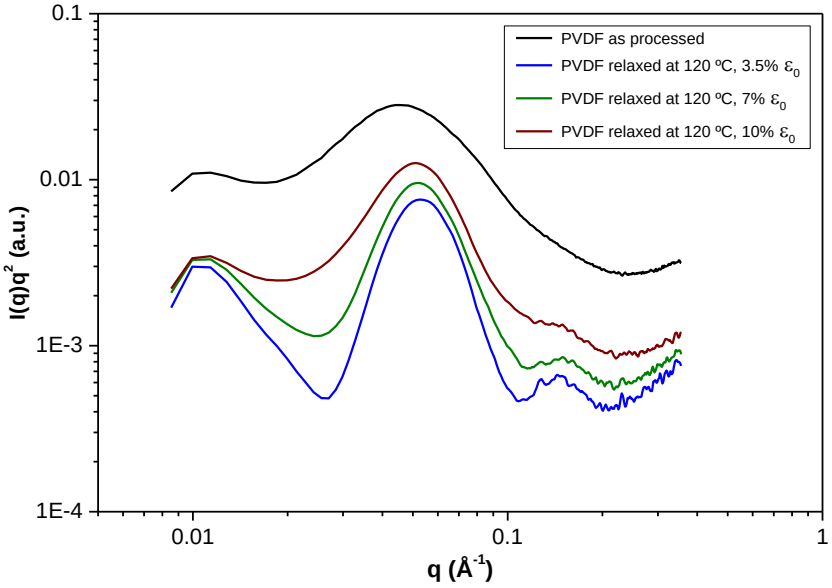

(c) PVDF relaxed at 120 ºC

Figure 42. Lorentz-corrected SAXS intensity profiles for as processed PVDF and samples relaxed at (a) 23 ºC, (b) 80 ºC and (c) 120 ºC.

Table 6. Long period deduced from Bragg's law and average domain size.

Sample	L_B (nm)	Average domain size (nm)
PVDF as processed	13.8	36.9
PVDF relaxed at 23 ºC, 3.5% ε_0	12.6	39.0
PVDF relaxed at 23 ºC, 7% ε_0	12.3	33.4
PVDF relaxed at 23 ºC, 10% ε_0	12.7	30.1
PVDF relaxed at 80 ºC, 7% ε_0	12.3	41.2
PVDF relaxed at 80 ºC, 10% ε_0	12.3	38.9
PVDF relaxed at 120 ºC, 3.5% ε_0	11.9	46.8
PVDF relaxed at 120 ºC, 7% ε_0	12.3	46.4
PVDF relaxed at 120 ºC, 10% ε_0	12.3	44.7

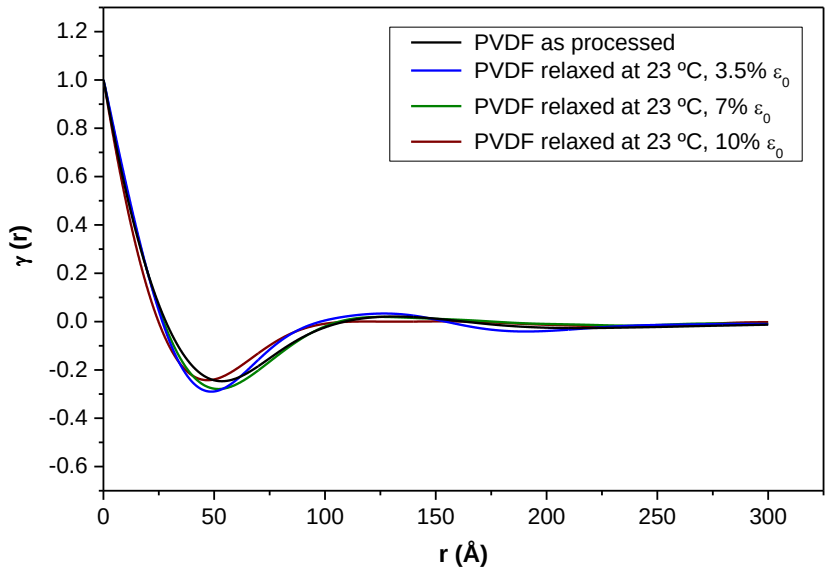

(a) PVDF relaxed at 23 ºC

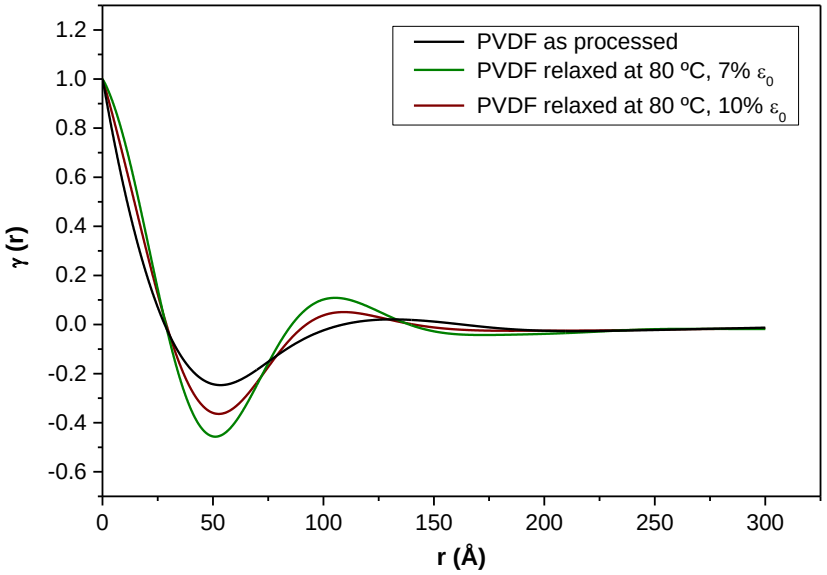

(b) PVDF relaxed at 80 ºC

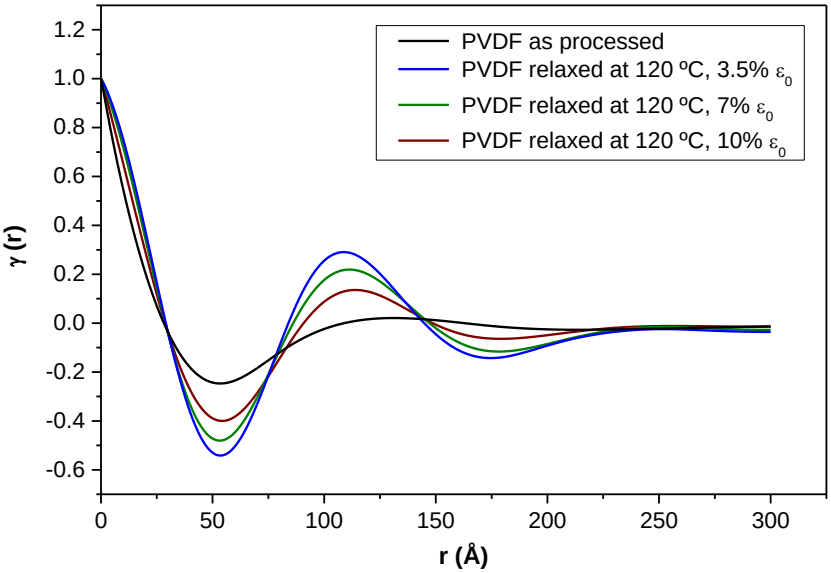

(c) PVDF relaxed at 120 ºC

Figure 43. Linear correlation γ(r) function for as processed PVDF and samples relaxed at (a) 23 ºC, (b) 80 ºC and (c) 120 ºC.

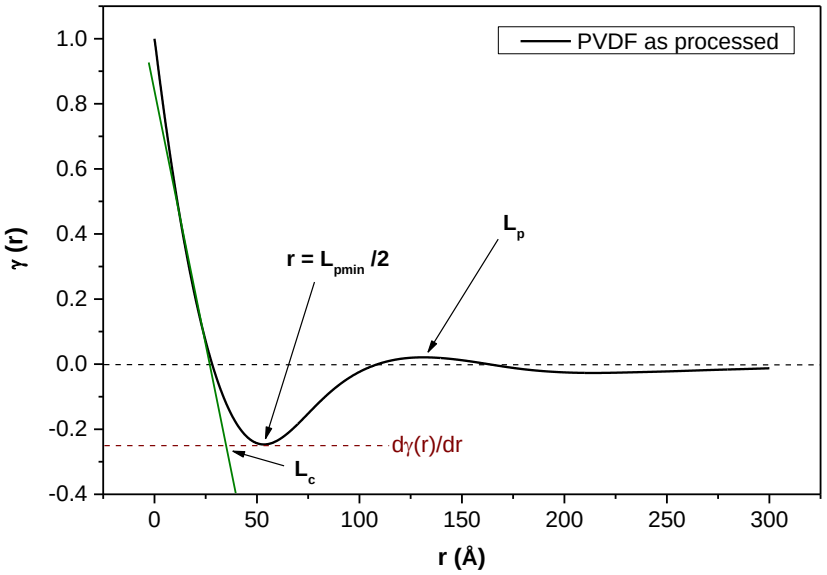

Figure 44. Linear correlation γ(r) function for as processed PVDF.

The long period (L_p), average amorphous thickness (L_a), average crystalline lamellae thickness (L_c) and average interface thickness (IT) values obtained for as processed PVDF were 13.1 nm, 7 nm, 3.7 nm and 1.3 nm, respectively (Table 7). Martins *et al.* [79] reported values of L_p, L_a, L_c and IT (calculated by the linear correlation γ(r) function) for PVDF, around 10 nm, 5.3 nm, 3.2 nm, and 1.2 nm, respectively. Likewise, Fatnassi *et al.* [76] found values of L_p, L_a, L_c and IT about 11 nm, 4.2 nm, 6 nm and 1 nm for PVDF, which was calculated from linear correlation γ(r) function method as well.

- In general, it can be noted that the relaxed samples presented lower values of long period L_p and the average amorphous thickness L_a (see Figure 45 - 47). In the cases of the long period L_p, for stress relaxation at 23 ºC, the reduction of this parameter was between 6 - 10%, showing that the long period decreased with the increase of stress relaxation temperature. The L_p obtained for samples relaxed at 80 and 120 ºC (10.5 - 11.4 nm) decreased between 13 - 20% compared with as processed PVDF. However, it is important to note that for higher temperatures (80 and 120 ºC), higher values of long period were obtained with the increase of the applied strain.
- The same behavior could be observed for amorphous thickness L_a. It can be observed that L_a decreased for relaxed samples (6 - 13% reduction). Besides, as the case

of L_p, the values of amorphous thickness L_a of samples relaxed at higher temperatures (80 and 120 ºC) increased with the increase of the strain.

- On the other hand, in the case of crystalline lamellae thickness L_c, relaxed samples at lower temperatures (23 ºC) showed slightly lower values of L_c. However, the reduction of Lc was not a significant change (considering an experimental error of 5%). In contrast, the values of L_c increased for stress relaxation at higher temperatures (80 and 120 ºC), reaching a maximum of 4.3 nm for stress relaxation at 120 ºC and 3.5% strain. The increase of L_c at higher temperatures was between 7 - 13%. Moreover, the average interface thickness (IT) presented a similar trend as the crystalline lamellae thickness L_c (as shown in Figure 45 - 47). It can be observed that values of interface thickness were practically the same for samples relaxed at lower temperature (23 ºC). Nevertheless, for high temperatures (80 and 120 ºC), higher interface thickness were obtained. The increase of interface thickness was about 13 - 32%.
- In Table 7 were presented the values of linear crystallinity (χ) within the lamellar stacks. Relaxed samples at lower temperature (23 ºC) showed almost the same values of linear crystallinity than as processed PVDF. However, higher values of linear crystallinity were obtained for samples relaxed at higher temperatures (80 and 120 ºC), showing a maximum of 40% for stress relaxation at 120 ºC and 3.5% strain. It was expected due to the increase in L_c at higher stress relaxation temperature. In addition, the non-ideality parameter was also calculated from $\gamma(r)$ function, and can be used as the value of the deviation from an ideal two-phase model. The samples relaxed at 80 and 120 ºC display smaller values of the NI parameters which indicate that they are closer to the ideal two-phase model than the samples relaxed at 23 ºC and as processed PVDF.

Overall, the results shows decrease of L_p induced by the stress relaxation process, showing lower values for higher stress relaxation temperature. The decrease of L_p was attributed to the decrease of amorphous layer thickness L_a, as a result of the chains recoil. With regard to L_c, this parameter did not change for stress relaxation at lower temperature (23 ºC). Nevertheless, at higher temperatures (80 and 120 ºC) the results suggest the growth of the thickness of crystalline layer induced by temperature occurs at expense of the amorphous layer thickness. Therefore, under these conditions (higher stress relaxation temperature), the interface thickness and the linear crystallinity within the lamellar stacks increased. Although, there was growth of the lamellar crystalline thickness at higher temperatures, it is important pointing out that the decrease in the amorphous thickness had a predominant effect on the reduction of long period.

Additionally, it is worth noting that long period deduced by Bragg's law was higher than those values found from the linear correlation γ(r) function. It could be explained considering that the Bragg long period would include the thickness of amorphous material outside the stacks in which it is embedded [17]. Therefore, the structural parameters (L_p, L_c and L_a) obtained from function γ(r) analysis are assumed to be more realistic.

Table 7. Structural parameters obtained by linear correlation γ(r) function.

Sample	L_p (nm)	L_a (nm)	L_c (nm)	IT (nm)	NI	χ (%)
PVDF as processed	13.1	7.0	3.7	1.3	0.04	35
PVDF relaxed at 23 ºC, 3.5% ε_0	12.7	6.3	3.6	1.3	0.05	36
PVDF relaxed at 23 ºC, 7% ε_0	12.5	6.7	3.7	1.3	0.03	35
PVDF relaxed at 23 ºC, 10% ε_0	11.8	6.1	3.4	1.2	0.04	36
PVDF relaxed at 80 ºC, 7% ε_0	10.5	6.2	4.0	1.6	0.001	39
PVDF relaxed at 80 ºC, 10% ε_0	10.9	6.6	4.0	1.5	0.001	38
PVDF relaxed at 120 ºC, 3.5% ε_0	10.9	6.4	4.3	1.7	0	40
PVDF relaxed at 120 ºC, 7% ε_0	11.1	6.5	4.1	1.6	0.002	39
PVDF relaxed at 120 ºC, 10% ε_0	11.4	6.9	4.0	1.5	0.002	37

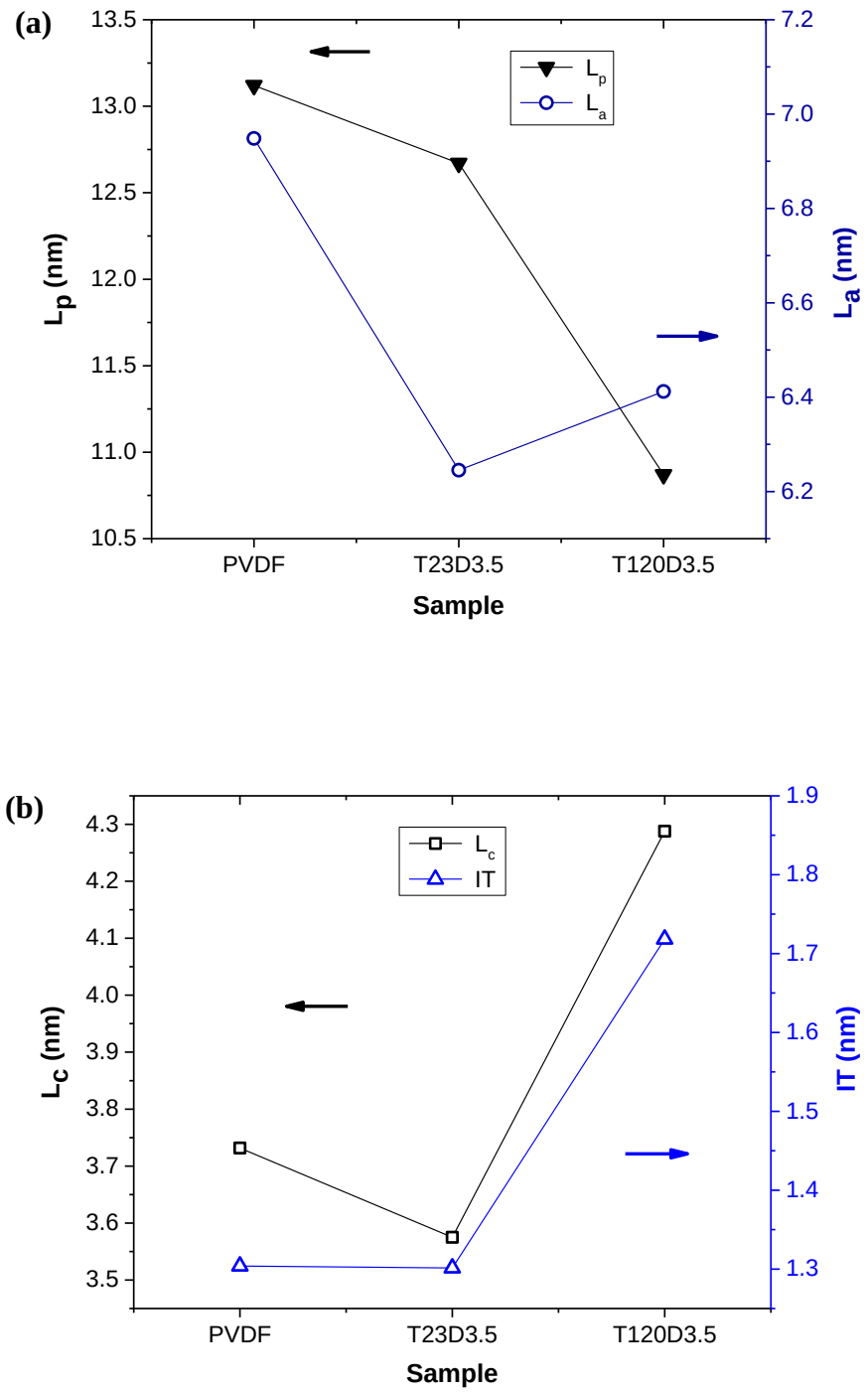

Figure 45. SAXS parameters: (a) long period (L_p), average amorphous layer thickness (L_a); (b) average crystalline layer thickness (L_c), average interface thickness (IT). Samples T23D3.5: PVDF relaxed at 23 °C and 3.5% ε_0; T80D3.5: PVDF relaxed at 80 °C and 3.5% ε_0 and T120D3.5: PVDF relaxed at 120 °C and 3.5% ε_0.

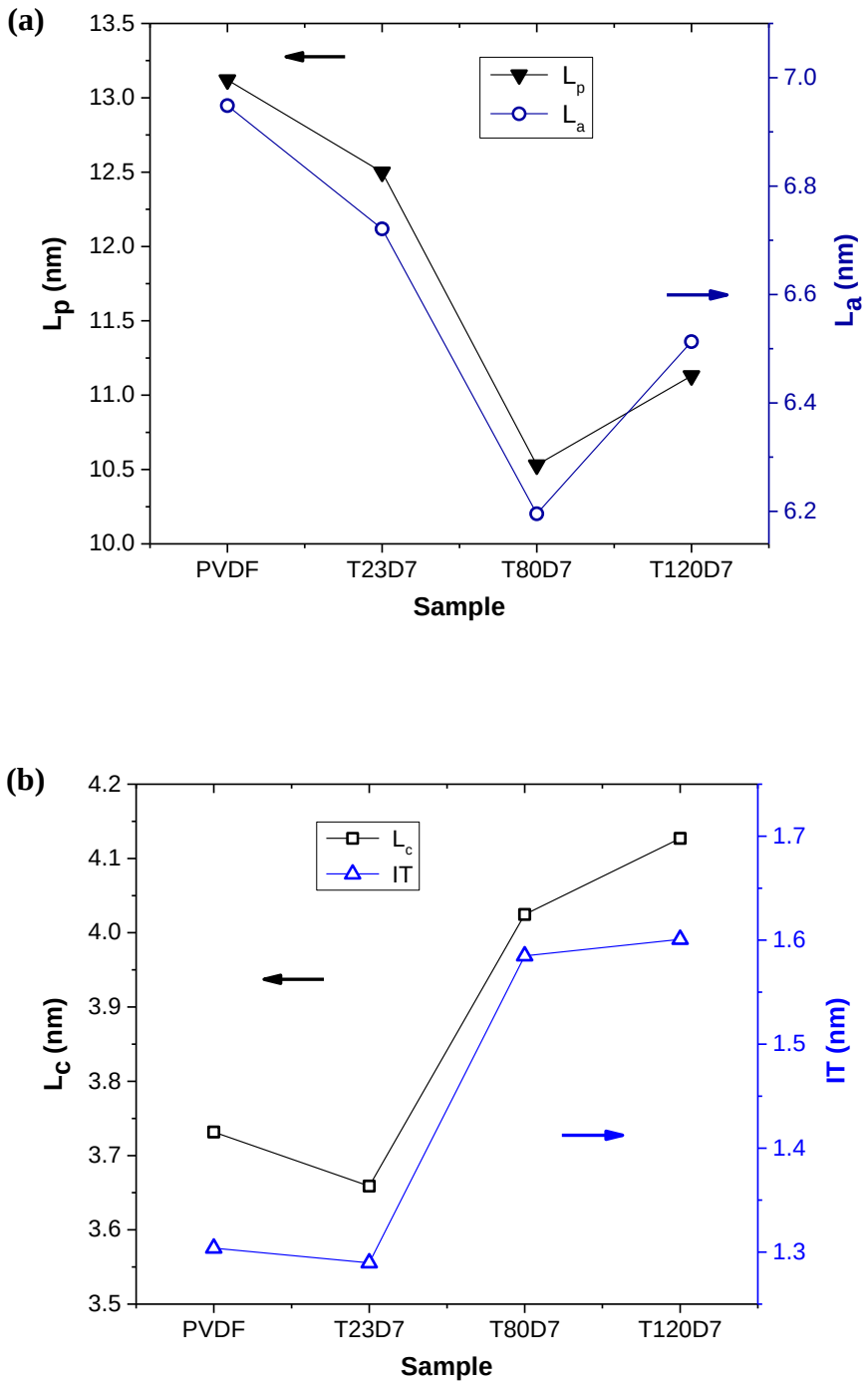

Figure 46. SAXS parameters: (a) long period (L_p), average amorphous layer thickness (L_a); (b) average crystalline layer thickness (L_c), average interface thickness (IT). Samples T23D7: PVDF relaxed at 23 °C and 7% ε_0; T80D7: PVDF relaxed at 80 °C and 7% ε_0 and T120D7: PVDF relaxed at 120 °C and 7% ε_0.

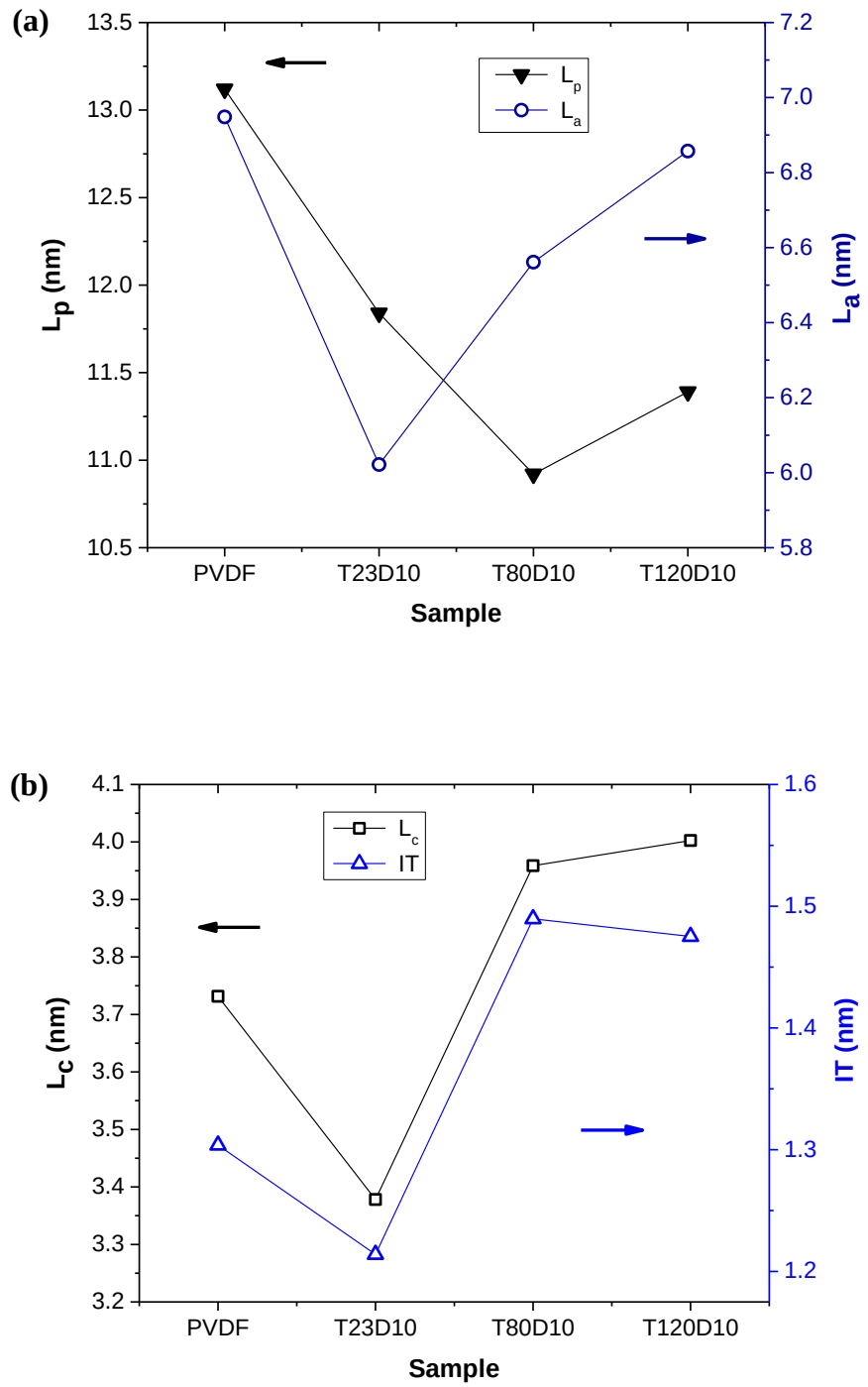

Figure 47. SAXS parameters: (a) long period (L_p), average amorphous layer thickness (L_a); (b) average crystalline layer thickness (L_c), average interface thickness (IT). Samples T23D10: PVDF relaxed at 23 °C and 10% ε_0; T80D10: PVDF relaxed at 80 °C and 10% ε_0 and T120D10: PVDF relaxed at 120 °C and 10% ε_0.

4.7. Influence of structural modifications on elastic modulus

4.7.1. Morphological changes detected by NMR

The as processed PVDF showed an elastic modulus (E) of 1292 MPa and f_{inter} around 41%. The stress relaxation at 23 and 80 ºC strained to 3.5% resulted in an increase of the f_{inter} to about 52%, and the elastic modulus dropped to 951 MPa, a 30% reduction in modulus for 27% increase in the intermediate region (as observed in Figure 48). As the material was relaxed at 120 ºC at 3.5% strain, the elastic modulus was reduced to 724 MPa (45% drop), and f_{inter} was raised 59%, showing a very strong dependency between the elastic modulus and its structural modification. The stress relaxation at 7% strain, for all stress relaxation temperatures tested in this work, f_{inter} was about 54%, and the elastic modulus tended to be in between 720 to 800 MPa. On the other hand, in the case of stress relaxation at 10% strain, the elastic modulus presented the same value as the 7% strain or a tendency of slight increase, and f_{inter} decreased its value, when compared to the previous deformation at the same temperature; in fact, the f_{inter} for the PVDF relaxed at 23 ºC and 10% strain was quite close to the value measured in the as processed material, while for the samples relaxed at 120 ºC this value increased 52%. Generally, it was observed that the drop in the elastic modulus could be correlated to the increase in the fraction of the intermediate region (f_{inter}) or a decrease in the rigid region (crystalline fraction), once mobile region was not changed.

It is shown in Figure 48 that stress relaxation process produced a reduction in the fraction of the rigid region (crystalline phase), increase in the intermediate region and no alteration in the mobile region. Under this condition, damage is generated in the material and the elastic modulus is the property most affected by it. In order to explain this behavior, the following proposal might be used for the structural evolution: as the material is stress relaxed, the polymer chains are pulled-out of the crystalline lamellae. The higher the temperature and the strain imposed, the lower becomes the crystalline region fraction, resulting in more amount of the constrained amorphous phase (intermediate region), as measured here.

In addition, at the end of stress relaxation test, the material is cooled down, and there is a partial chain recoil, particularly at constrained amorphous phase (intermediate region). Upon tensile testing the relaxed material, the recoiled chains can be stretched up with lower resistance to the imposed force, resulting in the lower elastic modulus

measured. This structure configuration explains the drop in elastic modulus and the nil influence of the stress relaxation on the tensile strength, while the elongation at break was quite reduced.

Many research about structural features have been conducted in severe plastic deformation [22, 68], mostly using tensile test. However, the structural evolution after stress relaxation had not been deeply studied. In this work, it was demonstrated that the combined effect of very small strain, time and low temperatures (such as stress relaxation at 23 ºC, at 3.5% strain, during 24 h), was able to strongly affect the material structure and its elastic modulus (with a drop of about 30%).

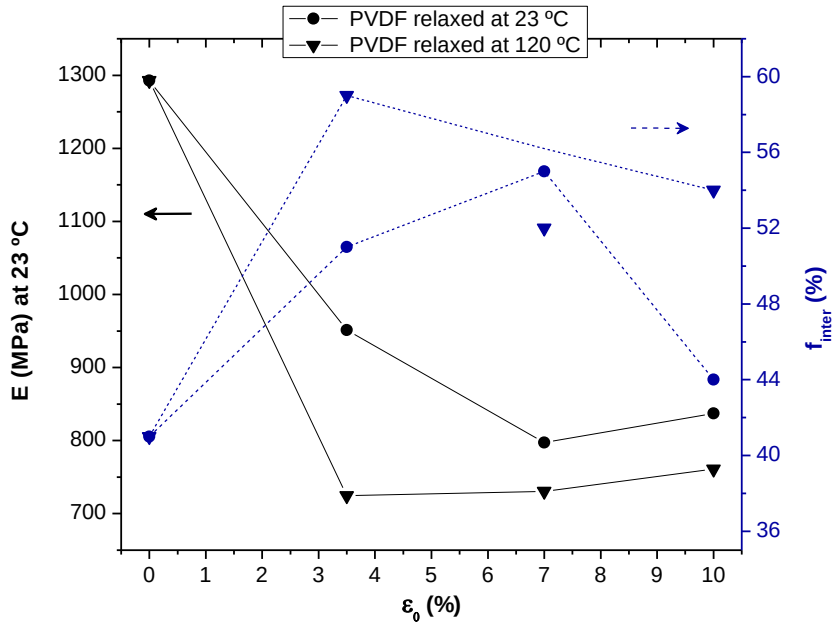

Figure 48. Correlation between elastic modulus (E) and fraction of the intermediate region (f_{inter}) after stress relaxation test.

4.7.2. Morphological changes detected by SAXS

Based on the results of structural parameters by SAXS, the structural evolution as results of the stress relaxation can be described in a morphological model shown in Figure 49.

Stress relaxation test consisted in subjected the specimen to a load up to a given strain value. Strain is maintained constant, and then stress decays with the test time. Thus, it can be considered that a first stage of the test is the stretching of the chains. This process stretches mainly the amorphous layers in a first stage, forcing mechanically the alignment of the polymer chains gradually in the interface. Thus, the long period would increase with strain increasing. Considering that the increase of long period depends mainly on extension of the chains in the amorphous layers between crystalline lamellae. On the other hand, a second stage consists of the stress relaxation process. Stress relaxation occurs by slow slipping of the chains to each other and by mechanical unwinding of the chains in the constrained region. Therefore, the long period decreases with stress decays due to the increase in the interface (IT) region. Thus, the decrease in the long period with the stress relaxation could indicate a partial reorganization of the amorphous layers within lamellar stacks.

The similar evolution character was found by Liu *et al.* [90] for step-cycle deformation (loading and unloading) tests at 28 ºC of poly(ethylene succinate). The L_p, L_a and L_c increases and decreases upon loading and unloading. The results showed that the major part of the long period variation during the step-cycle deformation originated from the amorphous phase. And L_c and L_a showed similar evolution character as L_p.

In this study, the evolution of the long period and crystalline and amorphous components as a result of stress relaxation is shown in Figure 49. Stress relaxation causes decrease in the long period and amorphous layer thickness, meanwhile the crystalline lamellae thickness is not affected at lower stress relaxation temperature (23 ºC). Furthermore, at high temperatures (80 and 120 ºC) the results suggest the growth of the thickness of crystalline layer due to crystallization by temperature activation. During crystallization the chains are pulled from the amorphous layers, in consequence the reduction of amorphous layer thickness is observed. The decrease of long period is also detected at high temperatures. These structural modifications indicate that the decrease of long period depends mainly on the reduction of amorphous layers thickness. The structural changes of PVDF induced by stress relaxation were represented in Figure 50.

This behavior was proposed from analysis based on the structural characterization of the polymer.

- The proposed model was suggested for investigating the variation of crystalline lamellae thickness with the drop in elastic modulus. Figure 51 presents the correlation between elastic modulus and thickness of crystalline lamellae. It can be clearly noted that at lower temperature the crystalline lamellae thickness did not change, but at higher temperatures it increases with decrease in elastic modulus. As already showed, overall, for the as processed PVDF with an elastic modulus of 1292 MPa, the average crystalline lamellae thickness is 3.7 nm. Relaxed PVDF showed a decrease of elastic modulus to 951 MPa - 724 MPa (30 - 45% drop). On the other hand, it could be detected that the crystalline lamellae thickness of samples varies only at higher temperatures, it increases to 4 - 4.3 nm (7 - 13% increase).

The crystalline lamellar thickness is an important parameter influencing the mechanical properties. The crystalline lamellar thickness is related to the rigidity (elastic modulus) of the material. Thus, the decrease of crystalline lamellar thickness as result of elastic modulus drop was expected, however, it was not observed here. The present work has demonstrated that the results obtained only from crystalline lamellar thickness cannot be relevant for prediction of the elastic behavior. And, therefore, the variation of crystalline phase fraction detected by NMR was more crucial to explain a lower modulus for PVDF induced by stress relaxation.

It appears from this work that the measurements by SAXS technique of the variation of the long period and crystalline and amorphous thickness induced by stress relaxation are a valuable method in order to characterize the nature of the polymer chains. Therefore, it is important to underline the measurement not only on the lamellae thickness but also on the crystalline phase region by complementary techniques.

Additionally, it is worth noting that, the differences in domain sizes estimated using SAXS and NMR methods hints at the existence of the constrained amorphous region within the spherulites. It should be mentioned that the NMR technique provides the total fraction of the rigid (crystalline), intermediate (constrained amorphous) and mobile (amorphous) regions in the polymer. The rigid-crystalline domain is composed of fibrils formed by stacks of crystalline lamellar and amorphous interlamellar regions. SAXS technique measured the thickness of the lamellar stacks inside the fibrils. Thus, the NMR method reveals increase of constrained amorphous region (f_{int}) at expense of the crystallinity, and SAXS reveals the increase of crystalline lamellar thickness (L_c) at

higher temperatures and that this parameter do not vary at lower temperatures, as result of the stress relaxation.

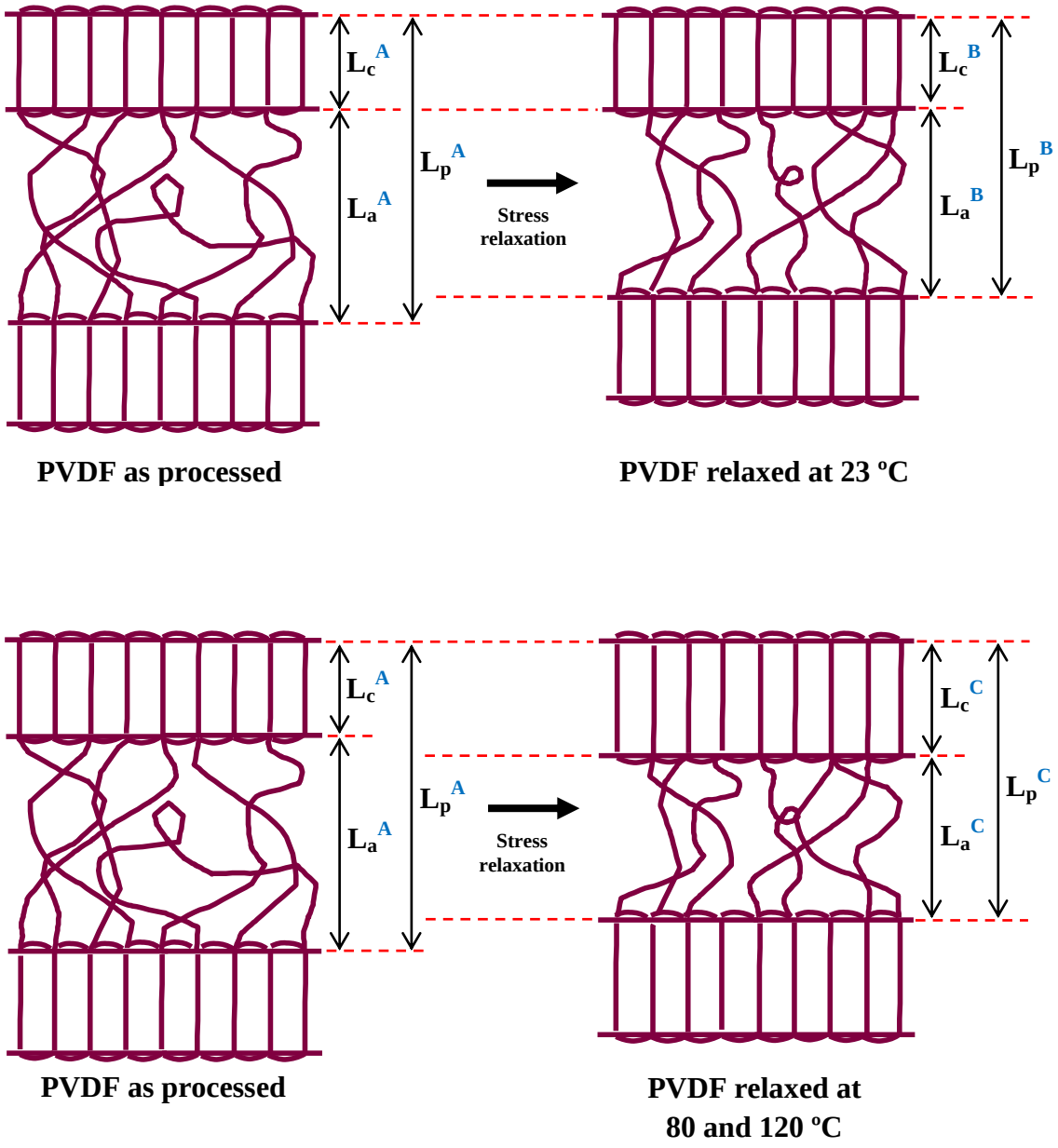

Figure 49. Structural parameters changes induced by stress relaxation. L_p: long period ($L_p^A > L_p^B, L_p^C$), L_a: average amorphous layer thicknes ($L_a^A > L_a^B, L_a^C$), L_c: average crystalline layer thickness ($L_c^A \sim L_c^B$; $L_c^A < L_c^C$).

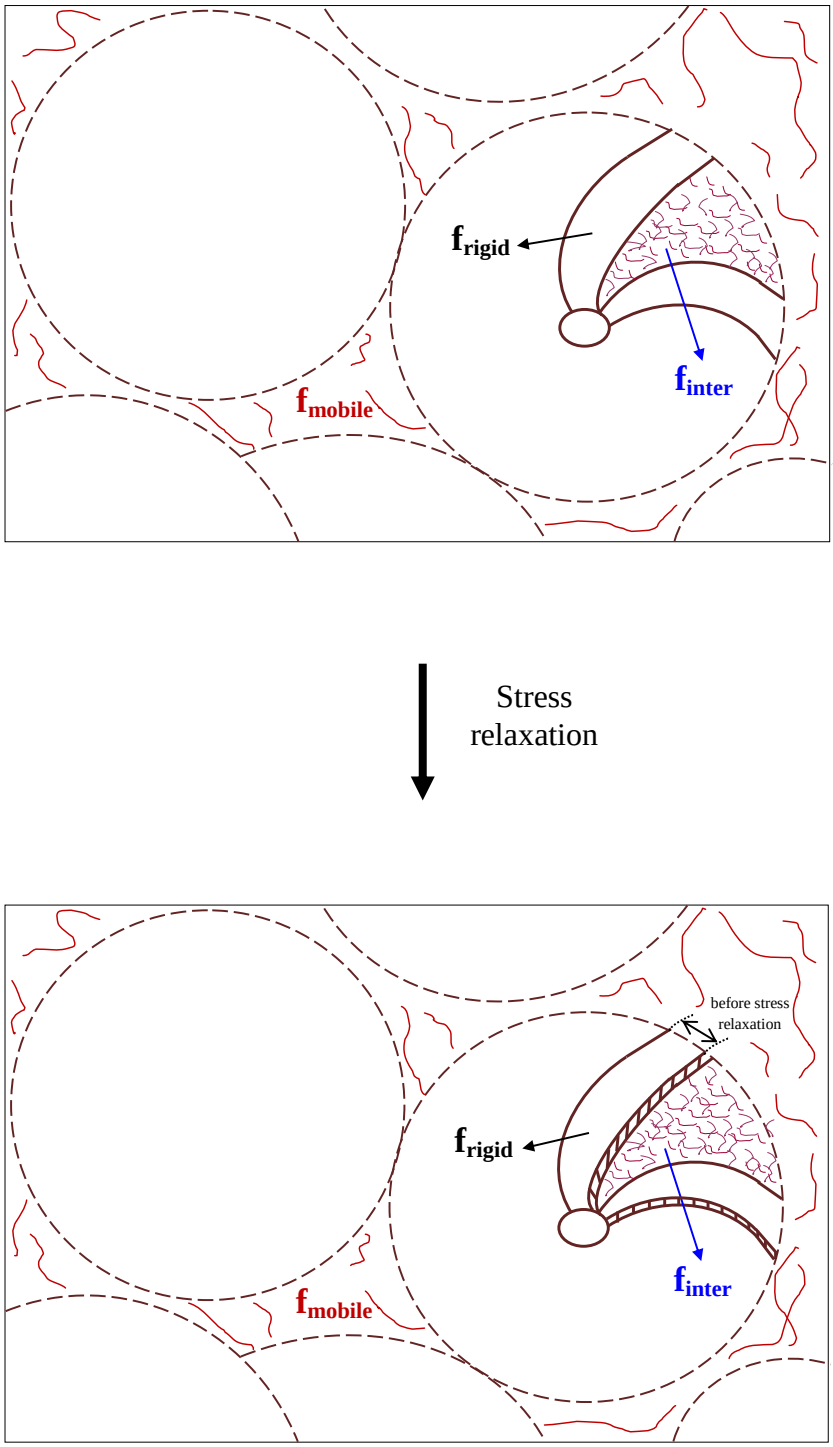

Figure 50. Structural evolution of PVDF induced by stress relaxation.

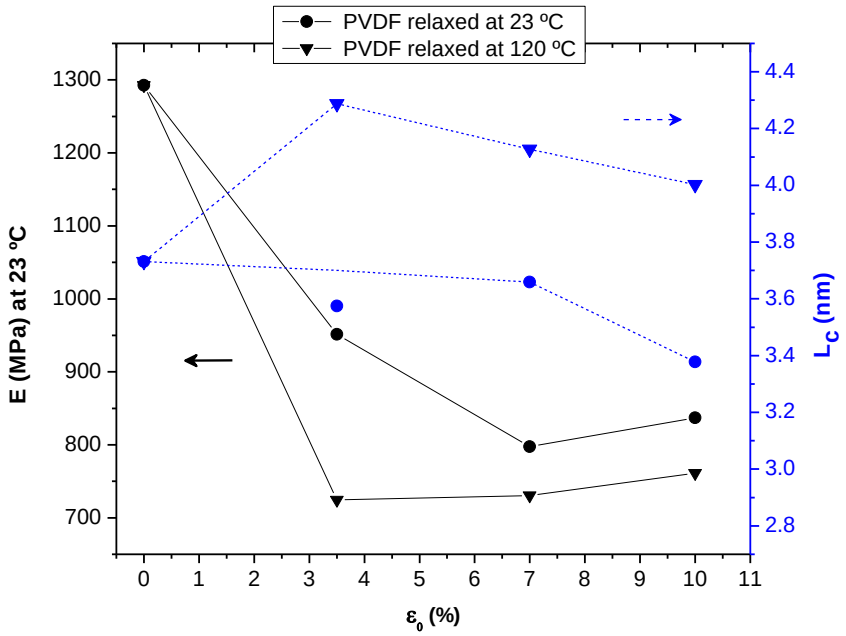

Figure 51. Correlation between elastic modulus (E) and crystalline lamellar thickness (L_c) after stress relaxation test.

Chapter 5

Conclusions

A series of studies have been carried out in this thesis to characterize structure-property relationships for PVDF induced by stress relaxation. This study permitted a better understanding of the structural modifications that were responsible for a particular mechanical behavior.

Solid-state NMR technique provided valuable information about the molecular scale phenomena and allowed to explain possible changes in morphology that are caused by the stress relaxation process. The crystalline fraction values detected by NMR decreased for all relaxed samples, while the constrained amorphous phase increases in fraction at the expense of the crystallinity. There was no variation in the free amorphous phase fraction of relaxed samples, indicating that the stress relaxation induces only the migration of chain segments from the crystalline phase to the constrained amorphous phase, whereas the free amorphous region remains unchanged.

It has shown that the elastic modulus is strongly dependent on the morphological changes. Comparing the elastic modulus obtained from tensile tests and the morphology from NMR and SAXS, a model structure-property investigation has been presented. The mechanical behavior of the polymer is closely related to the fraction of the crystalline, constrained amorphous and free amorphous phases present in the material. The change observed among these regions presents was ascribed to be responsible for the reduction of about 30 to 45% in elastic modulus after stress relaxation.

The structural characterization by means of SAXS mainly point that the stress relaxation process involves the reduction of long period and amorphous layer thickness between lamellae as a result of the chains recoil. Moreover, at lower stress relaxation temperatures, the crystalline thickness remained constant indicating that there is no crystal thickening during the stress relaxation process. Nonetheless, the increase in stress relaxation temperature has produced higher crystalline thickness values characterized by thick lamellar structures, due to crystallization induced by temperature.

The elastic modulus was affected in a significant way by the amount of amorphous constrained region within the spherulites and decrease of crystalline region detected by NMR. However; the variation (increase at higher temperatures) of crystalline lamellar thickness, measured from SAXS, did not affect the development of elastic modulus. Therefore, it can be said that drop of elastic modulus depended mainly on decrease of the crystalline fraction in the polymer. Thus, the present study demonstrates that solid-state NMR and SAXS methods provide complementary information about molecular-scale phenomena and changes in morphology that are caused by stress relaxation of PVDF.

The DMA measurements demonstrated that the β'-transition temperature was displaced at higher temperatures indicating that the stress relaxation increase the amount of amorphous region within the spherulites, namely constrained amorphous or intermediate region. On the other hand, the DSC was not able to detect any change in crystalline fraction for the PVDF tested here while NMR was. Furthermore, the DSC showed that the stress relaxation did not affect the melting and crystallization temperature confirming the stability of the crystal structure under the tests conditions used here.

References

[1] CONTRERAS, M., RABELLO, C., CUCINELLI, R., et al., 2018, "TD-NMR analysis of structural evolution in PVDF induced by stress relaxation", *Polymer Testing*, v. 68, pp. 153–159.

[2] VINOGRADOV, A., HOLLOWAY, F. , 2000, "Dynamic mechanical testing of the creep and relaxation properties of polyvinylidene fluoride," *Polymer Testing*, v. 19, n. 2, pp. 131–142.

[3] ALCHIKH, M., FOND, C., FRÈRE, Y., 2010, "Discontinuous crack growth in poly (vinyl fluoride) by mechanochemical ageing in sodium hydroxide", *Polymer Degradation and Stability*, v. 95, n. 4, pp. 440–444.

[4] REIS, J. M. L., MOTTA, E. P., DA COSTA MATTOS, H. S. , 2015, "Elasto-viscoplastic behaviour of a polyvinylidene fluoride (PVDF) in tension" , *Polymer Testing*, v. 46, pp. 9–13.

[5] SENCADAS, V., COSTA, C. M., GÓMEZ, J. L., et al., 2010, "Isothermal crystallization kinetics of poly(vinylidene fluoride) in the α-phase in the scope of the Avrami equation", *Journal of Materials Science*, v. 45, n. 5, pp. 1328–1335.

[6] DOS SANTOS, W. N., IGUCHI, C. Y., GREGORIO, R., 2008, "Thermal properties of poly(vinilidene fluoride) in the temperature range from 25 to 210 °C", *Polymer Testing*, v. 27, n. 2, pp. 204–208.

[7] FRYCZKOWSKI, R., FRYCZKOWSKA, B., BINIAŚ, W., et al., 2013,"Morphology of fibrous composites of PLA and PVDF" , *Composites Science and Technology*, v. 89, pp. 186–193.

[8] SAJKIEWICZ, P., WASIAK, A., GOCLOWSKI, Z., 1999, "Phase transitions during stretching of poly(vinylidene fluoride)", *European. Polymer Journal*, v. 35, n. 3, pp. 423–429.

[9] MANDAL, A., NANDI, A. K., 2011, "Physical properties of poly(vinylidene fluoride) composites with polymer functionalized multiwalled carbon nanotubes using nitrene chemistry", *Journal of Materials Chemistry*, v. 21, n. 39, pp. 15752–15763.

[10] SONG, R., XIA, G., XING, X., et al., 2013, "Modification of polymorphisms in polyvinylidene fluoride thin films via water and hydrated salt", *Journal of Colloid and Interface Science*, v. 401, pp. 50–57.

[11] MANO, J. F., SENCADAS, V., COSTA, A. M., et al., 2004, "Dynamic mechanical analysis and creep behaviour of β-PVDF films", *Materials Science and Engineering: A*, v. 370, n. 1–2, pp. 336–340.

[12] SENCADAS, V., LANCEROS-MÉNDEZ, S., SABATER, R., et al., 2012, "Relaxation dynamics of poly(vinylidene fluoride) studied by dynamical mechanical measurements and dielectric spectroscopy", *The European Physical Journal E*, v. 35, n. 5, pp. 1–11.

[13] ANDREASSEN, E., 1999, "Stress relaxation of polypropylene fibres with various morphologies", *Polymer (Guildf)*, v. 40, n. 14, pp. 3909–3918.

[14] BAEURLE, S. A., HOTTA, A., GUSEV, A. A., 2005, "A new semi-phenomenological approach to predict the stress relaxation behavior of thermoplastic elastomers", *Polymer (Guildf)*, v. 46, n. 12, pp. 4344–4354.

[15] BEZAZI, A., FRIOUI, N., SCARPA, F., 2011, "Tensile static, fatigue and relaxation behaviour of closed cell electret PVDF foams", *Mechanics of Materials*, v. 43, n. 9, pp. 459–466.

[16] ZHOU, H., 1997, *Structure-property relationships: model studies on melt extruded uniaxially oriented high density polyethylene films having well defined morphologies*. Ph.D. dissertation, Virginia Polytechnic Institute and State University, Blacksburg, USA.

[17] FATNASSI, M., BEN CHEIKH LARBI, F., DUBAULT, A., HALARY, J. L., 2005, "Structural study of semi-crystalline blends of poly(vinylidene fluoride) and poly(methyl methacrylate) by means of linear correlation and interface distribution functions", *E-Polymers*, n. 056, pp. 1–17.

[18] SCHÄLER, K., ROOS, M., MICKE, P., et al., 2015, "Basic principles of static proton low-resolution spin diffusion NMR in nanophase-separated materials with mobility contrast", *Solid State Nuclear Magnetic Resonance*, v. 72, pp. 50–63.

[19] ROOS, M., SCHÄLER, K., SEIDLITZ, A., et al., 2014, "NMR study of interphase structure in layered polymer morphologies with mobility contrast: Disorder and confinement effects vs. dynamic heterogeneities", *Colloid and Polymer Science*, v. 292, n. 8, pp. 1825–1839.

[20] ZHOU, H., WILKES, G. L., 1998, "Orientation-dependent mechanical properties and deformation morphologies for uniaxially melt-extruded high-density polyethylene films having an initial stacked lamellar texture", *Journal of Materials Science*, v. 33, n. 2, pp. 287–303.

[21] CHINAGLIA, D. L., RINALDO GREGÓRIO, J., VOLLET, D. R., 2012, "Structural Modifications in Stretch-Induced Crystallization in PVDF Films as Measured by Small-Angle X-ray Scattering", *Journal of Applied Polymer Science*, v. 151, n. 7, pp. 527–535.

[22] DEFEBVIN, J., BARRAU, S., STOCLET, G., et al., 2016, "In situ SAXS/WAXS investigation of the structural evolution of poly(vinylidene fluoride) upon uniaxial stretching", *Polymer (United Kingdom)*, v. 84, pp. 148–157.

[23] DU, C. H., ZHU, B. K., XU, Y. Y., 2005, "A study on the relationship between the crystal structure and hard elasticity of PVDF fibers", *Macromolecular Materials and Engineering*, v. 290, n. 8, pp. 786–791.

[24] WU, J., SCHULTZ, J. M., YEH, F., et al., 2000, "In-situ simultaneous synchrotron small- and wide-angle X-ray scattering measurement of poly(vinylidene fluoride) fibers under deformation", *Macromolecules*, v. 33, n. 5, pp. 1765–1777.

[25] BASSETT, D. C., 2006, "Linear nucleation of polymers", *Polymer (Guildf)*, v. 47, n. 15, pp. 5221–5227.

[26] GIRARD, D., CASTAGNET, S., GACOUGNOLLE, J. L., et al., 2007, "On the relevance of a notch creep test for the comprehension and prediction of slow crack growth in PVDF", *Polymer Testing*, v. 26, n. 7, pp. 937–948.

[27] PETERLIN, A., 1987, "Drawing and extrusion of semi-crystalline polymers", *Colloid and Polymer Science*, v. 265, n. 5, pp. 357–382.

[28] GUNEY, H. Y., 2005, "Elastic properties and mechanical relaxation behaviors of PVDF (poly (vinylidene fluoride)) at temperatures between -20 and 100°C and at 2 MHz ultrasonic frequency", *Journal of. Polymer Science Part B: Polymer Physics*, v. 43, n. 20, pp. 2862–2873.

[29] TEYSSEDRE, G., BERNES, A., LACABANNE, C., 1993, "Influence of the crystalline phase on the molecular mobility of PVDF", *Journal of. Polymer Science Part B: Polymer Physics*, v. 31, n. 13, pp. 2027–2034.

[30] EL MOHAJIR, B. E., HEYMANS, N., 2001, "Changes in structural and mechanical behaviour of PVDF with processing and thermomechanical treatments. 1. Change in structure", *Polymer (Guildf)*, v. 42, n. 13, pp. 5661–5667.

[31] LI, M., WONDERGEM, H., SPIJKMAN, M., *et al.*, 2013, "Revisiting the δ-

phase of poly(vinylidene fluoride) for solution-processed ferroelectric thin films", *Nature Materials*, v. 12, n. 5, pp. 433–438.

[32] IMAMURA, R., SILVA, A. B., GREGORIO, J. R., 2008, "Gamma-beta Phase Transformation Induced in Poly(vinylidene fluoride) by Stretching", *Journal of Applied Polymer Science*, v. 110, pp. 3242–3246.

[33] BOTELHO, G., LANCEROS-MENDEZ, S., GONÇALVES, A. M., et al., 2008, "Relationship between processing conditions, defects and thermal degradation of poly(vinylidene fluoride) in the β-phase", *Journal of Non-Crystalline Solids*, v. 354, n. 1, pp. 72–78.

[34] GREGORIO, R., CESTARI, M., 1994, "Effect of crystallization temperature on the crystalline phase content and morphology of poly(vinylidene fluoride)", *Journal of. Polymer Science Part B: Polymer Physics*, v. 32, n. 5, pp. 859–870.

[35] ESTERLY, D., 2002, *Manufacturing of Poly (vinylidene fluoride) and Evaluation of its Mechanical Propertie*s. M.S. dissertation, Virginia Polytechnic Institute and State University, Blacksburg, USA.

[36] GUO, H., ZHANG, Y., XUE, F., *et al.*, 2013, "In-situ synchrotron SAXS and WAXS investigations on deformation and α-β Transformation of uniaxial stretched poly(vinylidene fluoride)", *CrystEngComm*, v. 15, n. 8, pp. 1597–1606.

[37] SHARPLES, A., 1966, *Introduction to Polymer Crystallization*. 1ed. London, Edward Arnold Ltd.

[38] CALLISTER, W. D., 2001, *Fundamentals of Materials Science and Engineering An Interactive*. 5ed. New York, John Wiley & Sons, Inc.

[39] FOX, A., 2015, *Stress Relaxation Testing. STP 676*. 1ed. Kansas city, American Society for Testing and Materials 3.

[40] SMITH, W. H. J., 2010, *Foundations of Material Science and Engineering*. 1ed. New York, Mc Graw Hill.

[41] STACHURSKI, Z. H., 2002, "Micromechanics of stress relaxation in amorphous glassy PMMA. Part I. Molecular model for anelastic behaviour", *Polymer (Guildf)*, v. 43, n. 26, pp. 7409–7417.

[42] PFISTER, L. A., STACHURSKI, Z. H., 2002, "Micromechanics of stress relaxation in amorphous glassy PMMA part II: application of the RT model", *Polymer (Guildf)*, v. 43, pp. 7419–7427.

[43] MATHIESEN, D., VOGTMANN, D., DUPAIX, R., 2014, "Challenges In Mechanics of Time-Dependent Materials and Processes in Conventional and

Multifunctional Materials", v. 2, pp. 9–16.

[44] WORTMANN, F. J., SCHULZ, K. V., 1995, "Stress relaxation and time/temperature superposition of polypropylene fibres", *Polymer (Guildf)*, v. 36, n. 2, pp. 315–321.

[45] MIHÁLY VAS, P., LÁSZLÓ, N., 2006, "Investigating the Time Dependent Behavior of Thermoplastic Polymers under Tensile Load", *Macromolecular Symposia*, v. 239, pp. 176–181.

[46] LIU, G. SCHNEIDER, K., ZHENG, L., *et al.*, 2014, "Stretching induced phase separation in poly(vinylidene fluoride)/ poly(butylene succinate) blends studied by in-situ X-ray scattering", *Polymer (United Kingdom)*, v. 55, n. 10, pp. 2588–2596.

[47] MAIER, G. A., WALLNER, G., LANG, R. W., et al., 2005, "Structural changes during plastic deformation at crack tips in PVDF films: A scanning X-ray scattering study", *Macromolecules*, v. 38, n. 14, pp. 6099–6105.

[48] MAIER, G. A., WALLNER, G. M., LANG, R. W., et al., 2007, "Fracture of poly(vinylidene fluoride): A combined synchrotron and laboratory in-situ X-ray scattering study", *Journal of Applied Crystallography*, v. 40, n. 1, pp. 564–567.

[49] CASTAGNET, S., GIRAULT, S., GACOUGNOLLE, J. L., et al., 2000, "Cavitation in strained polyvinylidene fluoride: Mechanical and X-ray experimental studies", *Polymer (Guildf)*, v. 41, n. 20, pp. 7523–7530.

[50] FRÜBING, P., WANG, F., WEGENER, M., 2012, "Relaxation processes and structural transitions in stretched films of polyvinylidene fluoride and its copolymer with hexafluoropropylene", *Applied Physics A: Materials Science and Processing*, v. 107, n. 3, pp. 603–611.

[51] LAIARINANDRASANA, L., BESSON, J., LAFARGE, M., et al., 2009, "Temperature dependent mechanical behaviour of PVDF: Experiments and numerical modelling", *International Journal of Plasticity*, v. 25, n. 7, pp. 1301–1324.

[52] CASTAGNET, S., GACOUGNOLLE, J. L., DANG, P., 2000, "Correlation between macroscopical viscoelastic behaviour and micromechanisms in strained α polyvinylidene fluoride (PVDF)", *Materials Science and Engineering: A*, v. 276, n. 1–2, pp. 152–159.

[53] RAULT, J., SOTTON, M., RABOURDIN, C., et al., 1980, "Crystallization of polymers. Part I: Polydispersed polymers quenched from the liquid state",

Journal of Physics, v. 41, n. 12, pp. 1459–1467.

[54] KENNEDY, M. A., PEACOCK, A. J., MANDELKERN, L., 1994, "Tensile Properties of Crystalline Polymers: Linear Polyethylene", *Macromolecules*, v. 27, n. 19, pp. 5297–5310.

[55] BÉDOUI, F., DIANI, J., RÉGNIER, G., 2004, "Micromechanical modeling of elastic properties in polyolefins," *Polymer (Guildf)*, v. 45, n. 7, pp. 2433–2442.

[56] SCHÄLER, K., 2012, *Low-Field Nmr Studies of Structure and Dynamics in Semicrystalline Polymers*. Ph.D. dissertation, Martin-Luther-Universität Halle-Wittenberg , Halle/Saale, Germany.

[57] LEVITT, M. H., 2000, *Spin Dynamics. Basics of Nuclear Magnetic Resonance*. 2ed. Southampton, John Wiley & Sons Ltd.

[58] DUER, M. J., 2002, *Solid-State NMR Spectroscopy*. 1ed. Cambridge, Blackwell Science Ltd.

[59] HORNAK, J. P.. The Basics of NMR: Virtual book, 2017. Available in: <https://www.cis.rit.edu/htbooks/nmr/inside.htm>. Access in: 01 jul. 2018.

[60] JOHNSON, C., 1996, *Encyclopedia of Nuclear Magnetic Resonance*. 1ed. Chicester, Wiley.

[61] MARK, J. E., 2007, *Physical Properties of Polymers Handbook*. 1ed. Cincinnati, Springer Science Business Media.

[62] CALLAGHAN, P., 1991, *Principles of Nuclear Magnetic Resonance Microscopy*. 1ed. Oxford, Oxford University Press.

[63] ABRAGAM, A., 1961, *The Principles of Nuclear Magnetism*. 1ed. Oxford, Oxford University Press.

[64] GOLITSYN, Y., PULST, M., KRESSLER, J., et al., 2017, "Molecular Dynamics in the Crystalline Regions of Poly(ethylene oxide) Containing a Well-Defined Point Defect in the middle of the Polymer Chain", *The Journal of Physical Chemistry B*, v. 121, n. 17, pp. 4620–4630.

[65] CAVALCANTE, M. P., TOLEDO, A., RODRIGUES, E., et al., 2017, "Correlation between traditional techniques and TD-NMR to determine the morphology of PHB/PCL blends", *Polymer Testing*, v. 58, pp. 159–165.

[66] GAO, Y., ZHANG, R., LV, W., *et al.*, 2014, "Critical effect of segmental dynamics in polybutadiene/clay nanocomposites characterized by solid state ^{1}H NMR spectroscopy", *The Journal of Physical Chemistry C*, v. 118, n. 10, pp. 5606–5614.

[67] BÄRENWALD, R., CHAMPOURET, Y., SAALWÄCHTER, K., et al., 2012, "Determination of chain flip rates in poly(ethylene) crystallites by solid-state low-field ^{1}H NMR for two different sample morphologies", *The Journal of Physical Chemistry B*, v. 116, n. 43, pp. 13089–13097.

[68] LITVINOV, V. M., XU, J., MELIAN, C., et al., 2011, "Morphology, chain dynamics, and domain sizes in highly drawn gel-spun ultrahigh molecular weight polyethylene fibers at the final stages of drawing by SAXS, WAXS, and ^{1}H Solid-State NMR", *Macromolecules*, v. 44, n. 23, pp. 9254–9266.

[69] HSIAO, B. S., VERMA, R. K., 1998, "A novel approach to extract morphological variables in crystalline polymers from time-resolved synchrotron SAXS data", *Journal of Synchrotron Radiation*, v. 5, n. 1, pp. 23–29.

[70] CHU, B., HSIAO, B. S., 2001, "Small-angle X-ray scattering of polymers", *Chemical Reviews*, v. 101, n. 6, pp. 1727–1761.

[71] ZUBAVICHUS, Y. V, SLOVOKHOTOV, Y. L., 2001, "X-Ray synchrotron radiation in physicochemical studies", *Russian Chemical Reviews*, v. 70, n. 5, pp. 373–403.

[72] GLATTER, O., KRATKY, O., 1982, *Small Anlge X-ray Scattering*. 1ed. New York, Academic Press.

[73] SCHNABLEGGER, H., SINGH, Y., 2011, *The SAXS Guide*. 3ed. Graz, Anton Paar GmbH.

[74] SALOMONS, G. J., 1998, *Small-angle X-ray scattering study of crazing in bulk thermoplastic polymers*. Ph.D. dissertation, Queen's University, Kingston, Canada.

[75] RABIEJ, S., RABIEJ, M., 2011, "Determination of the parameters of lamellar structure of semicrystalline polymers using a computer program SAXSDAT", *Polimery/Polymers*, v. 26, n. 9, pp. 662–670.

[76] FATNASSI, M., LARBI, F. B. C., HALARY, J. L., 2010, "Quantitative analysis of semicrystalline blends SAXS data: Theoretical modeling versus linear correlation function", *International Journal of Polymer Science*, v. 2010, pp. 1–6.

[77] SANTA CRUZ, C., STRIBECK, N., ZACHMANN, H. G., et al., 1991, "Novel aspects in the structure of poly(ethylene terephthalate) as revealed by means of small angle x-ray scattering", *Macromolecules*, v. 24, n. 22, pp. 5980–5990.

[78] ERNZEN, J. R., BONDAN, F., LUVISON, C., et al., 2016, "Structure and properties relationship of melt reacted polyamide 6/malenized soybean oil",

Journal of Applied Polymer Science, v. 133, n. 8, pp. 1–10.

[79] MARTINS, J. N., BIANCHI, O., WANKE, C. H., et al., 2015, "Effects of POSS addition on Non-isothermal crystallization and morphology of PVDF", *Journal of Polymer Research*, v. 22, n. 11, pp. 1–10.

[80] PARADINHA, M. M., GONZALEZ, F., WANKE, C., et al., 2017, "Preparation and characterization of the ethylene-vinyl acetate copolymer partially hydrolyzed assisted by microwave radiation", *Journal of Applied Polymer Science*, v. 134, n. 10, pp. 1–9.

[81] ROBELIN, E., RAULT, J., 1989, "Origin of the Long Period and Crystallinity in Quenched. Semicrystalline Polymers", *Macromolecules*, v. 22, n. 9, pp. 3581–3594.

[82] Wang, Y., Jiang, Z., Fu, L., et al., 2014, "Lamellar thickness and stretching temperature dependency of cavitation in semicrystalline polymers", *PLOS One*, v. 9, n. 5.

[83] ASTM D 638, 2015, Standard test method for tensile properties of plastics 1, American Society for Testing and Materials 3, pp. 1–16.

[84] API RP 17B, 2002, Recommended Practice for Flexible Pipe, The American Petroleum Institute, Washington, DC, v. 44, pp. 71–90.

[85] ASTM D 618, 2000, Standard practice for conditioning plastics for testing, American Society for Testing and Materials, pp.7–10.

[86] SUN, N., WENZEL, M., ADAMS, A., 2014, "Morphology of high-density polyethylene pipes stored under hydrostatic pressure at elevated temperature", *Polymer (United Kingdom)*, v. 55, n. 16, pp. 3792–3800.

[87] MEKHILEF, N., 2001, "Viscoelastic and pressure-volume-temperature properties of poly(vinylidene fluoride) and poly(vinylidene fluoride)-hexafluoropropylene copolymers", *Journal of Applied Polymer Science*, v. 80, n. 2, pp. 230–241.

[88] LINARES, A., ACOSTA, J. L.,1997, "Tensile and dynamic mechanical behaviour of polymer blends based on PVDF", *European Polymer Journal*, v. 33, n. 4, pp. 467–473.

[89] TANG, X. G., HOU, M., ZOU, J., et al., 2013, "Poly(vinylidene fluoride)/halloysite nanotubes nanocomposites: The structures, properties, and tensile fracture behaviors", *Journal of Applied Polymer Science*, v. 128, n. 1, pp. 869–878.

[90] LIU, G., ZHENG, L., ZHANG, X., et al., 2013, "Stress induced lamellar thickening in poly(ethylene succinate)", *Polymer (United Kingdom)*, v. 54, n. 25, pp. 6860–6866.

[91] DU, C.-H., XU, Y.-Y., ZHU, B.-K., 2009, "Plasticizer Effect of Dibutyl Phthalate on the Morphology and Mechanical Properties of Hard Elastic Poly(vinylidene fluoride) Fibers", *Journal of Applied Polymer Science*, v. 114, pp. 3645–3651.

[92] NEIDHÖFER, M., BEAUME, F., IBOS, L., et al., 2004, "Structural evolution of PVDF during storage or annealing", *Polymer (Guildf)*, v. 45, n. 5, pp. 1679–1688.

[93] HOURSTON, D. J., HUGHES, I. D., 1977, "Poly(vinylidene fluoride) - poly(methyl methacrylate) blends", *Polymer (Guildf)*, v. 18, n. 11, pp. 1175–1178.

[94] CALADO, V., MONTGOMERY, D. C., 2003, *Planejamento de Experimentos usando Statistica*. 1ed. Rio de Janeiro, E-papers Serviços Editoriais.

Appendix I

Figures

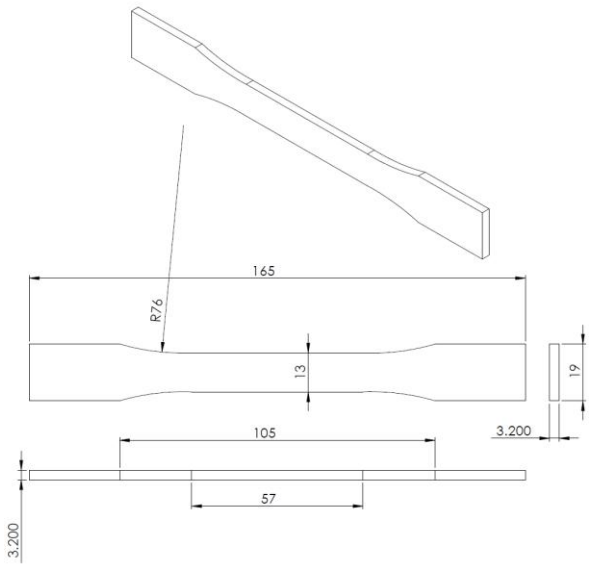

Figure 52. Sample dimensions according ASTM D 638 Type I.

Figure 53. Zwick/Roell machine (Kappa Multistation model) for stress relaxation tests. Laboratory of Materials Processing and Characterization (LPCM) – PEMM / UFRJ.

Figure 54. Universal testing machine Instron (model 5567). Laboratory of Materials Processing and Characterization (LPCM) – PEMM / UFRJ.

Figure 55. Netzsch DMA 242C instrument. Laboratory of Materials Processing and Characterization (LPCM) – PEMM / UFRJ.

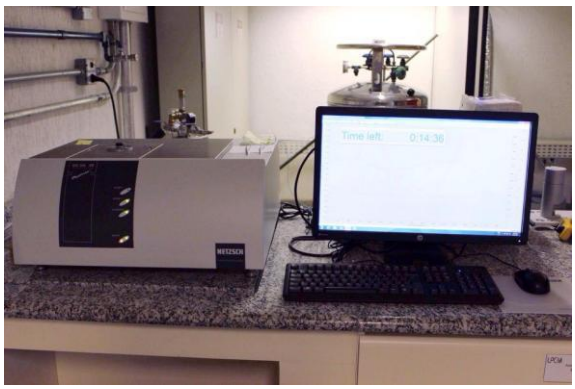

Figure 56. Netzsch DSC 204 F1 Phoenix calorimeter. Laboratory of Materials Processing and Characterization (LPCM) – PEMM / UFRJ.

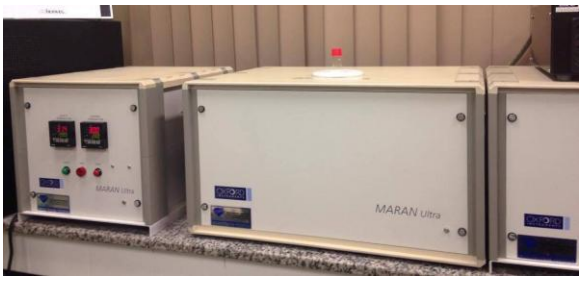

Figure 57. Maran Ultra spectrometer, electromagnetic field of 0.54 T (23.4 MHz for ^{1}H). Institute of Macromolecules Professor Eloisa Mano (IMA) – UFRJ.

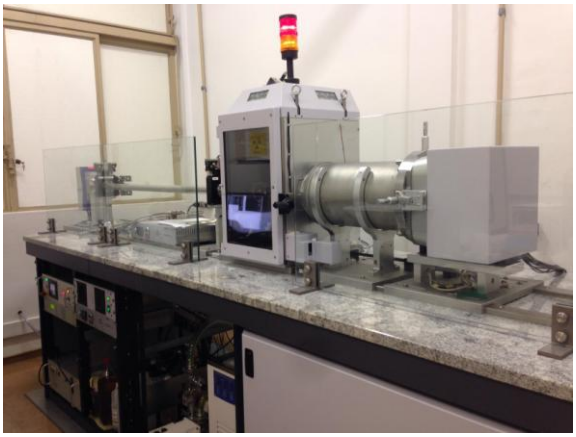

Figure 58. NanoSTAR SAXS system (Bruker AXS) coupled to Cu Kα radiation source Xenocs (Genix 3D Cu ULD) and to a Bruker Vantech 2000 detector. Institute of Physics – USP.

Appendix II

1. Representative curves of the stress relaxation tests

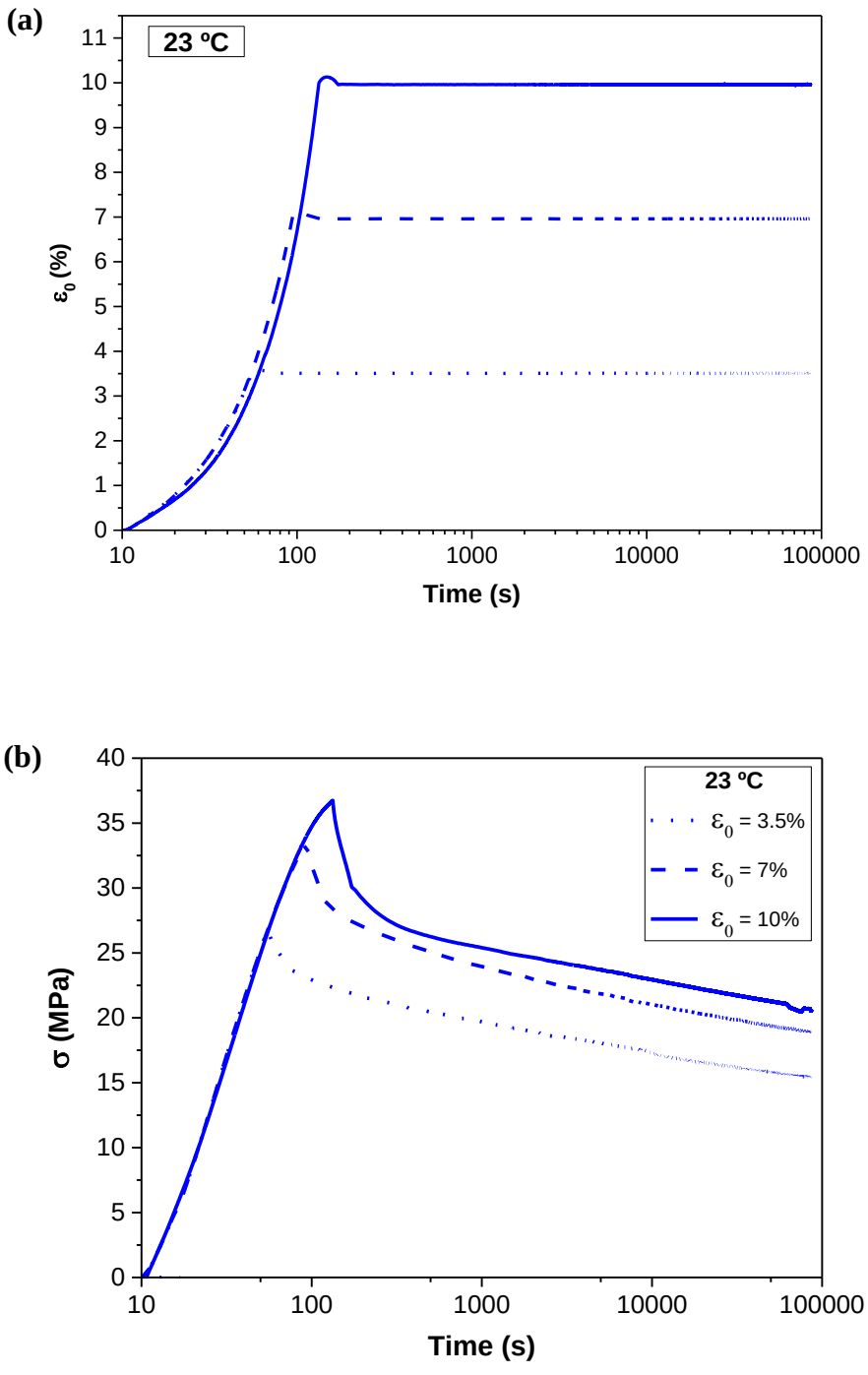

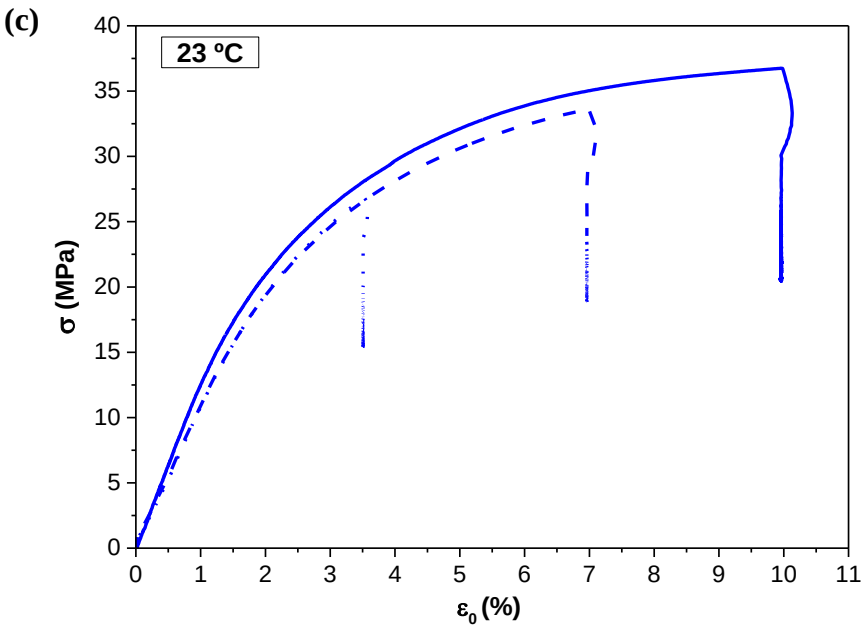

Figure 59. Relaxation results up to 24 h at 23 ºC: (a) Strain vs. time, (b) Stress vs. time, (c) Stress vs. strain.

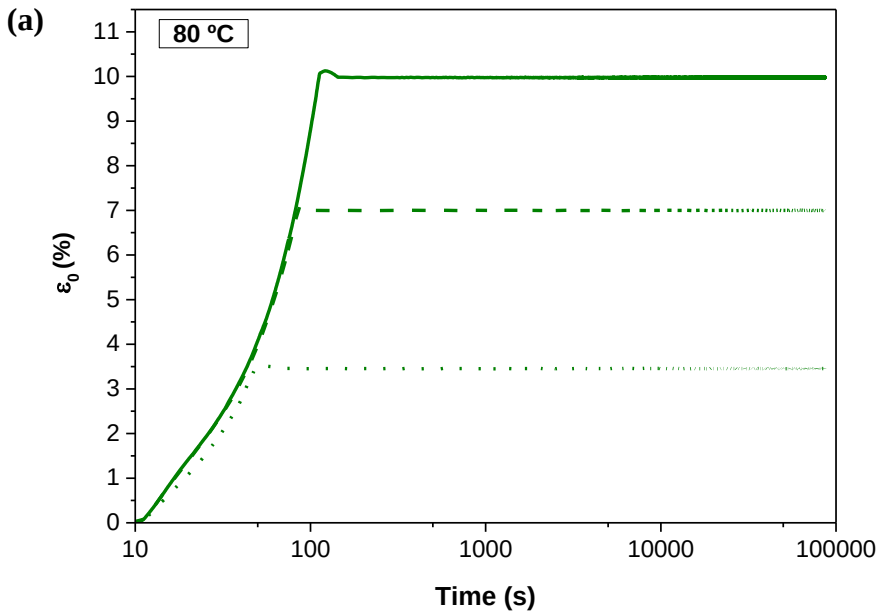

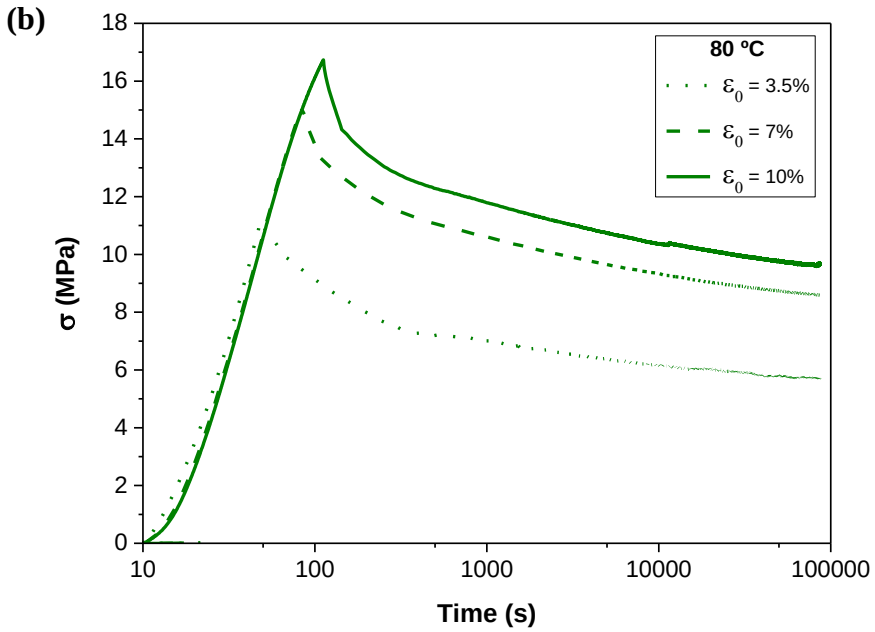

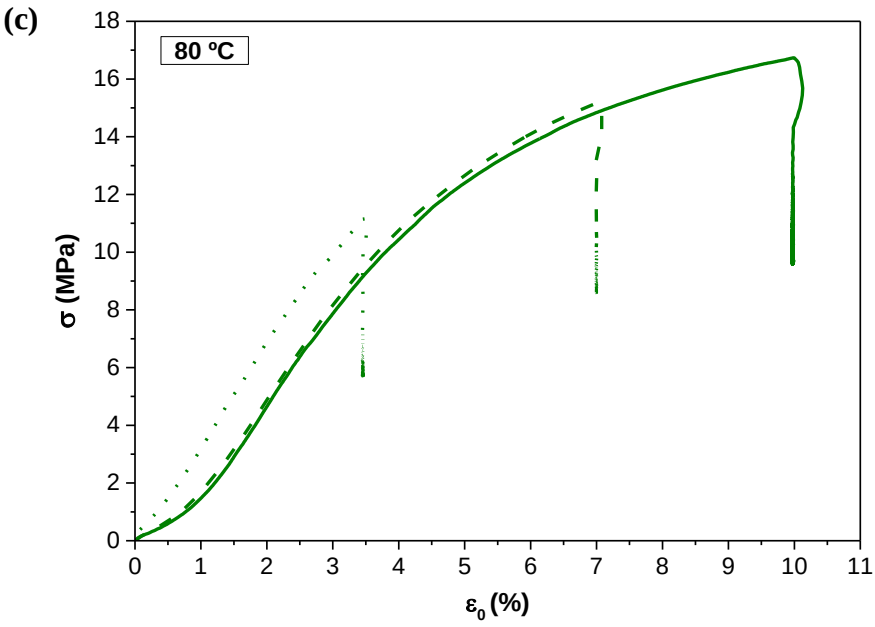

Figure 60. Relaxation results up to 24 h at 80 ºC: (a) Strain vs. time, (b) Stress vs. time, (c) Stress vs. strain.

(a)

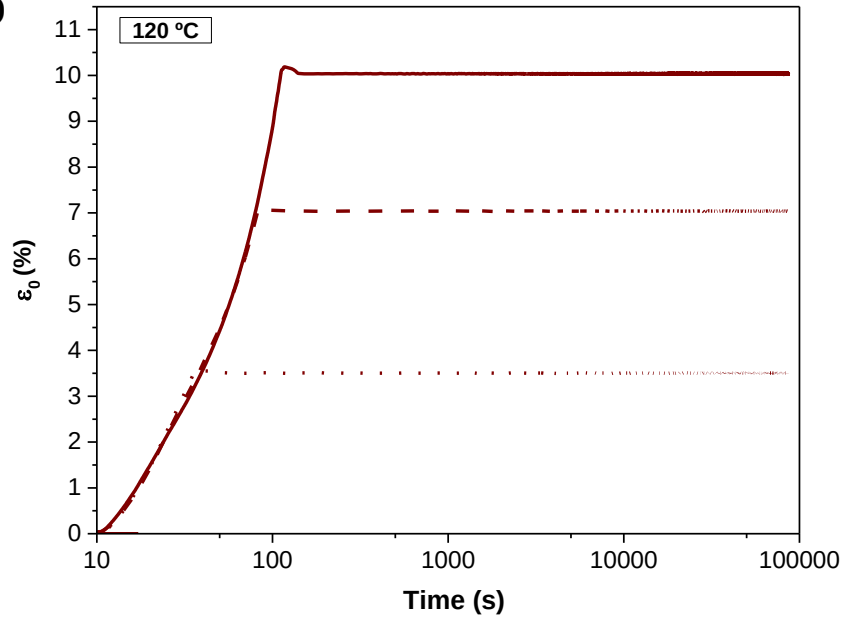
120 °C
ε0 (%)
Time (s)
0
1
2
3
4
5
6
7
8
9
10
11
10
100
1000
10000
100000

(b)

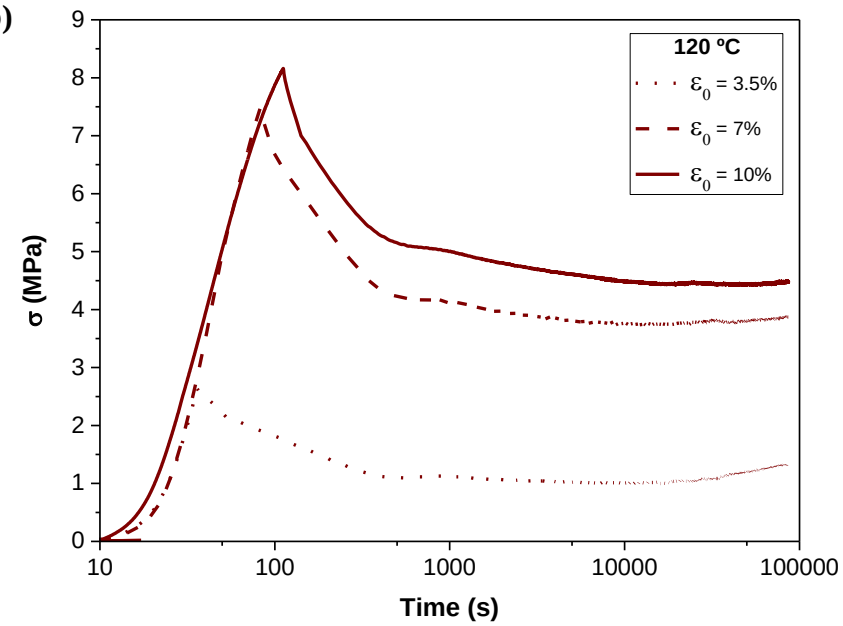
120 °C
ε0 = 3.5%
ε0 = 7%
ε0 = 10%
σ (MPa)
Time (s)
0
1
2
3
4
5
6
7
8
9
10
100
1000
10000
100000

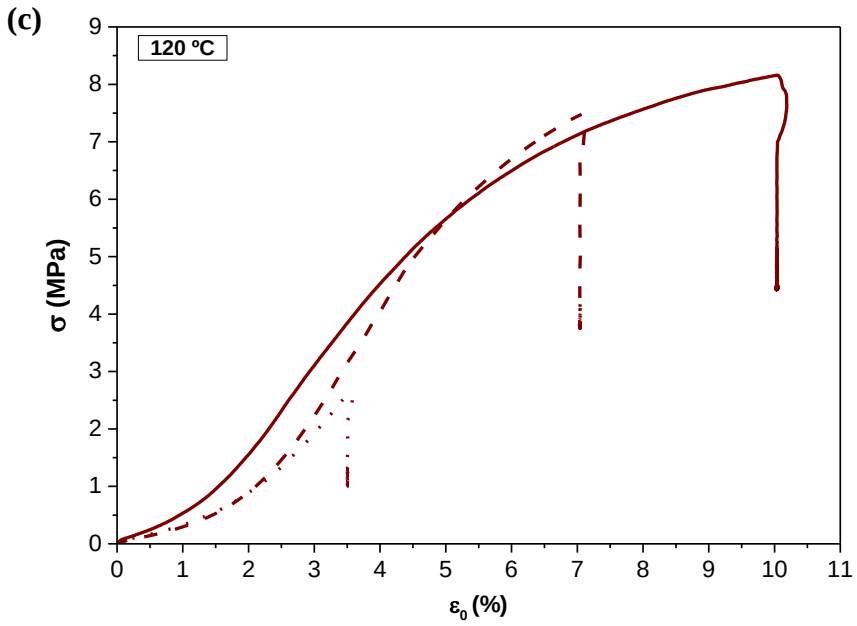

Figure 61. Relaxation results up to 24 h at 120 ºC: (a) Strain vs. time, (b) Stress vs. time, (c) Stress vs. strain.

2. Stress-strain curves of as processed PVDF and all relaxed samples (three samples for each condition)

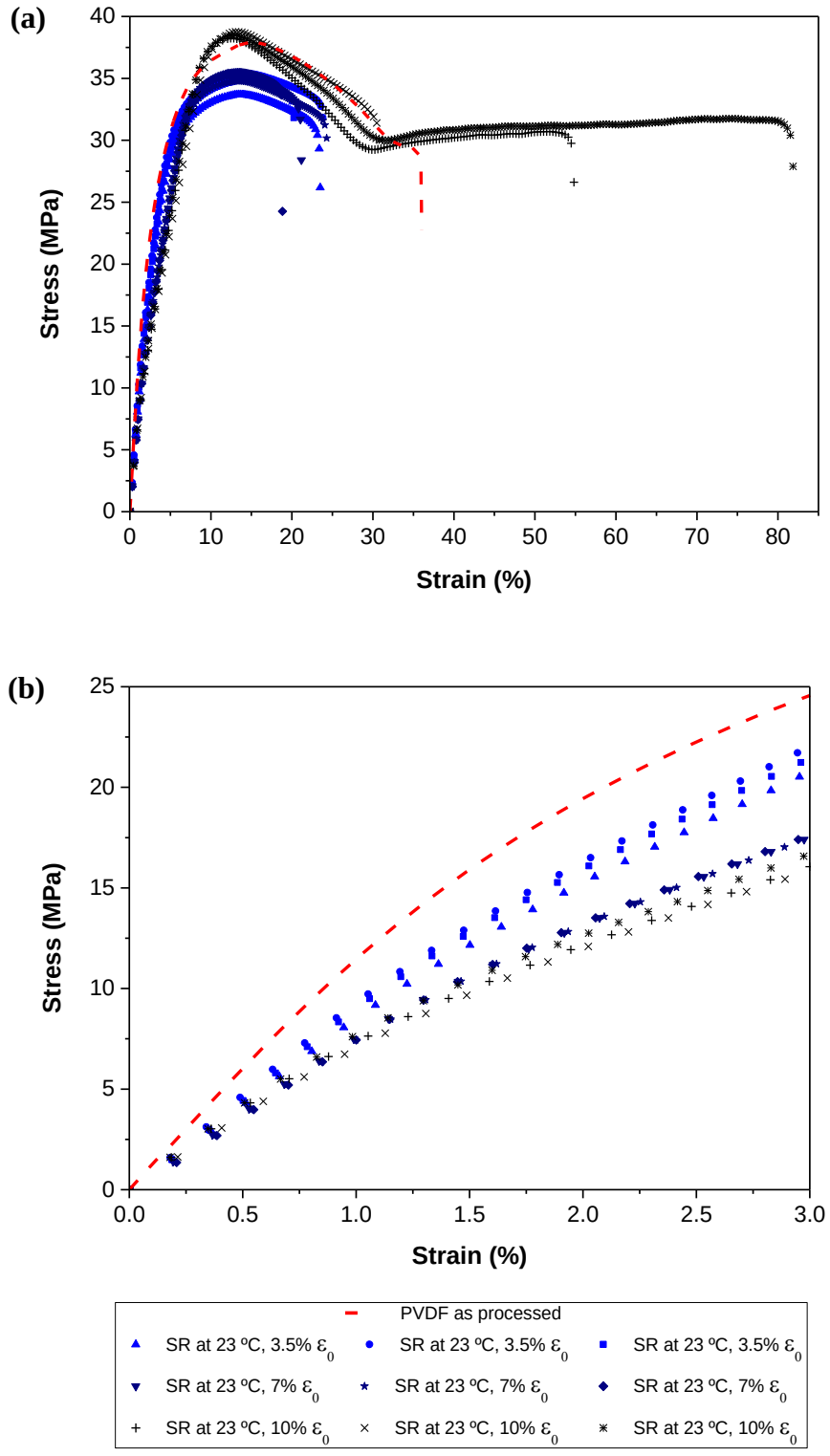

Figure 62. Strain-stress curves of as processed PVDF and all relaxed samples at 23 ºC. (a) Strain up to 85%, (b) Strain up to 3%.

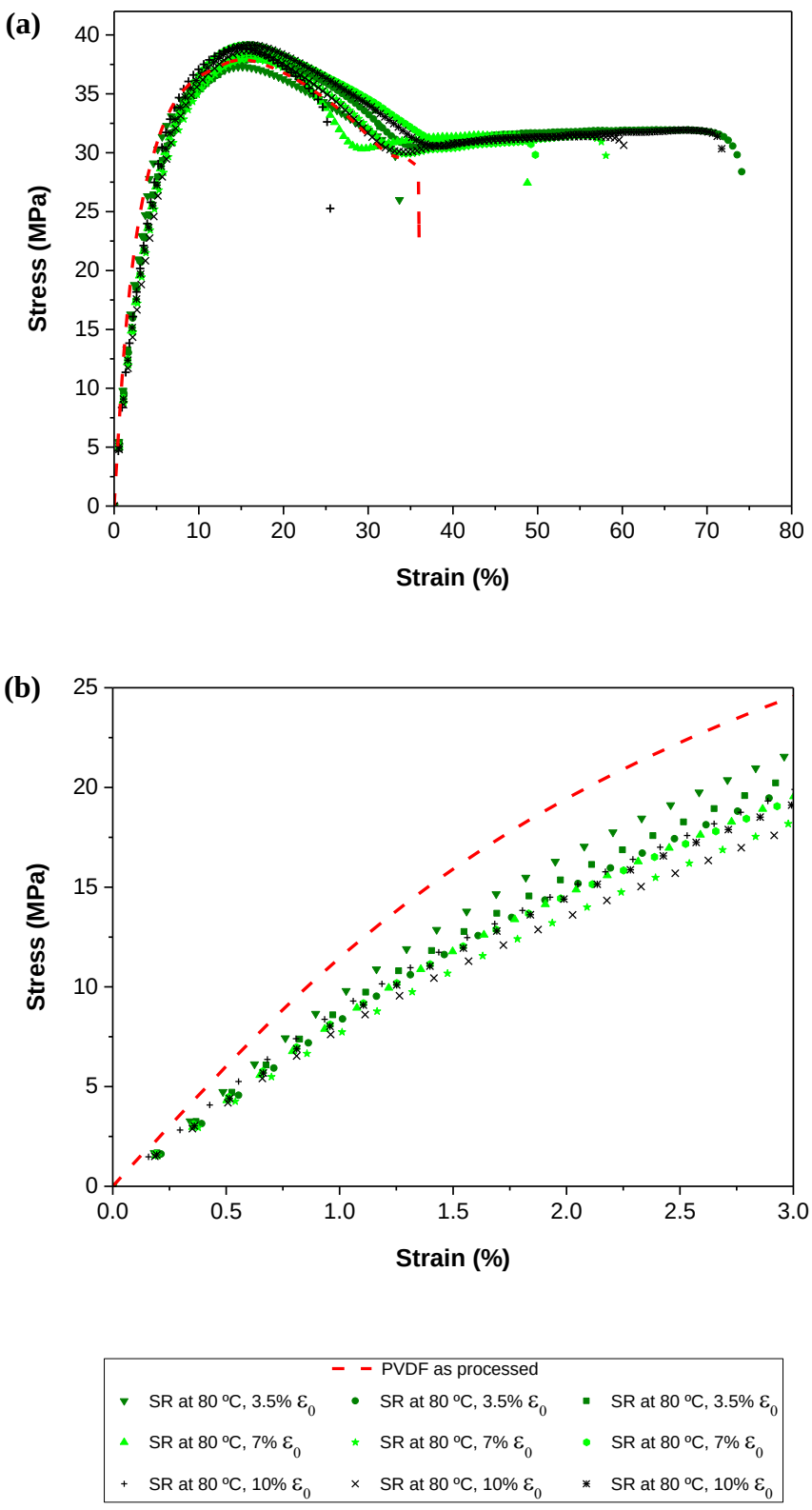

Figure 63. Strain-stress curves of as processed PVDF and all relaxed samples at 80 ºC. (a) Strain up to 80%, (b) Strain up to 3%.

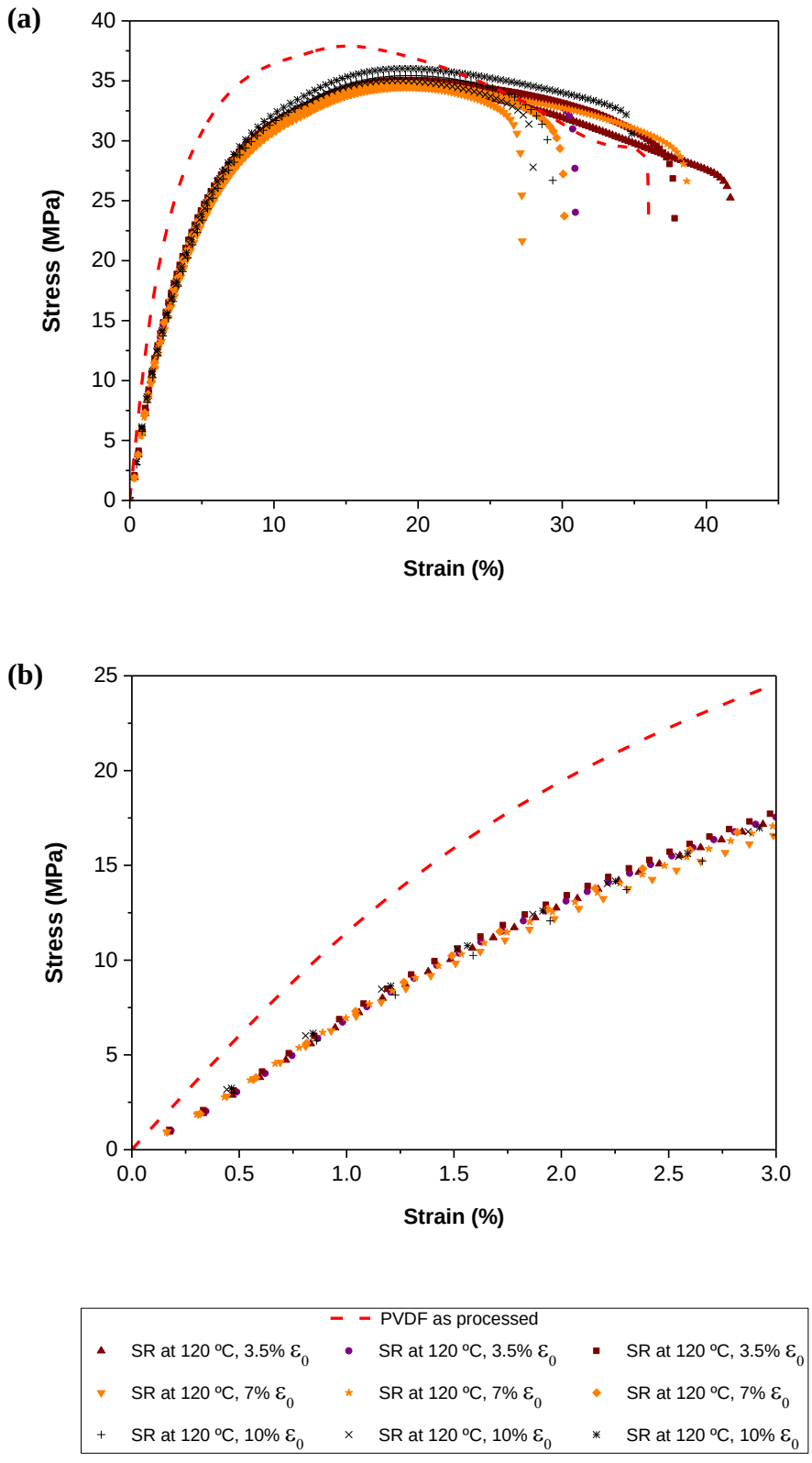

Figure 64. Strain-stress curves of as processed PVDF and all relaxed samples at 120 ºC. (a) Strain up to 45%, (b) Strain up to 3%.

3. Representative DSC thermograms and parameters

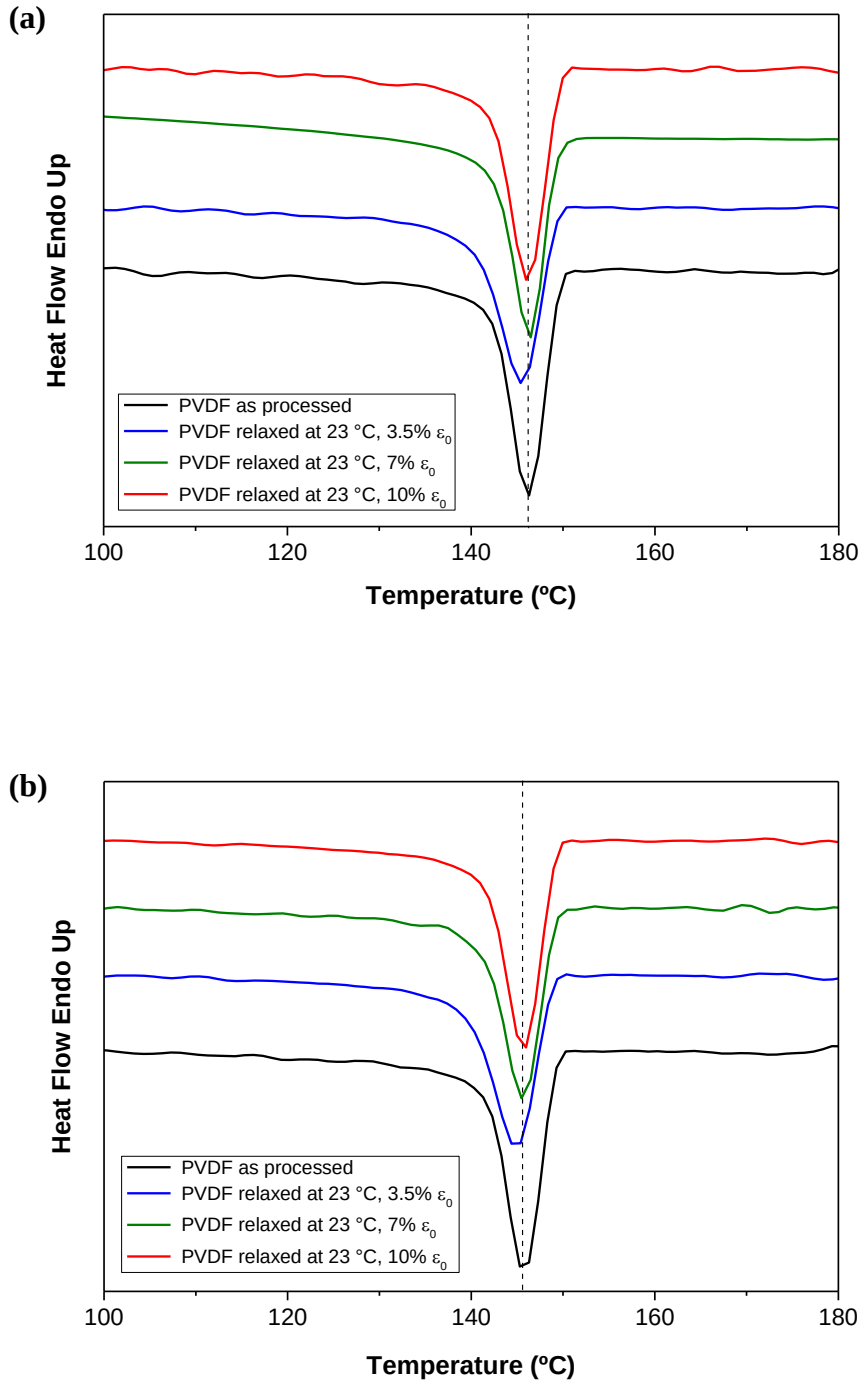

Figure 65. Representative DSC thermograms of as processed PVDF and samples relaxed at 23 ºC. (a) First cooling, (b) Second cooling.

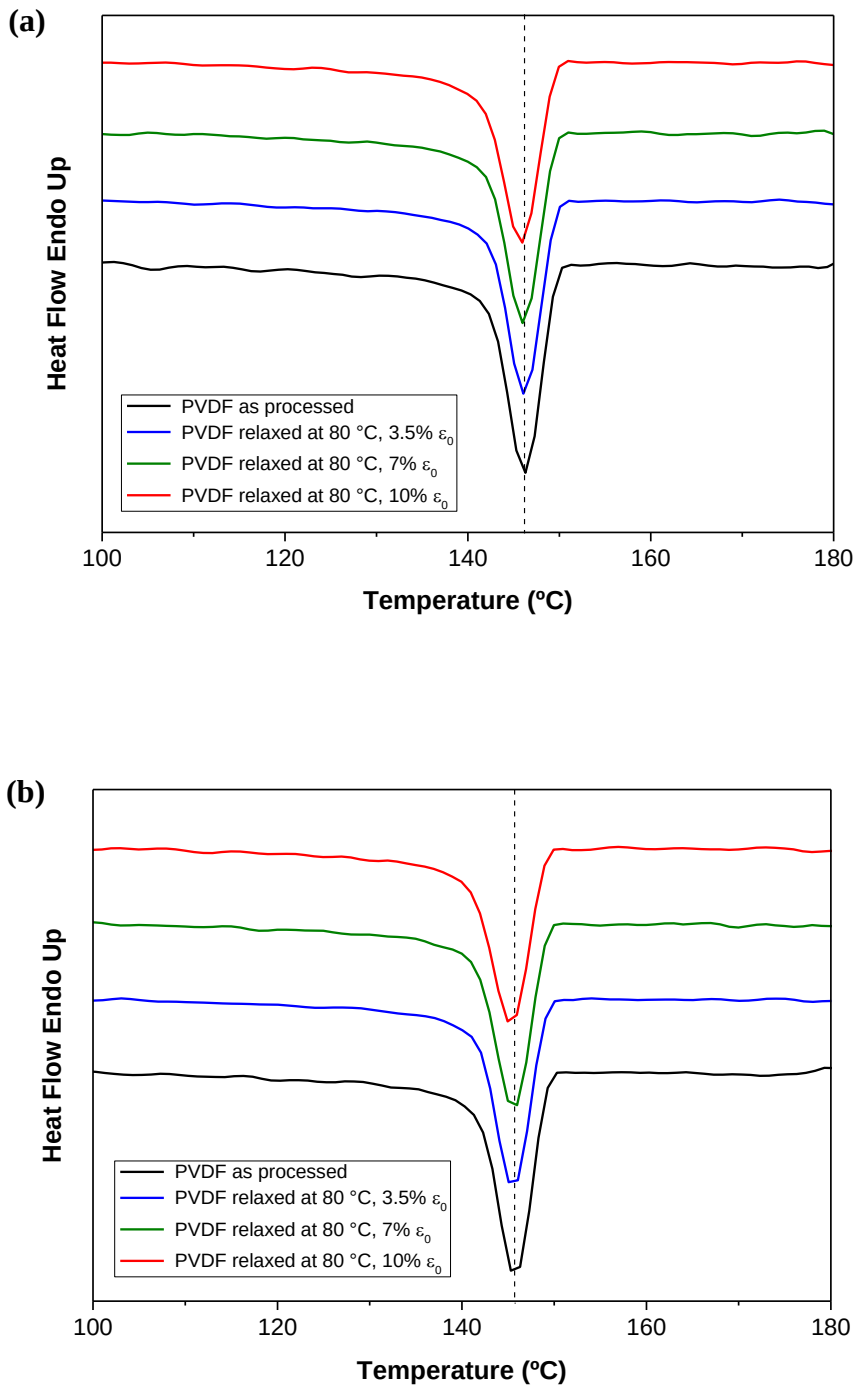

Figure 66. Representative DSC thermograms of as processed PVDF and samples relaxed at 80 ºC. (a) First cooling, (b) Second cooling.

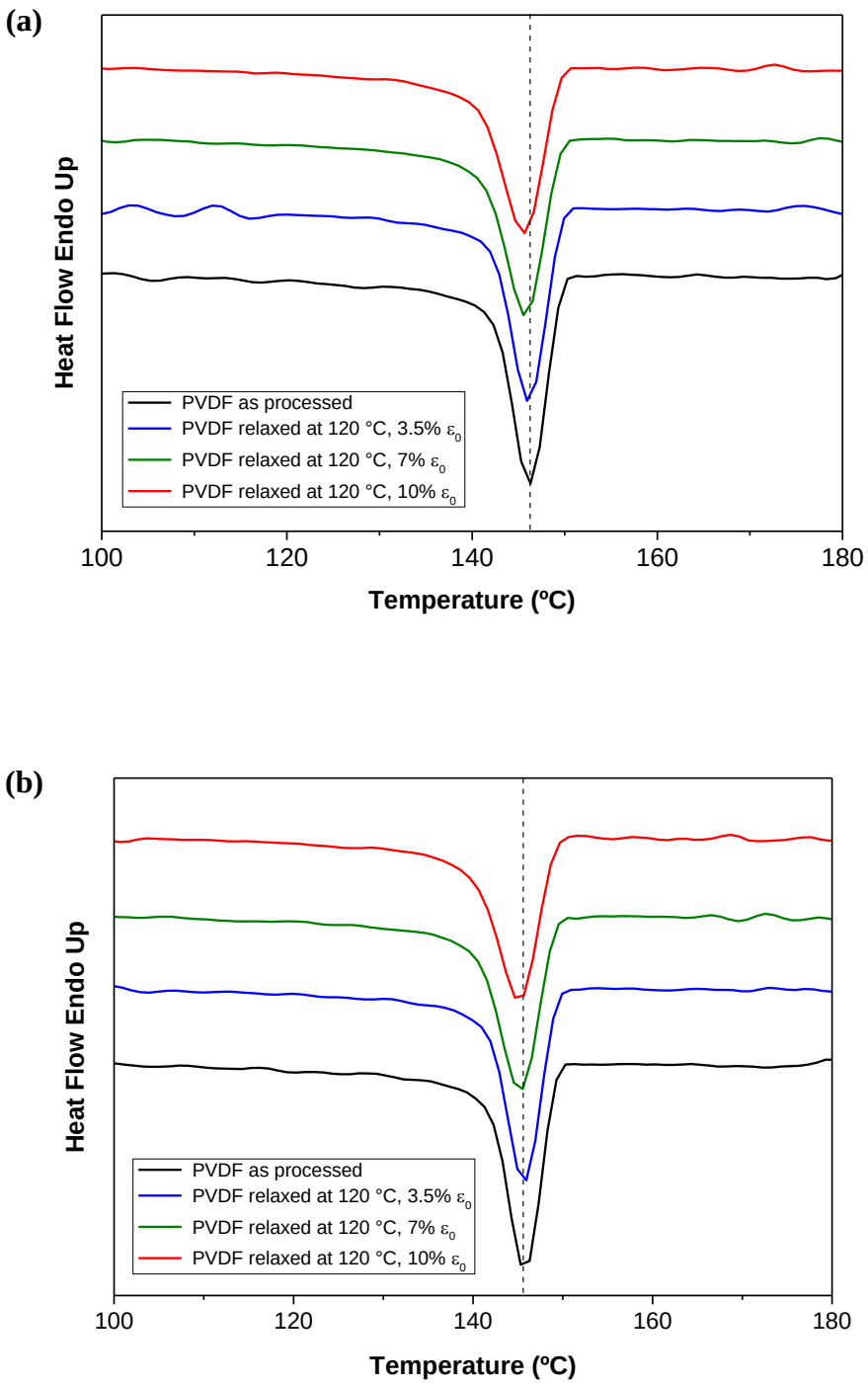

Figure 67. Representative DSC thermograms of as processed PVDF and samples relaxed at 120 ºC. (a) First cooling, (b) Second cooling.

Table 8. DSC parameters (average values) of as processed PVDF and relaxed samples.

Sample	ΔH_m[a] (J/g)		T_m[b] (ºC)[A]		T_c[c] (ºC)[A]	
	First heating	Second heating	First heating	Second heating	First cooling	Second cooling
PVDF	52.5	53.4	168.3	168.5	145.7	146.3
PVDF relaxed at 23 ºC, 3.5% ε_0	50.7	51.3	168.0	168.9	145.1	145.7
PVDF relaxed at 23 ºC, 7% ε_0	48.6	48.9	167.9	168.7	145.8	146.4
PVDF relaxed at 23 ºC, 10% ε_0	51.6	52.3	168.8	168.7	145.4	145.7
PVDF relaxed at 80 ºC, 3.5% ε_0	48.5	50.1	167.9	168.6	145.6	146.1
PVDF relaxed at 80 ºC, 7% ε_0	49.7	50.3	168.0	168.7	145.6	146.0
PVDF relaxed at 80 ºC, 10% ε_0	48.8	50.5	168.3	168.6	145.6	146.1
PVDF relaxed at 120 ºC, 3.5% ε_0	53.3	50.7	168.6	168.5	145.7	146.2
PVDF relaxed at 120 ºC, 7% ε_0	53.9	51.0	169.1	169.3	144.9	145.6
PVDF relaxed at 120 ºC, 10% ε_0	54.1	50.8	168.5	168.9	145.6	146.0

[a] ΔH_m = melting enthalpy (heat of fusion).

[b] T_m = melting temperature.

[c] T_c = crystallization temperature.

[A] Standard deviation ± 2ºC.

4. SAXS analysis

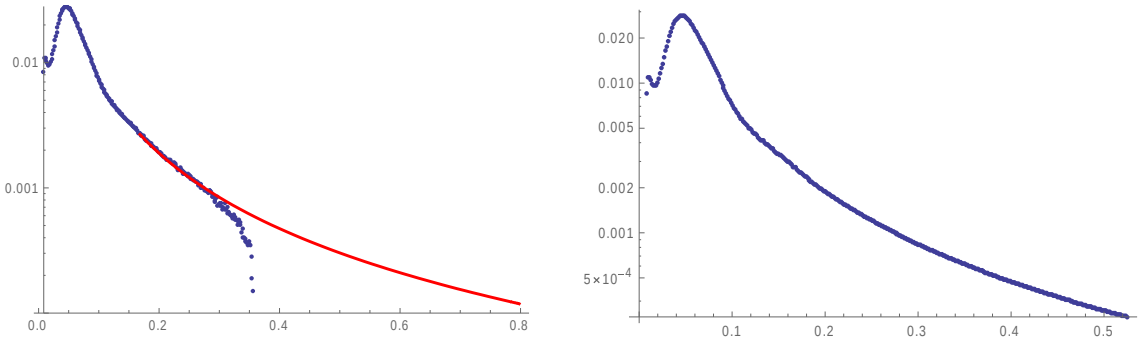

Figure 68. Extrapolated $I(q)q^2$ versus q curves, to high q values by applying Porod's law, of PVDF. Red line: Porod asymptote.

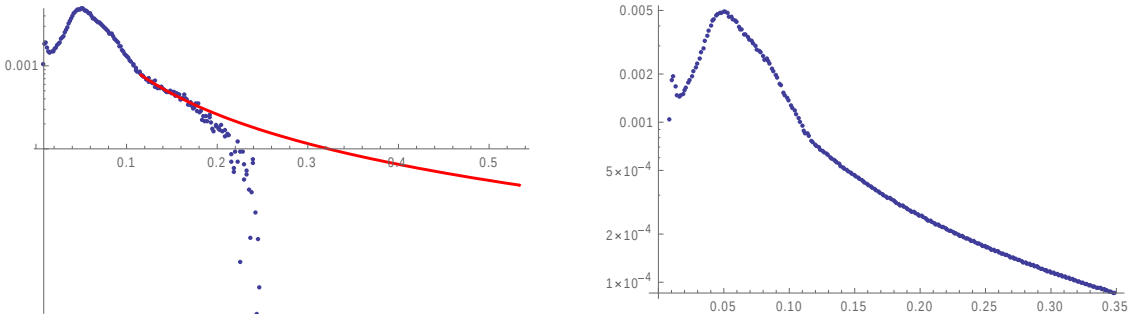

Figure 69. Extrapolated $I(q)q^2$ versus q curves, to high q values by applying Porod's law, of PVDF relaxed at 23 ºC and 3.5% strain. Red line: Porod asymptote.

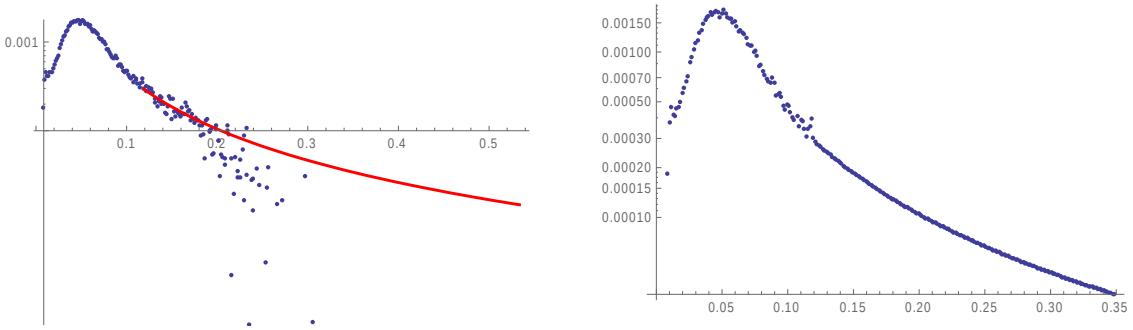

Figure 70. Extrapolated $I(q)q^2$ versus q curves, to high q values by applying Porod's law, of PVDF relaxed at 23 ºC and 7% strain. Red line: Porod asymptote.

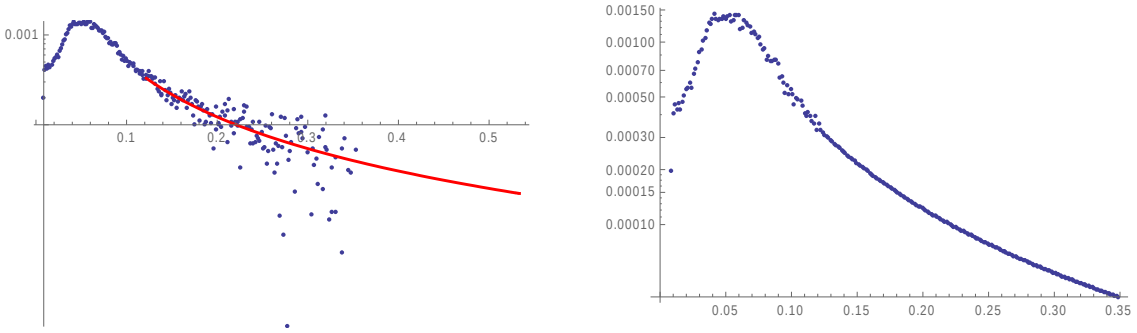

Figure 71. Extrapolated $I(q)q^2$ versus q curves, to high q values by applying Porod's law, of PVDF relaxed at 23 ºC and 10% strain. Red line: Porod asymptote.

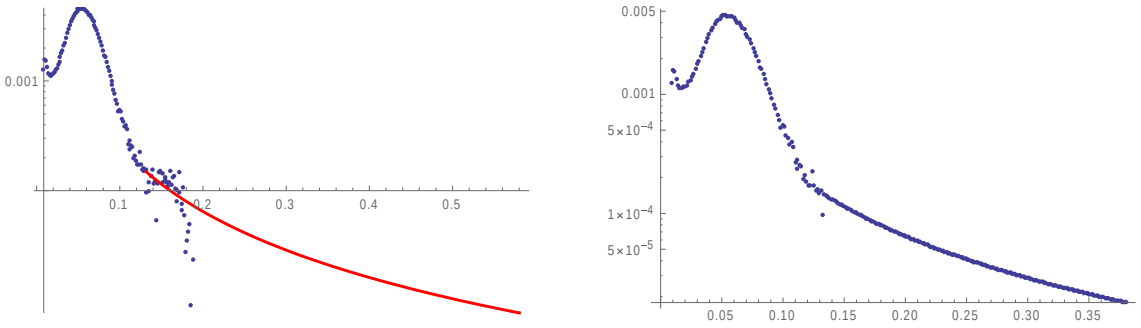

Figure 72. Extrapolated $I(q)q^2$ versus q curves, to high q values by applying Porod's law, of PVDF relaxed at 80 ºC and 7% strain. Red line: Porod asymptote.

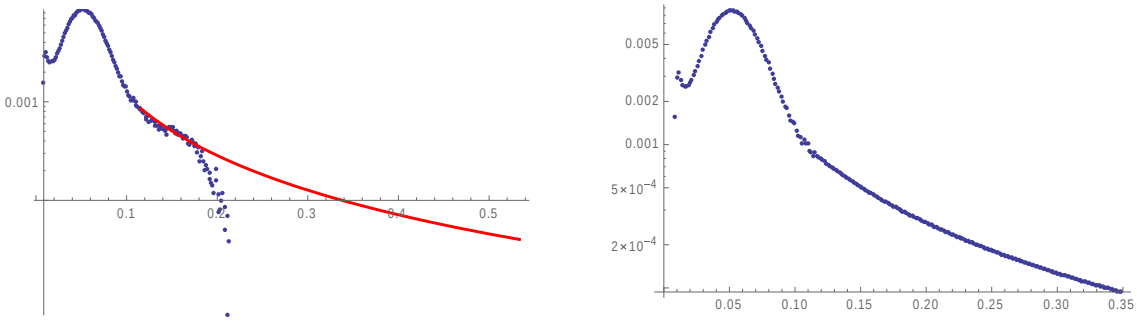

Figure 73. Extrapolated $I(q)q^2$ versus q curves, to high q values by applying Porod's law, of PVDF relaxed at 80 ºC and 10% strain. Red line: Porod asymptote.

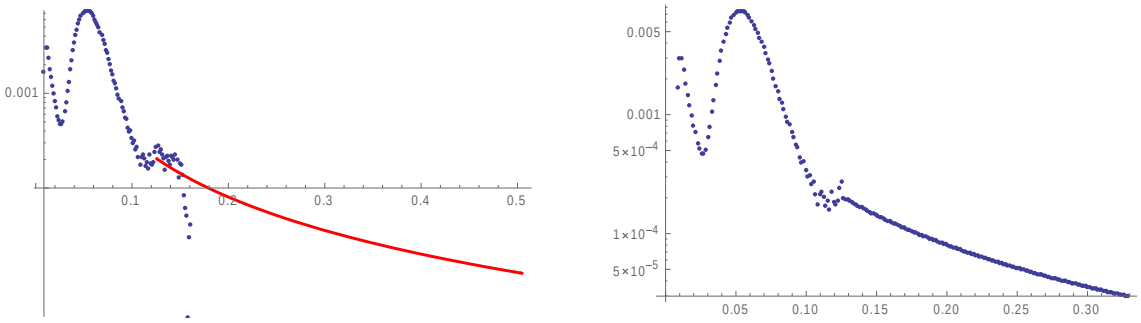

Figure 74. Extrapolated $I(q)q^2$ versus q curves, to high q values by applying Porod's law, of PVDF relaxed at 120 ºC and 3.5% strain. Red line: Porod asymptote.

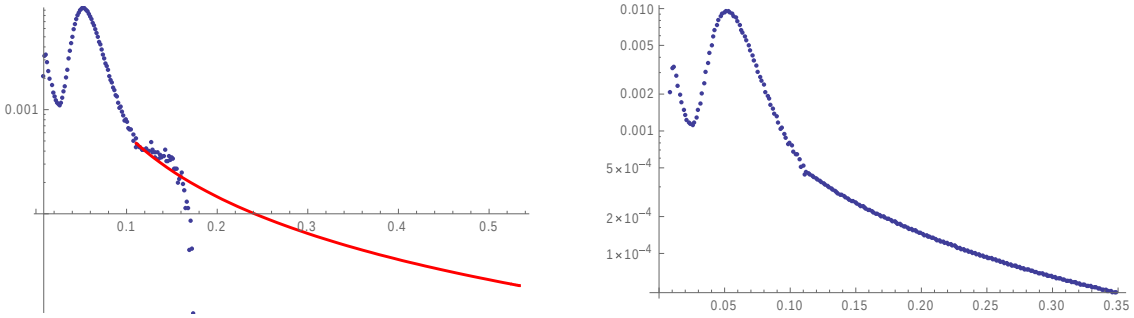

Figure 75. Extrapolated $I(q)q^2$ versus q curves, to high q values by applying Porod's law, of PVDF relaxed at 120 ºC and 7% strain. Red line: Porod asymptote.

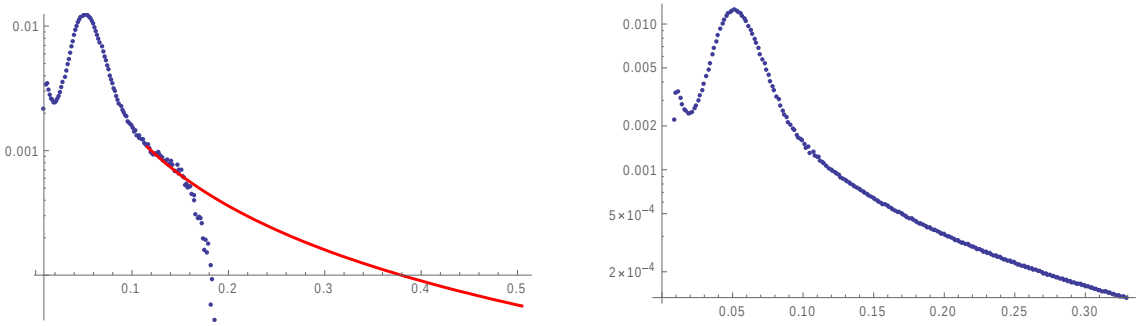

Figure 76. Extrapolated $I(q)q^2$ versus q curves, to high q values by applying Porod's law, of PVDF relaxed at 120 ºC and 10% strain. Red line: Porod asymptote.

Appendix III

1. Statistical analysis

The mean values of the results in this work were assessed by statistical analysis using the Statistica 10 software. The mean ($\bar{x}$), the absolute standard deviation (s) and the coefficient of variation (CV) were calculated by the following equations [94]:

$$\bar{x} = \frac{1}{n}\sum_{i=1}^{n} x_i \qquad (31)$$

$$s = \sqrt{\frac{\sum_{i=1}^{n}(x_i - \bar{x})^2}{n - 1}} \qquad (32)$$

$$CV = \frac{s}{\bar{x}} \times 100 \qquad (33)$$

where n is the size of the data populations analyzed. Difference between the mean pairs was verified by analysis of variance (ANOVA), and then the Fisher's least significant difference (Fisher's LSD) method was applied. The data (the difference between pairs of sample means) were statistically significant for values of $p < 0.05$, equivalent to a level of confidence of 95%.

The test statistic for the null hypothesis H_0 ($\mu_i = \mu_j$) is presented according to the following equation [94]:

$$t_0 = \frac{\bar{x}_i - \bar{x}_j}{\sqrt{MQ\left(\frac{1}{n_i} + \frac{1}{n_j}\right)}} \qquad (34)$$

The mean pairs will be statistically different if:

$$\bar{x}_i - \bar{x}_j > LSD = t\left(\alpha/2,\ N - a\ \sqrt{MQ\left(1/n_1 + 1/n_2\right)}\right) \qquad (35)$$

Statistical analysis was applied for the results of the tensile tests, DMA and DSC experiments; and are shown below.

2. Variation of elastic modulus (tensile test)

Univariate Tests of Significance for E (Tg)
Sigma-restricted parameterization
Effective hypothesis decomposition

Effect	SS	Degr. of Freedom	MS	F	p
Intercept	23258205	1	23258205	7535,627	0,000000
amostra	748017	9	83113	26,928	0,000000
Error	61729	20	3086		

Tests of Homogeneity of Variances (Tg)
Effect: amostra

	Hartley F-max	Cochran C	Bartlett Chi-Sqr.	df	p
E	812,5621	0,310828	15,75504	9	0,072177

LSD test; variable E (Tg)
Probabilities for Post Hoc Tests
Error: Between MS = 3086,4, df = 20,000

Cell No.	amostra	{1} 1292,7	{2} 837,06	{3} 797,32	{4} 951,37	{5} 899,74	{6} 868,23	{7} 942,70	{8} 760,99	{9} 730,38	{10} 724,42
1	Sem relax		0,000000	0,000000	0,000000	0,000000	0,000000	0,000000	0,000000	0,000000	0,000000
2	Relax_23C_10def	0,000000		0,391378	0,020347	0,182291	0,499945	0,030470	0,109077	0,029037	0,022001
3	Relax_23C_7def	0,000000	0,391378		0,002867	0,035290	0,133705	0,004446	0,432522	0,155575	0,123672
4	Relax_23C_3def	0,000000	0,020347	0,002867		0,268488	0,081747	0,850320	0,000444	0,000092	0,000068
5	Relax_80C_10def	0,000000	0,182291	0,035290	0,268488		0,495235	0,354925	0,006196	0,001310	0,000964
6	Relax_80C_7def	0,000000	0,499945	0,133705	0,081747	0,495235		0,116277	0,028299	0,006482	0,004810
7	Relax_80C_3def	0,000000	0,030470	0,004446	0,850320	0,354925	0,116277		0,000694	0,000144	0,000106
8	Relax_120C_10def	0,000000	0,109077	0,432522	0,000444	0,006196	0,028299	0,000694		0,507570	0,429602
9	Relax_120C_7def	0,000000	0,029037	0,155575	0,000092	0,001310	0,006482	0,000144	0,507570		0,896710
10	Relax_120C_3def	0,000000	0,022001	0,123672	0,000068	0,000964	0,004810	0,000106	0,429602	0,896710	

3. Variation of tensile strength (tensile test)

Univariate Tests of Significance for E (Tg)
Sigma-restricted parameterization
Effective hypothesis decomposition

Effect	SS	Degr. of Freedom	MS	F	p
Intercept	40383,66	1	40383,66	177056,3	0,000000
amostra	94,56	9	10,51	46,1	0,000000
Error	4,56	20	0,23		

Tests of Homogeneity of Variances (Tg)
Effect: amostra

	Hartley F-max	Cochran C	Bartlett Chi-Sqr.	df	p
E	22,26427	0,335286	6,822524	9	0,655591

Cell No.	LSD test; variable E (Tg) Probabilities for Post Hoc Tests Error: Between MS = ,22808, df = 20,000 amostra	{1} 38,367	{2} 38,499	{3} 35,202	{4} 34,651	{5} 38,910	{6} 38,517	{7} 37,863	{8} 35,499	{9} 34,566	{10} 34,821
1	Sem relax		0,737872	0,000000	0,000000	0,179313	0,704541	0,210629	0,000000	0,000000	0,000000
2	Relax_23C_10def	0,737872		0,000000	0,000000	0,305215	0,964313	0,118174	0,000000	0,000000	0,000000
3	Relax_23C_7def	0,000000	0,000000		0,173023	0,000000	0,000000	0,000001	0,454659	0,118537	0,340621
4	Relax_23C_3def	0,000000	0,000000	0,173023		0,000000	0,000000	0,000000	0,041755	0,829653	0,666925
5	Relax_80C_10def	0,179313	0,305215	0,000000	0,000000		0,325971	0,014237	0,000000	0,000000	0,000000
6	Relax_80C_7def	0,704541	0,964313	0,000000	0,000000	0,325971		0,108902	0,000000	0,000000	0,000000
7	Relax_80C_3def	0,210629	0,118174	0,000001	0,000000	0,014237	0,108902		0,000006	0,000000	0,000000
8	Relax_120C_10def	0,000000	0,000000	0,454659	0,041755	0,000000	0,000000	0,000006		0,026610	0,097456
9	Relax_120C_7def	0,000000	0,000000	0,118537	0,829653	0,000000	0,000000	0,000000	0,026610		0,520059
10	Relax_120C_3def	0,000000	0,000000	0,340621	0,666925	0,000000	0,000000	0,000000	0,097456	0,520059	

4. Variation of α-transition temperature, Tα (DMA experiments)

Effect	Univariate Tests of Significance for Talfa (Tg) Sigma-restricted parameterization Effective hypothesis decomposition SS	Degr. of Freedom	MS	F	p
Intercept	111930,7	1	111930,7	27637,22	0,000000
amostra	294,6	8	36,8	9,09	0,002637
Error	32,4	8	4,1		

	Tests of Homogeneity of Variances (Tg) Effect: amostra Hartley F-max	Cochran C	Bartlett Chi-Sqr.	df	p
Talfa	20,75309	0,259414	1,705261	7	0,974342

Cell No.	LSD test; variable Talfa (Tg) Probabilities for Post Hoc Tests Error: Between MS = 4,0500, df = 8,0000 amostra	{1} 86,150	{2} 79,500	{3} 78,350	{4} 75,900	{5} 87,150	{6} 82,200	{7} 84,800	{8} 86,750	{9} 87,300
1	Sem relax		0,010788	0,004702	0,000938	0,632623	0,147692	0,521227	0,773191	0,583395
2	Relax_23C_10def	0,010788		0,583395	0,111434	0,005227	0,305201	0,030010	0,006956	0,004702
3	Relax_23C_7def	0,004702	0,583395		0,258135	0,002372	0,156907	0,012517	0,003105	0,002147
4	Relax_23C_3def	0,000938	0,111434	0,258135		0,000516	0,033855	0,002219	0,000653	0,000473
5	Relax_80C_10def	0,632623	0,005227	0,002372	0,000516		0,079485	0,276540	0,847408	0,942414
6	Relax_80C_7def	0,147692	0,305201	0,156907	0,033855	0,079485		0,322297	0,102097	0,072322
7	Relax_80C_3def	0,521227	0,030010	0,012517	0,002219	0,276540	0,322297		0,360942	0,249320
8	Relax_120C_7def	0,773191	0,006956	0,003105	0,000653	0,847408	0,102097	0,360942		0,791548
9	Relax_120C_3def	0,583395	0,004702	0,002147	0,000473	0,942414	0,072322	0,249320	0,791548	

5. Variation of crystallinity index (DSC experiments)

a. First heating

Univariate Tests of Significance for Xc1aquec (Tg)
Sigma-restricted parameterization
Effective hypothesis decomposition

Effect	SS	Degr. of Freedom	MS	F	p
Intercept	47682,50	1	47682,50	77099,38	0,000000
amostra	80,95	9	8,99	14,54	0,000124
Error	6,18	10	0,62		

Tests of Homogeneity of Variances (Tg)
Effect: amostra

	Hartley F-max	Cochran C	Bartlett Chi-Sqr.	df	p
Xc1aquec	834,5679	0,546523	11,63490	9	0,234683

LSD test; variable Xc1aquec (Tg)
Probabilities for Post Hoc Tests
Error: Between MS = ,61845, df = 10,000

Cell No.	amostra	{1} 50,090	{2} 49,205	{3} 46,365	{4} 48,340	{5} 46,600	{6} 47,460	{7} 46,255	{8} 51,650	{9} 51,460	{10} 50,850
1	Sem relax		0,286723	0,000796	0,050243	0,001259	0,007437	0,000645	0,075410	0,112108	0,356631
2	Relax_23C_10def	0,286723		0,004758	0,297139	0,007846	0,050788	0,003776	0,011079	0,016742	0,062943
3	Relax_23C_7def	0,000796	0,004758		0,030839	0,771193	0,193990	0,891536	0,000052	0,000071	0,000197
4	Relax_23C_3def	0,050243	0,297139	0,030839		0,051338	0,289300	0,024261	0,001803	0,002655	0,009627
5	Relax_80C_10def	0,001259	0,007846	0,771193	0,051338		0,299788	0,670207	0,000076	0,000104	0,000300
6	Relax_80C_7def	0,007437	0,050788	0,193990	0,289300	0,299788		0,156461	0,000334	0,000473	0,001535
7	Relax_80C_3def	0,000645	0,003776	0,891536	0,024261	0,670207	0,156461		0,000044	0,000059	0,000163
8	Relax_120C_10def	0,075410	0,011079	0,000052	0,001803	0,000076	0,000334	0,000044		0,813971	0,333005
9	Relax_120C_7def	0,112108	0,016742	0,000071	0,002655	0,000104	0,000473	0,000059	0,813971		0,455897
10	Relax_120C_3def	0,356631	0,062943	0,000197	0,009627	0,000300	0,001535	0,000163	0,333005	0,455897	

b. Second heating

Univariate Tests of Significance for Xc2aquec (Tg)
Sigma-restricted parameterization
Effective hypothesis decomposition

Effect	SS	Degr. of Freedom	MS	F	p
Intercept	47289,76	1	47289,76	252319,7	0,000000
amostra	25,29	9	2,81	15,0	0,000109
Error	1,87	10	0,19		

Tests of Homogeneity of Variances (Tg)
Effect: amostra

	Hartley F-max	Cochran C	Bartlett Chi-Sqr.	df	p
Xc2aquec	12,12071	0,235727	3,505152	9	0,940871

LSD test; variable Xc2aquec (Tg)
Probabilities for Post Hoc Tests
Error: Between MS = ,18742, df = 10,000

Cell No.	amostra	{1} 51,010	{2} 49,950	{3} 46,650	{4} 48,970	{5} 48,210	{6} 48,005	{7} 47,875	{8} 48,500	{9} 48,675	{10} 48,415
1	Sem relax		0,034347	0,000001	0,000826	0,000072	0,000040	0,000028	0,000173	0,000304	0,000133
2	Relax_23C_10def	0,034347		0,000018	0,047072	0,002442	0,001156	0,000731	0,007373	0,014657	0,005306
3	Relax_23C_7def	0,000001	0,000018		0,000320	0,004820	0,010692	0,017864	0,001628	0,000871	0,002225
4	Relax_23C_3def	0,000826	0,047072	0,000320		0,109697	0,049923	0,029905	0,303111	0,511078	0,228769
5	Relax_80C_10def	0,000072	0,002442	0,004820	0,109697		0,646004	0,456944	0,518109	0,308011	0,646004
6	Relax_80C_7def	0,000040	0,001156	0,010692	0,049923	0,646004		0,770109	0,279507	0,152751	0,365933
7	Relax_80C_3def	0,000028	0,000731	0,017864	0,029905	0,456944	0,770109		0,179416	0,094367	0,240693
8	Relax_120C_10def	0,000173	0,007373	0,001628	0,303111	0,518109	0,279507	0,179416		0,694553	0,848276
9	Relax_120C_7def	0,000304	0,014657	0,000871	0,511078	0,308011	0,152751	0,094367	0,694553		0,561489
10	Relax_120C_3def	0,000133	0,005306	0,002225	0,228769	0,646004	0,365933	0,240693	0,848276	0,561489	